AUS DER ABTEILUNG FÜR NEUROPATHOLOGIE
Prof. Dr. med. Markus J. Riemenschneider

DER FAKULTÄT FÜR MEDIZIN
DER UNIVERSITÄT REGENSBURG

REELIN/DISABLED-1-SIGNALING
IN GLIOMA CELL MIGRATION AND INVASION

Inaugural Dissertation
zur Erlangung des Doktorgrades der Medizin

der Fakultät für Medizin der Universität Regensburg

vorgelegt von

Stefan Bernd Swoboda

2018

AUS DER ABTEILUNG FÜR NEUROPATHOLOGIE
Prof. Dr. med. Markus J. Riemenschneider

DER FAKULTÄT FÜR MEDIZIN
DER UNIVERSITÄT REGENSBURG

REELIN/DISABLED-1-SIGNALING
IN GLIOMA CELL MIGRATION AND INVASION

Inaugural Dissertation
zur Erlangung des Doktorgrades der Medizin

der Fakultät für Medizin der Universität Regensburg

vorgelegt von

Stefan Bernd Swoboda

2018

Dekan: Prof. Dr. Dr. Torsten E. Reichert

1. Berichterstatter: Prof. Dr. med. Markus J. Riemenschneider

2. Berichterstatter: Prof. Dr. rer. nat. Eugen Kerkhoff

Table of Contents

Abbreviations

Abbreviations	
'	minute(s)
''	second(s)
2D	two dimensional
3D	three dimensional
A	ampere
ADF	actin depolymerizing factor
ADP	adenosine diphosphate
APS	ammonium persulfate
ARF1	ADP-ribosylation factor 1
ATP	adenosine triphosphate
bp	base pairs
BSA	bovine serum albumin
$CaCl_2$	calcium chloride
cDMEM	complete Dulbecco's modified Eagle's medium
cDNA	complementary DNA
CNS	central nervous system
CO_2	carbon dioxide
d	distance
D	distance from origin
DAB1	Disabled-1
DAPI	4',6-diamidino-2-phenylindole
dH_2O	destillated H_2O
DMEM	Dulbecco's modified Eagle's medium
DMSO	dimethyl sulfoxide
DNA	deoxyribonucleic acid
dNTP	deoxyribonucleotide triphosphate
E. coli	Escherichia coli
ECM	extracellular matrix
EGF	epidermal growth factor
EGFR	epidermal growth factor receptor
EGFRvIII	epidermal growth factor receptor variant III
F	phenylalanine
F-actin	filamentous actin
FCS	fetal calf serum
g	acceleration due to gravity (9.81 m/s2)
G418	geneticindisulfat
G-actin	globular actin
GBM	glioblastoma multiforme
GFP	green fluorescent protein

h	hour(s)
HEPES	4-(2-hydroxyethyl)-1-piperazineethanesulfonic acid
HRP	horseradish peroxidase
IDH	isocitrate dehydrogenase
KCl	potassium chloride
kDa	kilo Dalton
Kip1	Cyclin-dependent kinase inhibitor 1B
LIMK	LIM (Lin-11/Isl-1/Mec-3)-domain-containing protein kinase
$MgCl_2$	magnesium chloride
MGMT	O-6-methylguanine-DNA methyltransferase
$MnCl_2$	manganese (II) chloride
mRNA	messenger RNA
MRT	magnetic resonance tomography
NaCl	sodium chloride
NaOH	sodium hydroxide
NP-40	nonylphenolethoxylate
O/N	overnight
p27	Cyclin-dependent kinase inhibitor 1B
p53	tumor protein p53
PAGE	polyacrylamide gel electrophoresis
PBS	phosphate buffered saline
P-cofilin	phosphorylated cofilin
PCR	polymerase chain reaction
PDGFR	platelet-derived growth factor receptor
PFA	paraformaldehyde
PI3K	phosphatidylinositol-4,5-bisphosphate 3-kinase
RNA	ribonucleic acid
RT	room temperature
SDS	sodium dodecyl sulfate
sec	second(s)
STAT	signal transducer and activator of transcription
TBS	Tris-buffered saline
TCGA	The Cancer Genome Atlas
TEMED	tetramethylethylenediamine
Triton X-100	t-octylphenoxypolyethoxyethanol
Tween 20	polyoxyethylene (20) sorbitan monolaurate
V	volt
v	volume
w	weight
w/o	without
WT	wildtype
Y	tyrosine

1 Introduction

Primary tumors of the brain and spinal cord represent about 2 - 3% of all diagnosed tumors and are therefore rather rare cancer entities (Schlegel et al. 2003). Gliomas comprise about 80% of all malignant brain tumors and more than half of all gliomas are glioblastomas (Ostrom et al. 2016). Despite extensive research, treatment of glioblastomas is still lacking highly effective therapies leaving patients with an average survival time of less than two years (Tonn et al. 2006, Louis 2007). In terms of basic research, the *Reelin/Disabled-1* signaling pathway has emerged as a new potential tumor suppressor over the last decade.

1.1 Reelin/Disabled-1 signaling pathway

The role and the biological mechanisms of the *Reelin/Disabled-1* signaling pathway have already been an object of research for the last decades. Especially its function during embryonic brain development as an inhibitor of neuronal migration has been the topic of intensive research. Much less is known about the meaning of *Reelin/Disabled-1* signaling in cancers, especially in brain tumors. However, previous work of our laboratory for *Reelin* and *Disabled-1* suggested a potential role as tumor suppressor in high-grade gliomas.

1.1.1 Reelin

Several studies have unraveled the functions in regulation of neuronal migration of the extracellular glycoprotein *Reelin* but, primarily, it has been discovered by D. S. Falconer at the Institute of Animal Genetics, Edinburgh, in the 1950s. The name of this protein is derived from the *reeler* mouse, an autosomal recessive mutant mouse showing pronounced neurological symptoms, like dystonia, ataxia and tremors (Falconer 1951) and striking abnormalities in the telencephalic and cerebellar cortices (Goffinet 1984). These mice were later found to lack functioning *Reelin* due to a certain homozygous gene mutation (D'Arcangelo et al. 1995). Over the last six decades, *Reelin* and the *reeler* mouse have been

extensively studied as a model for brain development, proclaiming *Reelin* as a key regulator of neuronal migration.

The *Reelin* gene (*RELN*, GenBank-Accession-No.: AAC51105.1), is widely conserved through vertebrates and transcribed into a linear mRNA of 11'571 bp with an open reading frame (ORF) of 10,383 nucleotides. *RELN* is encoding for a large protein consisting of 3461 amino acids resolving in a molecular mass of about 388 kDa (DeSilva et al. 1997). Three different alleles, situated at the chromosomal region 7q22, were found responsible for the *reeler* mutant, with each of them displaying a partial deletion of the *RELN* coding sequence (D'Arcangelo et al. 1995, Takahara et al. 1996).

X-ray cristallography has revealed that *Reelin* comprises several domains (see *Figure 1*) consisting of a signaling sequence (S), followed by the *reeler domain* which can also be found in the extracellular proteins F-spondin and mindin (SP) (Feinstein et al. 1999). Next comes another unique region containing an epitope for the Cajal-Retzius cell marker 50 (CR-50) (H), an immunohistochemical marker for cells that are producing *Reelin*. The *Reelin* producing Cajal-Retzius cells are important during corticogenesis (see *Figure 2*). Then, the combination of a central epidermal growth factor (EGF) motif surrounded by two different sequences, A and B, is repeated eight times, each of these containing 350-390 amino acids (Yasui et al. 2007). The final reelin domain contains a highly basic and short C-terminal region (+) with a length of 32 amino acids. This region is highly conserved, being 100% identical in all mammals. In contrast to previous results, this region is not required for secretion but is necessary to activate downstream signaling efficiently (Nakano et al. 2007).
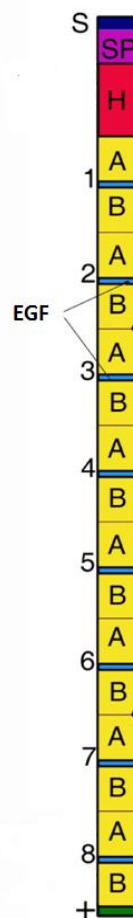
Figure 1: Scheme of the *Reelin* protein.
Reelin exhibits a multidomain architecture that starts with a signaling sequence (S) and the typical *reeler domain* (SP). It further comprises an epitope for the Cajal-Retzius cell marker 50 (H) and eight tandem repeats of which each repeat is divided into two different subrepeats (A and B) by an epidermal growth factor (EGF) motif. *Reelin* ends with a short, highly basic C-terminal region (+).
Taken from (CopperKettle 2013).

Canonical signaling downstream of *Reelin* is mediated by binding to the very-low-density lipoprotein receptor (VLDLR) and the ApoE receptor 2 (ApoER2) which results in the activation of the cytoplasmic adapter protein *Disabled-1* (*DAB1*) by tyrosine phosphorylation (Hiesberger et al. 1999). Both receptors are able to stimulate *DAB1* phosphorylation, however clustering of these receptors at the plasma membrane is necessary for recruitment of SRC family tyrosine kinases (SFKs) (see *chapter 1.1.2*), further downstream signaling and especially for its effect on neuronal migration (Strasser et al. 2004).

The role of *Reelin* during embryonic brain development has been most extensively studied in the neocortex of mice as a model system. Here, *Reelin* is required for the proper formation and positioning of the neuronal cell layers in the cortical plate (Honda et al. 2011). The cortical plate is a neuronal region that neuroblasts reach through migration guided by radial glia during corticogenesis to form the six layers of the neocortex (Herz & Chen 2006).

A very profound study on the influences of deficient *Reelin* signaling during embryonic development is summed up in *Figure 2*:

Generally speaking, lack of *Reelin* leads to an inversion of the six cell layers of the neocortex. The schematic drawings show a part of the cerebral cortex of an embryonic mouse brain at three successive points in time (i, ii and iii). The presence of *Reelin* is shown by the blackened Cajal-Retzius neurons (CR) and black dots in wild type mice (a). These cells, together with subplate neurons (SP), represent the preplate (PP) which will later be the marginal zone (MZ) of the brain. The Arabic numbers of the indicated neurons mark the future layers of the neocortex (1-6). The newly born neurons that are formed by wild-type mice in the ventricular zone (VZ) migrate past the subplate and stop beneath the marginal zone. Later generated neurons overtake the subplate as well as the earlier neurons and reach the top of the developing cortex. As a consequence, the earlier-generated neurons are located beneath the later-born ones.

In *reeler* mice, the preplate appears to be normal. However, the Cajal-Retzius cells are unable to generate *Reelin* which is indicated by the uncolored CR neurons. Furthermore, the neurons of this cortex are not able to migrate past the subplate and therefore the preplate does not split into two layers but becomes the superplate (SPP). Thus, earlier-generated neurons stack at the top of the cortex whilst later-generated neurons reside in the deeper layers. Moreover, neurons in the upper layer near the internal plexiform zone (IPZ) show a formation of horizontally or even inversely oriented dendrites. Briefly summarized, the neocortex of *reeler* mice, opposed to that of wild-type mice, shows an outside-in sequence of neuronal positioning (Honda et al. 2011).
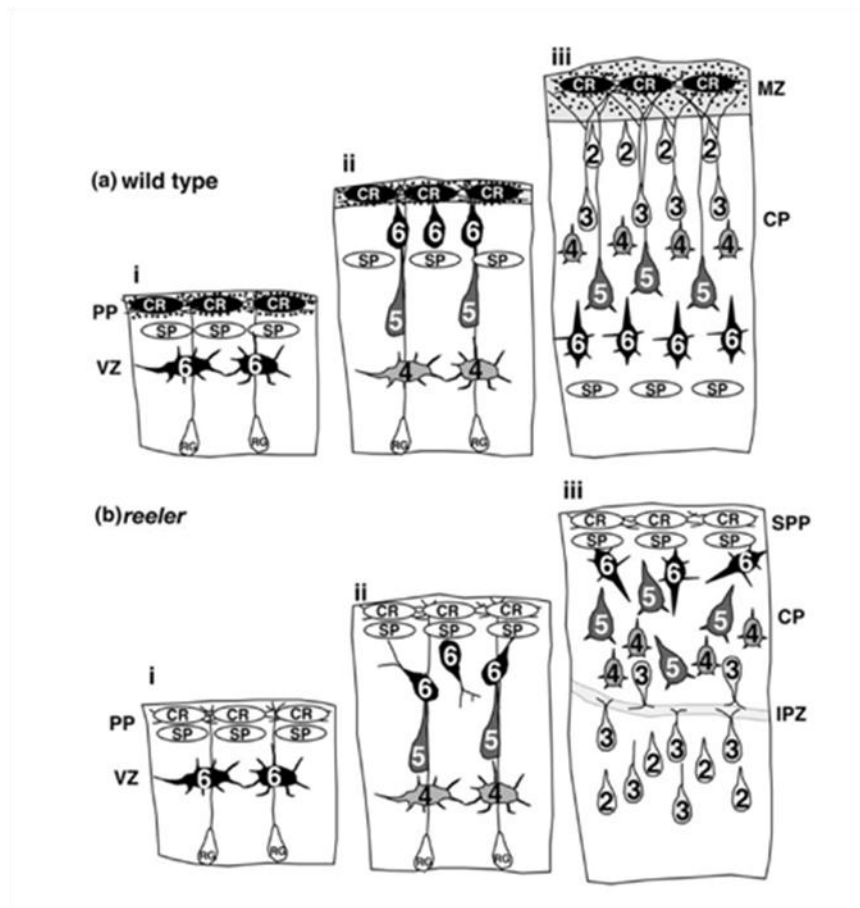
Figure 2: Development of the cerebral cortex in wild type and reeler mice.
(a) depicts the influences that *Reelin*, secreted by Cajal-Retzius neurons (CR, black cells), has on corticogenesis at three successive points in time (i, ii, iii) whereas (b) is showing failed cortical development due to absence of *Reelin* (CR, white cells). Cajal-Retzius cells (CR) and subplate neurons (SP) represent the preplate (PP) becoming the marginal zone (MZ) later. The Arabic numbers of the indicated neurons mark the future layers of the neocortex (1-6).
(a) In wild-type mice newly born neurons are formed in the ventricular zone (VZ) and migrate past the subplate (SP). Finally, earlier-generated neurons are located beneath the later-born ones.
(b) In *reeler* mice neurons are not able to migrate past the subplate (SP) and therefore earlier-generated neurons stack at the top of the cortex, whilst later-generated neurons reside in the deeper layers. Further cortical anomalies found here, are formation of a superplate (SPP) and an internal plexiform zone (IPZ) where neurons show a formation of horizontally or inversely oriented dendrites. The neocortex of *reeler* mice shows an outside-in sequence of neuronal positioning.
Modified from (Honda et al. 2011, S. 1272).

However, proper lamination in the central nervous system is not only a result of direct interaction of *Reelin* with migrating neurons. Additionally, radial glial cells are activated by the *Reelin* signaling cascade. Radial glial cells of the neocortex seem in general only mildly affected, whereas the development of the dentate gyrus shows severely altered neuronal positioning and formation of radial processes in the absence of *Reelin* (Förster et al. 2002, Hartfuss et al. 2003). This considerable morphological phenotype was found independently of

Reelin signaling in neurons. This suggests that *Reelin* is directly affecting glial cells (Brunne et al. 2013).

Although the functions of *Reelin/DAB1* signaling during embryonic development are very well understood, only little is known about its importance for the adult brain. It has been shown that *Reelin* is expressed continuously even after disappearance of the Cajal-Retzius cells at the end of the neuronal migration phase. Instead, *Reelin* is produced by a group of GABA-ergic (γ-aminobutyric acid) interneurons (Herz & Chen 2006). Some studies indicate that *Reelin/DAB1* signaling influences the growth of dendrites (Jossin & Goffinet 2007) and is a potential modulator of neurotransmission. It was shown that *Reelin* and its receptors ApoER2 and VLDLR influence cognition and plasticity of synapses in mice. Loss of one of these receptors leads to defects in long term potentiation, a major cellular mechanism that underlies learning and memory. These findings might contribute to understand the pathophysiology of alterations of cognitive functions and loss of synapses in patients with Alzheimer's disease (Weeber et al. 2002).

Besides the importance for Alzheimer's disease, further analyses showed that *Reelin/DAB1* signaling seems to play an emerging role in other neurological and neuropsychiatric disorders of the adult brain. Lower levels of *Reelin* have been found in patients suffering from schizophrenia, bipolar disorder and autism (Fatemi et al. 2000, Fatemi et al. 2005). Again, the effects of *Reelin* on long term potentiation which lead to a reduction of NMDA receptors were proposed to contribute to these disorders (Coyle 2006). Other findings suggest that *Reelin/DAB1* signaling is required to maintain neuroanatomical integrity in the adult brain as *Reelin* malfunction leads to dispersed positioning of dentate granule cells in patients with epilepsy (Heinrich et al. 2006). This malpositioning of neurons is correlated to the wake of seizures, especially to that of temporal lobe epilepsy (Haas et al. 2002, Heinrich et al. 2006). Genetic defects of the *Reelin* gene were found to result in a form of lissencephaly with cerebellar hypoplasia. Lissencephaly is a human brain disorder that is characterized by the absence or reduction of cerebral convolutions (Hong et al. 2000).

For quite a long time it was believed that only traces of *Reelin* could be detected outside the brain, however, about 15 years ago, it was shown that *Reelin* is present in plasma of rats, mice and humans. Moreover, western blotting and immunocytochemistry revealed expression in the liver, the pituitary gland and a subgroup of chromaffin cells in the adrenal medulla (Smalheiser et al. 2000). Only little is known about the physiological role of *Reelin/DAB1* signaling in these and other peripheral tissues but findings suggest rather little importance of

this pathway for normal organic functions. Nonetheless, some studies on non-brain cancers proposed a function in tumor suppression for the *Reelin* protein (see *chapter 1.1.4* for more information).

1.1.2 Disabled-1

As mentioned above, the key target for further transmission of *Reelin* signaling in embryonic development of the brain is the protein *Disabled-1* (*DAB1*) (~ 63 kDa), whose gene represents a homologue of the drosophila protein *disabled* (Ware et al. 1997). This insight was gained by experiments with mice that were deficient of the *DAB1* gene. These mouse mutants, called *scrambler* and *yotari* (both of them containing different mutations of the *DAB1* gene), show a phenotype that is indistinguishable from the one in reeler mice (Howell et al. 1997b).

DAB1 interacts with the *Reelin* receptors ApoER2 and VLDLR through binding to a cytoplasmic domain that contains a typical sequence of amino acids. This amino-terminal phosphotyrosine binding (PTB) domain contains a sequence of asparagin (N), proline (P), an arbitrary amino acid (x) and tyrosine (Y) and is therefore abbreviated as NPxY motif (Howell et al. 2000). Binding of *Reelin* leads to clustering of its receptors which finally induces tyrosine phosphorylation of *DAB1* (Hiesberger et al. 1999). Additionally, it could be shown that binding of *Reelin* to co-receptors like Cadherin-related neuronal receptors (CNRs) is necessary for the initiation of *DAB1* phosphorylation through Src family kinases (*SFKs*) (Senzaki et al. 1999).

Figure 3 explains the structure of the human *DAB1* protein. Human *DAB1* contains three domains, the PTB, DabH1 and DabH2 domain, that represent regions of homology to the related mouse gene. The percentage of identity varies between 54 and 73%. Next to the
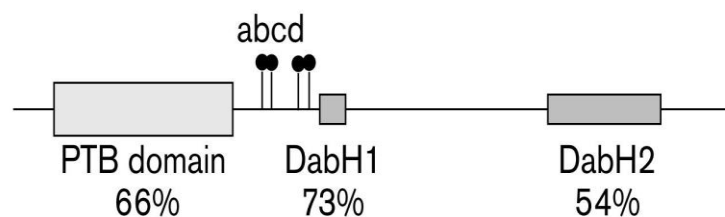
Figure 3: Protein structure of DAB1.
Human *DAB1* comprises three domains (PTB domain, DabH1 and DabH2) that show high sequence-homology to its related mouse gene. The percentage of identy is given below each region. Furthermore, *DAB1* consists of four genetic regions (a, b, c and d) that contain five potential phosphorylation sites. Taken from (Howell et al. 2000).

PTB domain, four genetic regions, containing five phosphorylation sites, Tyr185 (a), Tyr198/Tyr200 (b), Tyr220 (c) and Tyr232 (d), are marked (Howell et al. 2000). Additionally, the sequence around Tyr198 resembles a sequence of the platelet derived growth factor receptor containing two tyrosines (equivalent to Tyr198 and Tyr200) which are both supposed

to be phosphorylated (Mori et al. 1993). Two of these four sites have already been proved as targets for phosphorylation by analyzing several mutants replaced by phenylalanine instead of tyrosine. A *DAB1* protein with mutation of all five tyrosines is called 5F mutant (Howell et al. 2000).

Tyrosine-phosphorylated *DAB1* only extents its whole potential as a transmitter of *Reelin* signaling in the presence of Src family kinases (*SFKs*), especially of the members Src, Fyn and Abl. *SFKs* are non-receptor tyrosine kinases that interact with multiple cytosolic, nuclear and membrane proteins (Howell et al. 1997a). Studies show that *DAB1* is a physiological substrate and also an activator of *SFKs* in neurons, meaning that *DAB1* can potentiate its own phosphorylation level through these kinases. Furthermore, mutations of certain *SFKs* lead to similar changes of mouse cortices present in the *reeler* mutant, suggesting that the cellular reaction to *Reelin* normally includes activation of *SFKs* (Bock & Herz 2003). The above information on *DAB1* so far is summed up in *Figure 4*.
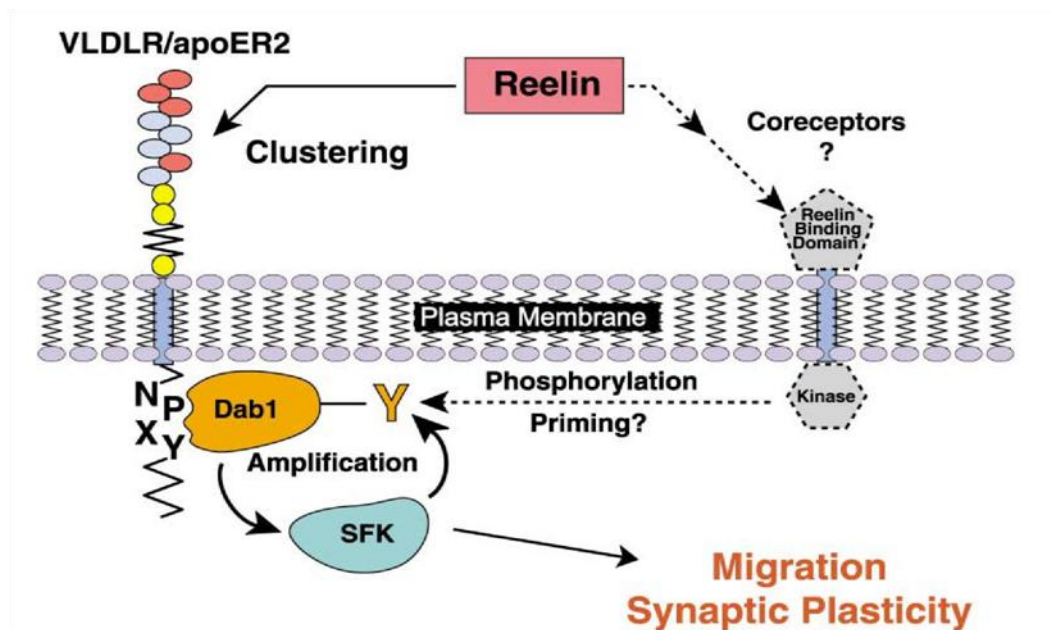
Figure 4: Hypothetical model for SFK activation by Reelin.
Reelin binds to its receptors, the very-low-density lipoprotein receptor (VLDLR) and the ApoE receptor 2 (apoER2), which leads to clustering of these receptors and binding of *DAB1* to the intracellular NPxY amino-acid sequence. Additionally, *Reelin* might bind unknown coreceptors that induce primary tyrosine-phosphorylation (Y) of *DAB1*. Once activated, *DAB1* is capable of amplifying its own phosphorylation through Src family kinases (SFK). This finally leads to reduced migration and enhanced synaptic plasticity of neurons. Taken from (Bock & Herz 2003).

Another interesting finding is that the intracellular protein *DAB1* is generally stable in its inactivated form. However, in response to its activator *Reelin*, it is polyubiquitinated and

degraded by proteasome complexes, proposing that tyrosine phosphorylation is important for the degradation of *DAB1* (Arnaud et al. 2003). This conclusion is also in accordance with findings in *reeler* mutants: The levels of *DAB1* protein are much higher in embryonic brain tissue from *reeler* mutant mice than compared to controls (Howell et al. 2000).

DAB1 contains not only tyrosine phosphorylation sites but can also be phosphorylated at serine491 through the Cyclin-Dependent Kinase 5 (*Cdk5*). It has been shown that *Cdk5* as well as its regulatory subunits p35 and p39 are regulating neuronal migration during corticogenesis independently of *Reelin* signaling. Mice that lack *Cdk5*, p35, or both p35 and p39 have defects of lamination in the neocortex similar yet not identical to *reeler* mice. Further significance of *DAB1* serine phosphorylation is unknown. However, these findings suggest that *DAB1* represents a molecular interface of two distinct signaling pathways regulating cell positioning (Keshvara et al. 2002).

1.1.3 Overview of known downstream targets

Proper development of the mammalian brain requires extensive coordination between migration, differentiation, proliferation and survival of future neurons and glial cells. Some of the known downstream targets of *Reelin/DAB1* signaling are contributing to these cellular functions during embryonic development.

As briefly mentioned above, it was shown that Cadherin-related neuronal receptors (CNRs) are co-receptors of *Reelin* in the cell membrane of neurons. CNR family proteins are supposed to be involved in formation and reorganization of synaptic connections in the nervous system. Inhibition of *Reelin* binding through antibodies against proteins of the CNR family (anti-RBD CNR antibody) leads to reduced tyrosine phosphorylation of *DAB1* (Senzaki et al. 1999). It has also been proved that CNRs interact with Fyn, a member of the SFKs (Hamada & Yagi 2001), suggesting that *Reelin* is also capable of modulating the phospho-tyrosine level of *DAB1* through other receptors than ApoER2 and VLDLR. *Figure 5* gives an overview of this hypothetical pathway of *Reelin* signaling.
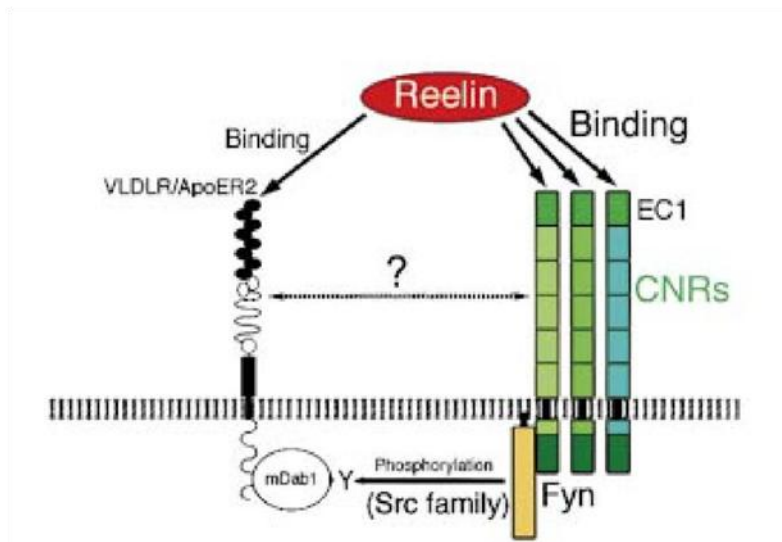
Figure 5: Hypothetical pathway of Reelin interacting with CNR family proteins.
Binding of *Reelin* to the N-terminal EC1 domain of Cadherin-related neuronal receptors (CNRs) is capable of modulating the tyrosine-phosphorylation (Y) of mouse *DAB1* (mDab1) through Fyn, a Src family kinase. Probably, an interaction of CNRs and the main *Reelin* receptors, the very-low-density lipoprotein receptor (VLDLR) and the ApoE receptor 2 (ApoER2), has additional influences on the activation of *DAB1*.
Modified from (Senzaki et al. 1999).

A proved target further downstream of *Reelin*/*DAB1* signaling is the phosphatidylinositol 3-kinase (PI3K). Stimulation of PI3K by *Reelin* leads to activation of the protein kinase B (PKB, also known as Akt). PI3K/PKB signaling is highly conserved in all cells of higher eukaryotes (Manning & Cantley 2007) and known to control a very diverse group of cellular functions like cell growth, proliferation, migration and intracellular trafficking. These components of *Reelin* signaling are enriched in axonal growth cones, contributing to proper neuronal positioning during brain development (Beffert et al. 2002). Further studies revealed that PI3K and PKB activity regulated through *Reelin* are both crucial for corticogenesis (Jossin & Goffinet 2007, Leemhuis & Bock 2011, Ohkubo et al. 2003).

Besides the downstream targets above, migration and cellular motility is also often corresponding to expression of and interaction with integrins. These proteins are necessary for establishment of cell-matrix junctions. Integrins are transmembrane receptors containing two different chains, an α and a β subunit, and can trigger intracellular signaling pathways. Research on *Reelin* signaling has particularly turned the spotlight on two specific integrins: α3β1 integrin (also known as laminin receptor) and α5β1 integrin (also called fibronectin receptor).

The receptor α3β1 integrin is mainly known for binding laminin but collagen I and IV or entactin/nidogen are described as ligands as well. However, α3β1 integrin is more than a

simple adhesion receptor, but has a rather complex role as signaling molecule that can modulate multiple cellular functions like proliferation, differentiation and migration (Kreidberg 2000). It was also proved that α3β1 integrin is able to bind the extracellular protein *Reelin* which leads to inhibition of neuronal migration during brain development. Further data suggests that activation of the laminin receptor modulates targets of *Reelin* signaling, as a reduction of *DAB1* levels could be found in α3β1-deficient mice (Dulabon et al. 2000).

α5β1 integrin is the primary receptor for fibronectin and able to support matrix assembly of fibronectin as well as promoting cell migration (Arnaout et al. 2007, Zhang et al. 1993). Recent studies showed that binding of *Reelin* to its receptors can activate integrin α5β1 through a pathway that includes *DAB1*. Consequently, the activation of α5β1 integrin through this inside-out signaling promotes neuronal adhesion to fibronectin. Additional data indicates that this pathway influences neuronal migration and is crucial for proper layering of the neocortex during brain development (Sekine et al. 2012).

Migrating cells do not only show changes of integrin activity but most often also exhibit mechanisms to modulate their cytoskeletal structure. It is known that *Reelin* is capable of controlling at least two pathways that reorganize the actin cytoskeleton.

The neuronal Wiskott-Aldrich syndrome protein (N-WASP) is known to promote invasion by activating the Arp2/3 complex, a protein initiating the polymerization of actin and inducing formation of filopodia (Tang et al. 2013). Unphosphorylated/inactive *DAB1* binds N-WASP directly and starts the signaling pathway by activating N-WASP. Phosphorylated/active *DAB1* in turn is degraded through ubiquitinylation and thus can no longer activate these mechanisms leading to reduced filopodia formation and decreased cell motility (Suetsugu et al. 2004).

A second pathway influencing actin filament dynamics and reorganization includes ADF/cofilin family proteins (hereafter referred to as cofilin for simplicity). Active, unphosphorylated cofilin binds globular (G)-actin as well as filamentous (F)-actin and can enhance the disassembly of F-actin by stimulating severance and depolymerization of actin filaments. This results in higher actin turnover (Pollard & Borisy 2003). *Reelin/DAB1* signaling leads to activation of the enzyme *LIM kinase 1* and *2* (*LIMK1/2*) which phosphorylates cofilin at serine3 and converts the protein into an inactive form. With this modification it is no longer capable of binding actin and thus promotes actin polymerization and cytoskeletal stability. As a consequence, actin turnover is suppressed and cell motility

reduced (Chai et al. 2009, Kruger et al. 2010). *Figure 6* illustrates the interactions of cofilin and actin.
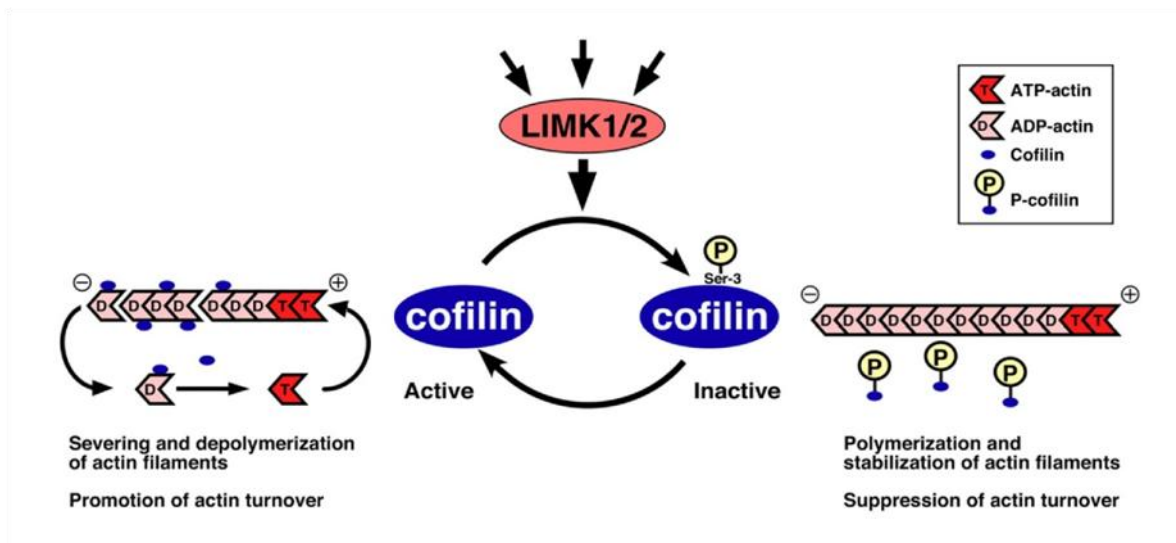
Figure 6: Control of actin filament dynamics by phospho-regulation.
Amongst other proteins, LIMK1/2 is activated by *Reelin*, which leads to phosphorylation of cofilin at serine3 converting it from an active into an inactive state. Unphosphorylated cofilin is binding ADP-actin and induces formation of ATP-actin, leading to enhanced severing and depolymerization of actin filaments and stimulation of actin turnover. Phosphorylated cofilin is unable of binding actin and is therefore suppressing actin turnover by promoting polymerization and stabilization of actin filaments.
Modified from (Mizuno 2013).

1.1.4   Reelin/Disabled-1 signaling in other cancers

As mentioned above in *chapter 1.1.1*, expression of *Reelin* is not restricted to the brain, but can be found in many other tissues. Although existing data rather suggests little importance for physiological mechanisms of *Reelin/DAB1* signaling (Ikeda & Terashima 1997), *Reelin* might act in reducing invasion of multiple non-brain cancers. This presumption was established after having compared the expression of *Reelin* protein in several cancers (e.g. hepatocellular carcinoma, breast cancer, esophageal cancer or pancreatic cancer) to levels in normal tissues. Most of the samples showed a reduced level of expression of *Reelin* compared to the control cases (Okamura et al. 2011, Sato et al. 2006, Stein et al. 2010, Yuan et al. 2012).

Research on hepatocellular carcinoma revealed that up to 80% of the samples showed a clearly reduced level of *Reelin* expression. Again, about half of these tumors were found to be hypermethylated on the *RELN* gene promoter preventing synthesis of *Reelin* mRNA.

Moreover, clinical data suggested *Reelin* as a regulator gene being inversely correlated to the reoccurrence of hepatocellular carcinoma (Okamura et al. 2011).

Similar results were found in a study on breast cancer that found that hypermethylation of *RELN* promoter leads to poorer prognosis and positive lymph node status. Besides that, it was proved that overexpression of *Reelin* and incubation with exogenous *Reelin* was capable of suppressing cell migration, invadopodia formation and invasiveness in vitro (Stein et al. 2010). Similar findings are provided in a study on pancreatic cancer. Knockdown of *RELN* or its downstream target *DAB1* using small interfering RNA in cells that retained expression of *Reelin* exhibited enhanced cell migration and invasiveness (Sato et al. 2006).

However, a study by Perrone et al. showed a completely different result: whereas a down-regulation of *Reelin* was found in the carcinomas described above and several other entities, an increased expression of this protein was associated with high-grade disease in prostate cancer. Elevated levels were significantly correlated with aggressive phenotypic behavior of cancer cells. Interestingly, benign prostatic tissue did not show any expression of *Reelin* (Perrone et al. 2007).

Moreover, also the protein *DAB1* has been found to function in a pathway that is promoting invasion and metastasis of colorectal cancers. The phosphorylation level of *DAB1* as well as interaction with the tyrosine kinase ABL seem to play a crucial role in a signaling system that is induced by the transmembrane receptor protein NOTCH (Sonoshita et al. 2015).

1.2   General information on glioblastoma

The preceding chapter gave an overview of the pathological role of *Reelin*/*DAB1* signaling in non-neoplastic tissue and multiple cancers. However, there is no existing study investigating the influence of this pathway on glioblastoma or other brain tumors, except for two immunohistochemical studies in gangliogliomas. This low-grade tumor which is often associated with focal epilepsy in young patients, showed significantly reduced levels of *DAB1* protein in its tissue but no mutations of the *DAB1* gene could be detected (Becker et al. 2002, Kam et al. 2004).

The chapter below will provide some general information on glioblastoma that is necessary to understand the contents and experiments of this doctoral thesis and will also give a short summary of the data on *Reelin/DAB1* signaling in glioblastoma that was raised in our workgroup so far.

1.2.1 Overview and epidemiology

Tumors of the central nervous system (CNS) represent about 2 - 3% of all cancers diagnosed displaying a rather seldom but most often highly-malignant tumor entity in adults (Schlegel et al. 2003). In childhood, in reverse, brain tumors are the most common type of neoplasms after leukemias (Kaatsch 2010).

Gliomas are subdivided according to histological and biochemical similarities to astrocytic, oligodendroglial or ependymal cells. However, the cellular origin of gliomas is still unknown but studies of tumor suppressor mouse models suggest that gliomas arise from stem/progenitor cells (Alcantara Llaguno et al. 2009). Another study states that gliomas can also be induced by oncogenes via dedifferentiation of both neurons and astrocytes (Friedmann-Morvinski et al. 2012). Astrocytic gliomas are the most common primary tumors of the CNS (Tonn et al. 2006).

Gliomas are classified by means of histological and molecular criteria as stated in the World Health Organisation (WHO) classification of tumors of the central nervous system in its latest version from 2016 (first edition: 1979). The WHO classification is dividing brain tumors in four grades by assigning a certain grade of malignancy ranging from WHO grade I (benign) to WHO grade IV (highly malignant) to each histological subtype. Tumor classification is necessary for finding suitable therapeutic strategies and can give a prediction on the patient's prognosis (Louis et al. 2016).

WHO grade I tumors display neoplasms that show only a low proliferation rate and little degeneration. As they are normally histologically well-circumscribed, they can be cured completely by radical and maximal surgical resection. A typical grade I glioma is the pilocytic astrocytoma which is also the most common primary brain tumor in pediatric patients (Tonn et al. 2006, Louis 2007).

Tumors classified as WHO grade II, e.g. the diffuse astrocytoma, also show a low proliferation rate but are infiltrating healthy surrounding brain tissue in contrast to WHO grade I tumors. Therefore, these tumors tend to reoccur after surgical excision and the median survival is reduced to 4 years (Medical Disability Guidelines 2012).

A WHO grade III neoplasia like the anaplastic astrocytoma is characterized by microscopic features of malignancy and is normally accompanied by restricted life expectancy. Histologically, these tumors show nuclear and cellular atypia, as for example chromatin richness, disproportion of nuclear-cytoplasm ratio and an elevated mitotic activity (Tonn et al. 2006, Louis 2007).

Glioblastomas, also known as glioblastoma multiforme (GBM), are highly malignant tumors due to diffuse infiltration of healthy brain tissue and high mitotic and proliferative activity. They are therefore classified as WHO grade IV tumors. Besides high cellularity, nuclear and cytoplasmic pleomorphism, the presence of microvascular proliferation and central necrosis is essential for the diagnosis. Without effective treatment, these tumors have an average survival time of only a few months that can be extended to about 15 months with the standard of current therapy including surgery, chemotherapy and radiation. Due to the overall poor prognosis, patients have a 2-year survival rate of about 27% (Tonn et al. 2006, Louis 2007, Omuro 2013).

Table 1 gives an overview on classification and grading of the most common glioma entities.

Table 1: Classification and grading of the most common astrocytic gliomas according to the WHO classification of tumors of the central nervous system.
Modified from (Huse et al. 2013, Louis et al. 2007, Riemenschneider & Reifenberger 2009).

Tumor type	WHO grade
Astrocytic gliomas with more circumscribed growth	
Pilocytic astrocytoma	I
Pilomyxoid astrocytoma	II
Pleomorphic xanthoastrocytoma	II
Subependymal giant cell astrocytoma	I
Diffusely infiltrating astrocytic gliomas	
Diffuse astrocytoma	II
Anaplastic astrocytoma	III
Glioblastoma	IV
Giant cell glioblastoma	IV
Gliosarcoma	IV
Mixed gliomas	
Oligoastrocytoma	II
Anaplastic oligoastrocytoma	III

Glioblastomas are deemed to be the most prevalent and also most aggressive primary brain tumors accounting for approximately half of all functional tissue CNS tumor cases and 20% of all intracranial tumors (Ohgaki & Kleihues 2005). It is estimated that approximately 2 - 3 new cases per 100'000 residents occur annually in western countries affecting slightly more

men than women. Glioblastomas may appear at any age, but older people with a peak of incidence between 50 and 70 years are more often afflicted (Tonn et al. 2006).

The majority of glioblastomas develops in the cerebral hemispheres and can spread into the basal ganglia or the contralateral hemisphere. The brain stem is a rare localization in adults but can be particularly found in children. Macroscopically, these tumors present most often as necrotic masses with frequent central hemorrhages that are surrounded by oedematous brain tissue (Tonn et al. 2006) as shown in *Figure 7*.
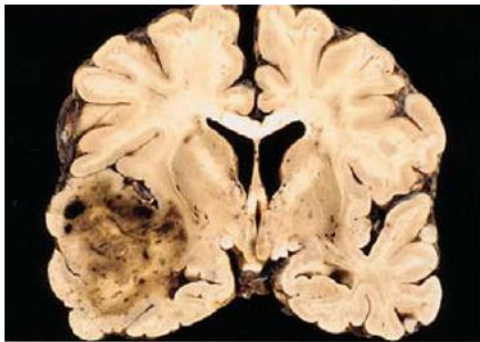
Figure 7: Glioblastoma of the temporal lobe.
A necrotic mass with central hemorrhages can be identified in the temporal lobe. Most likely, macroscopic appearance suggests glioblastoma multiforme.
Taken from (Tonn et al. 2006).

1.2.2 Etiology

Research efforts from many individual groups and more recent data collections from multiinstitutional research networks, like The Cancer Genome Atlas (TCGA) (Brennan et al. 2013), identified several genetic mutations (see *chapter 1.2.4*) and novel aspects on the etiology of glioblastomas. Besides that, genetic syndromes caused by inherited mutations, like Li-Fraumeni syndrome or Neurofibromatosis, are found in about 1% of all glioblastoma patients (Farrell & Plotkin 2007).

Most patients with glioblastomas present with a very short clinical history due to the very fast and spontaneous development of these tumors. Without any evidence of longer precedent malignant progression, these neoplasms are called primary glioblastomas. Opposed to these, cases of secondary glioblastomas are less common and evolve from pre-existing low-grade diffuse or anaplastic astrocytoma. Secondary glioblastomas are more common in younger adults (30-45 years), whereas primary glioblastomas occur mostly in older patients (mean age 55 years) (Kleihues et al. 2002). A morphological differentiation between both entities is not possible because of identical histological features; however, these tumors can be distinguished by their genetic and epigenetic aberrations (Huse et al. 2013). More information on the molecular pathology in glioblastoma can be found in *chapter 1.2.4*.

1.2.3 Symptoms, diagnosis and treatment

Due to the rapid growth of glioblastomas, health complaints usually arise within only a few weeks or months. Most patients primarily suffer from non-specific neurological symptoms like nausea, vomiting and headache which can be accompanied by seizures, memory loss or hemiparesis. However, the array of symptoms produced by these tumors is very diverse and depends highly on their localization. A glioblastoma of the frontal cerebral lobe might lead to personality changes, whereas a tumor next to the optic nerve can cause visual loss. Other locations lead rather to cerebral oedema and increased cerebral pressure which explains the general symptoms listed above (Kleihues et al. 2002).

Malignant cells of glioblastomas carried in the cerebrospinal fluid can result in gliomatosis of the meninges or may spread to the spinal cord. Metastases beyond the central nervous system are extremely unusual but dissemination to regional lymph nodes, lung, pleura, liver and bone has been described in very rare cases (Frappaz et al. 1999, Pasquier et al. 1980).

Nowadays, patients with newly developed unclear neurological symptoms are usually quickly subjected to cranial tomography like magnetic resonance imaging (MRI). Here, glioblastomas normally appear as an intracerebral space-occupying lesion with ring-enhancement due to peripheral vascularization of the mass and a central hypointense area which is corresponding to tumor necrosis. These radiological findings underscore the suspicion of a glioblastoma, however, cerebral abscess or metastasis of another malignant tumor have to be taken into account as differential diagnoses (Smirniotopoulos et al. 2007). A definitive diagnosis of glioblastoma requires a stereotactic biopsy or a craniotomy with tumor resection and pathologic confirmation by an experienced neuropathologist. Lately, diagnostic methods have been extended by more advanced imaging, like measurement of blood perfusion or of tumor metabolite concentration. However, neuropathologic examination remains the gold standard for diagnosis of a glioblastoma (Nikiforova & Hamilton 2011).

The goal of glioblastoma therapy is to slow down the tumor growth and improve the quality of life. All therapy strategies are non-curative interventions but are at most life-prolonging. The standard treatment of glioblastoma is based on three pillars: surgery, radiation and chemotherapy.

Surgical intervention is usually the first step intending to remove as much tumor as possible without destroying any functional brain tissue and thus increasing survival (Lacroix et al.

2001). Normally, the operation is followed by a combined radio- and chemotherapy in which radiation is the mainstay of treatment for glioblastoma. Studies could show that patients who received a radiotherapy had a median survival time of more than double of those who did not (Walker et al. 1978). The chemotherapeutic drug of choice at the moment is temozolomide which seems to sensitize the tumor cells to radiation but also has direct anti-tumorigenic effects itself (Chamberlain et al. 2007). This treatment showed a significant influence as patients receiving radio- and chemotherapy survived 2.5 months longer than a control group with radiation alone, extending the median survival from 12.1 to 14.6 months (Stupp et al. 2005). Besides this, older patients whose tumor tissue exerts *MGMT*-methylation (see *chapter 1.2.4*) are exclusively treated with temozolomide due to the high toxicity of combined chemoradiation. These patients have a higher benefit from temozolomide alone (Malmstrom et al. 2012).

1.2.4 Molecular diagnosis and pathology of gliomas

Molecular markers are gaining more and more importance in neurooncology as histology no longer serves as sole diagnostic tool for correct brain tumor classification (Louis et al. 2016). Additionally, molecular testing attributes to survival prognosis of tumor patients and can give predictive information on response to certain treatments (Dietmaier et al. 2015).

As the schematic representation of molecular markers during pathogenesis of gliomas in *Figure 8* explains, a large number of biological alterations is known in glioblastomas and astrocytic tumors of which the following represent important markers for everyday clinical practice or have been reported to be involved in glioma cell migration and invasion.

The methylation level of the *O6-Methylguanin-DNA-methyltransferase* (*MGMT*)-gene promoter is among the most frequently analyzed molecular markers in human brain tumors (Dietmaier et al. 2015). This gene, located on the chromosomal region 10q26, encodes for a DNA repair gene that removes alkyl groups from the O^6 of guanine (Watanabe et al. 2007) and is hypermethylated in 40% of all glioblastomas. Elevated methylation levels of the *MGMT* promoter predict a better response to treatment with the alkylating chemotherapeutic drug temozolomide which is translating into a prolonged patient survival (Hegi et al. 2005).

Mutations of the substrate binding domain of the *isocitrate dehydrogenase* (*IDH*) *1* gene and its homologue *IDH2* display another biological marker analyzed frequently that allows to differentiate between several low-grade astrocytomas. For example, approximately 70% of

diffuse astrocytomas show a mutation of amino acid 132 in the *IDH1* gene whereas pilocytic astrocytomas express mainly wildtype *IDH1*. Furthermore, 90% of all secondary glioblastomas, opposed to primary glioblastomas, are also tested positive for this mutation as they most often develop from these precursor lesions (Dietmaier et al. 2015, Yan et al. 2009). Besides *MGMT* promoter methylation and *IDH1/2* methylation, complete loss of the long arm of chromosome 1 and the short arm of chromosome 19 (1p/19q deletion) is an entity-defining alteration in oligodendroglial tumors and may guide to consideration of oligodendroglial differentiation in diagnosis of oligoastrocytomas (Louis et al. 2016). Additionally, detection of 1p19q deletion predicts favorable prognosis for tumors with oligodendroglial features and responsiveness to polychemotherapy with procarbazine, lomustine and vincristine (Cahill et al. 2015, Cairncross et al. 2006, Dietmaier et al. 2015, Riemenschneider et al. 2013).

Apart from these biochemical markers analyzed with regard to diagnosis of brain tumors, gliomas show multiple genetic alterations like mutation of the epidermal growth factor receptor (EGFR), of the tumor suppressor protein p53 or of PI3 kinase pathway genes. These markers are less applicable for molecular diagnosis as usually no information on prognosis or response to treatment is gained due to their identification (Ceccarelli et al. 2016, Huse et al. 2013, Riemenschneider & Reifenberger 2009).

Numerous studies have shown that the EGFR is not only frequently amplified or overexpressed in glioblastomas but also in multiple other cancers. Very often, a truncated EGFR protein which forms a constitutively active mutant called EGFR variant III (EGFRvIII) is present in these tumor cells (Libermann et al. 1985, Schlegel et al. 1994, Sugawa et al. 1990). With regards to gliomas, a positive correlation between EGFR overexpression and enhanced invasiveness of tumor cells (Lund-Johansen et al. 1990) as well as promotion of glioblastoma cell migration and tumor growth by the epidermal growth factor (EGF), a ligand of the EGFR (Tysnes et al. 1997), was reported.

The p53 protein is among the best known of all tumor suppressors and – when mutated – is capable of promoting migration and invasion, as well as inhibiting cellular aging and apoptosis in various human cancers (Muller et al. 2011). It was recently shown that p53 has a crucial role in gliomagenesis by inducing accumulation of cooperative oncogenic alterations (Wang et al. 2009). It is therefore reasonable that mutations of p53 are frequently found and can be similarly observed in lower grade malignant gliomas like diffuse astrocytoma as well as in secondary glioblastomas (Ohgaki et al. 2004).

Besides EGFR and p53 mutations, oncogenes of the PI3 kinase pathway play a crucial role in development of glioblastomas. PI3 kinases are involved in many cellular functions such as

cell growth, differentiation, motility and survival and are hence capable of promoting tumorigenesis when misregulated. Additionally, the phosphatase and tensin homologue (PTEN), an antagonist of the PI3 kinase pathway, is absent in up to 30% of all primary glioblastomas (Bleeker et al. 2014, Huse et al. 2013, Riemenschneider & Reifenberger 2009). An overview on known molecular alterations that are frequently found in astrocytic gliomas is given in *Figure 8*. Some of the genetic mutations listed below have been explained in greater detail in this chapter. Additionally, a distinction is made between alterations that are preferentially found in primary glioblastomas on the one hand and secondary glioblastomas on the other.
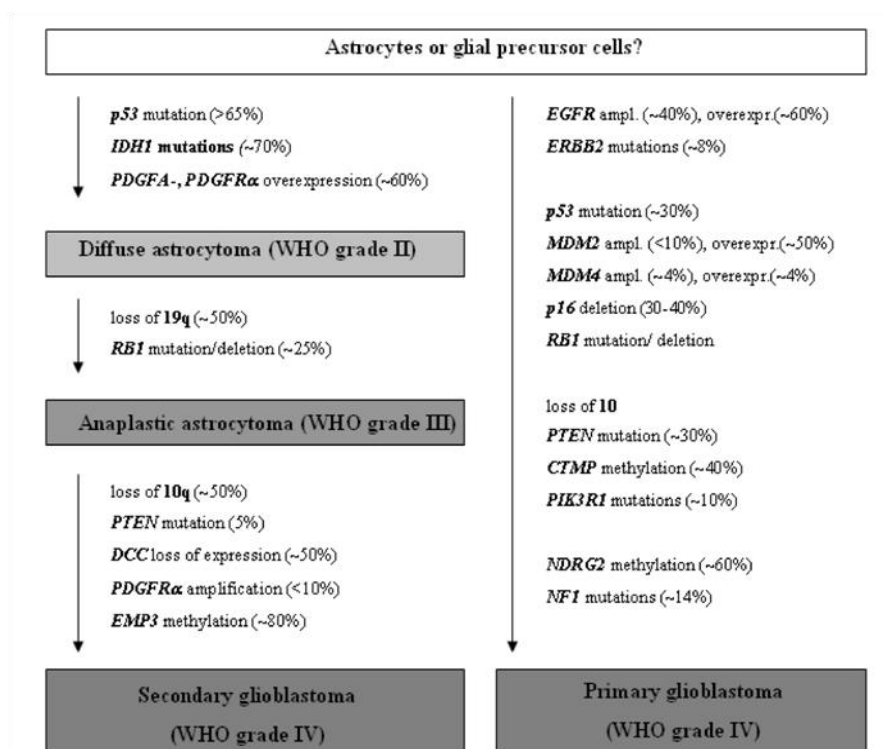
Figure 8: Schematic representation of the molecular pathogenesis and progression of astrocytic gliomas. Note that a distinction between genetic mutations that are preferentially found in primary or secondary glioblastomas can be made. Taken from (Riemenschneider & Reifenberger 2009).

1.3 Reelin/DAB1 signaling in glioblastoma

As explained extensively in *chapter 1.1.4*, *Reelin/DAB1* signaling has an important effect on non-brain tumors suggesting a tumor supressive function in several cancers like hepatocellular carcinoma, breast cancer, esophageal cancer or pancreatic cancer (Okamura et al. 2011, Sato et al. 2006, Stein et al. 2010, Yuan et al. 2012). Although *Reelin* acts particularly during development of the central nervous system, none of these studies have

ever examined the influence of *Reelin* and members of its canonical signaling on gliomas so far.

Previous work of our laboratory supports the hypothesis of *Reelin* being a tumor suppressor, as promising data on the methylation status of the *RELN* promoter and mRNA levels of *Reelin* and *DAB1* in glioblastoma and astrocytic tumors was raised. Furthermore, an influence of *Reelin/DAB1* signaling on the proliferation of glioblastoma cells could be proved. The following chapters are briefly summarizing these findings.

1.3.1   RELN promoter hypermethylation

Real-time PCR analysis of mRNA levels of *Reelin* and *DAB1* revealed that these proteins show reduced expression in multiple tested astrocytic tumor samples. Furthermore, downregulation of *Reelin* and *DAB1* correlates with higher grade of malignancy, whereas at the same time, the *Reelin* receptors VLDLR and ApoER2 are upregulated with increasing WHO grade (Violonchi 2009). Survival analysis of data of the Rembrandt and The Cancer Genome Atlas (TCGA) databases reinforced these findings (data raised by Dr. Markus Schulze). As a reason for the reduced expression of *Reelin*, a hypermethylation pattern of the *RELN* promoter sequence was found via bisulfite conversion which is seen particularly often in glioblastomas. Treatment of these tumors with demethylating agents led to strong reexpression of *Reelin* mRNA compared to untreated controls (Violonchi 2009).

1.3.2   DAB1 induced proliferation block

Not only the genomic analysis of *RELN* in glioblastoma cells, but also cell biological testing of cell growth had revealed promising results proposing *Reelin/DAB1* signaling as an important tumor suppressor pathway. A proliferation assay in U87 and U251 cells stably overexpressing the downstream target *DAB1* showed that *Reelin* is significantly inhibiting cell division in a *DAB1*-dependent fashion compared to control cells with only very low endogenous *DAB1* expression or cells expressing the 5F *DAB1* mutant (data raised by Dr. Markus Schulze).

1.4 Aims of this study

As a basis for this doctoral thesis, preliminary findings of our laboratory revealed that *Reelin/DAB1* signaling is associated with the grade of malignancy in glioblastomas and generated the hypothesis that *Reelin* acts as a tumor suppressor in astrocytic tumors. A crucial characteristic for highly malignant cancers is increased cell motility and diffuse infiltration of healthy tissue. It is also known that these cell processes can be influenced by *Reelin/DAB1* signaling. In order to follow up on this hypothesis, the research for this doctoral thesis aimed at analyzing the effects of the *Reelin/DAB1* signaling pathway on the migrational and invasive phenotype of glioblastoma cells.

To investigate on the overall role of *Reelin* on these cellular functions and to distinguish between *DAB1*-dependent and -independent effects a unique set of experiments was performed:

- The preceding chapters already displayed that *Reelin* and *DAB1* are regulators of neuronal migration, thus the main part of my research focused on glioblastoma migration and the contribution of the canonical *Reelin* signaling axis. Therefore, a live imaging based assay to observe 2D cell migration on fibronectin and laminin was used to examine the influences of *Reelin* and the involvement of integrin binding in motility of glioblastoma cells.

- To pursue the findings obtained in the migration assay, these experiments were extended through an invasion assay. *Reelin* has already been described as an inhibitor of diffuse tumor infiltration in multiple other cancers. Therefore, we sought to examine the influences of *Reelin/DAB1* signaling in a classical invasion assay. The invasive behavior of the same set of cells as in the migration assay was observed on matrigel, a protein mixture which resembles complex extracellular matrix found in many tissues.

- Cell lines that show a migratory phenotype often exhibit altered regulation of the actin cytoskeleton. As the assay for migration delivered promising results, immunocytochemistry of filamentous actin and of the actin reorganizing protein phospho-cofilin was performed to examine morphological changes like formation of stress fibers or cell membrane ruffling under *Reelin* stimulation.

- Only little information on downstream targets of *Reelin/DAB1* signaling in cancers is available. For further investigation on these molecular mechanisms, protein analysis of

multiple known and potential members of this signaling cascade was performed using the standard western blotting technique. Amongst others, the phosphorylation levels under *Reelin* stimulation of the following proteins were analyzed:

- Focal adhesion kinase (FAK), a regulator of cell-matrix junctions,
- Total phospho-tyrosine levels via the antibody 4G10,
- Kip1/p27, a CDK inhibitor,
- STAT3, an activator of transcription and
- Cofilin, a reorganizing protein of the cytoskeleton.

The experiments of this study were chosen to contribute to a deeper understanding of the role of *Reelin/DAB1* signaling in astrocytic tumor pathogenesis and pathology. The results of this doctoral thesis on migration and invasion of glioblastoma are hopefully one day conducive to an effective anti-invasive therapy of brain tumors.

2 Materials

2.1 Chemicals

Chemical	Manufacturer
4-(2-hydroxyethyl)-1-piperazineethanesulfonic acid (HEPES)	Roth
4',6-diamidino-2-phenylindole (DAPI)	Sigma-Aldrich
Ammonium persulfate (APS)	Roth
Bovine serum albumin	Applichem
Calcium chloride ($CaCl_2$)	Roth
Dimethylsulfoxide (DMSO)	Roth
Ethanol 100%	Roth
Ethanol 70%	Fischar
Ethylenediaminetetraacetic acid (EDTA)	Roth
Glycerol	Roth
Glycine	Roth
Hydrochloric acid (HCl)	Roth
Hydrogen peroxide (H_2O_2)	Sigma-Aldrich
Igepal	Fluka
Isopropanol	Merck
Magnesium chloride (MgCl2)	Roth
Manganese (II) chloride (MnCl2)	Roth
Methanol Rotipuran 99.9%	Roth
Nonfat dry milk powder	Roth
Normal goat serum	PAN™-Biotech
Paraformaldehyde (PFA)	Sigma-Aldrich
Phosphatase Inhibitor Cocktail	Roche
Phos-tag™	Wako Pure Chemical Industries
Ponceau S Solution	Sigma Life Science
Potassium chloride (KCl)	Roth
Protease Inhibitor Cocktail	Roche
RNAse free water	Roth

Rotiphorese® Gel 30 (37.5:1) Acrylamide 30%	Roth
Saponin	Sigma Life Science
Sodium azide (NaN$_3$)	Roth
Sodium chloride (NaCl)	Roth
Sodium deoxycholate	Roth
Sodium dodecyl sulfate (SDS)	Roth
Sodium hydroxide (NaOH)	Roth
SYBR Green 2x SensiFAST SYBR Green	Bioline
Tetramethylethylenediamine (TEMED)	Roth
TrisBase Trizma® base	SAFC®
Tris-HCl	Roth
Triton X-100	Roth
Tween-20	Sigma-Aldrich
β-mercaptoethanol	Roth

2.2   Cell culture reagents

Reagent	Manufacturer
CO$_2$-Independent Medium	gibco® life technologies
Dulbecco´s modified Eagle´s medium 4.5 g/l glucose	Sigma Life Science
Dulbecco´s modified Eagle´s medium w/o phenolred 4.5 g/l glucose	Sigma Life Science
Dulbecco´s phosphate buffered saline	Sigma Life Science
Fetal calf serum	PAN™-Biotech
Fibronectin, human	Sigma Aldrich
Geneticindisulfate (G418) 50.0 mg/ml	Calbiochem® Millipore
Hank's balanced salt solution	Sigma Life Science
Laminin, human	Sigma Aldrich
L-glutamine	gibco® life technologies
Penicillin / streptomycin	gibco® life technologies
Poly-L-lysine 0.01% solution	Sigma Life Science
Trypsin / EDTA	Sigma Life Science

2.3   Cell culture materials

Material	Manufacturer
µ-Slide 8 well ibiTreat	ibidi®
24 well plate	Corning Life Sciences
Cell culture flasks 75 cm^2	CellStar® Breiner Bio-One
Control inserts 8.0 Micron	Corning BioCoat™
Cryo Pure Tube 1.6ml	Sarstedt
Falcon tube 15 ml	Sarstedt
Falcon tube 50 ml	Sarstedt
Growth Factor Reduced Corning® Matrigel® Invasion Chamber 8.0 Micron	Corning BioCoat™
Lab-Tek II Chamber Slide 8 well	LAB-TEK® Thermo Fisher Scientific
Plastic pipettes 5 ml, 10 ml, 25 ml, 50 ml	Sarstedt
Tissue culture dishes Ø 15, 30 and 100 mm	Sarstedt

2.4   Primers

All primers used for this doctoral thesis were obtained by Eurofins MWG/Eurofins Genomics, Ebersberg, Germany. Detailed information will be listed in the corresponding chapter (see *chapter 3.2.3*).

2.5   Antibodies for western blotting

2.5.1   Primary antibodies

Antibody	Target species	Host	Dilution	Manufacturer
4G10	all	mouse	1:1000	Millipore
Cofilin	human	rabbit	1:1000	Cell Signaling
P-DAB1 (Tyr220)	human	rabbit	1:1000	Cell Signaling
P-FAK (Tyr297)	human/mouse	rabbit	1:1000	Invitrogen
P-Kip1/P-p27 (Thr198)	human	rabbit	1:1000	R&D
P-STAT3 (S727)	human	rabbit	1:1000	Cell Signaling

Total DAB1	human/mouse	rabbit	1:1000	Cell Signaling	
Total Kip1/p27	human	rabbit	1:1000	Cell Signaling	
Total STAT3	human/mouse	mouse	1:1000	Cell Signaling	
Tubulin (Clone DM1A)	human/mouse	mouse	1:10.000	Sigma-Aldrich	

2.5.2   Secondary antibodies

Antibody	Conjugat	Dilution	Manufacturer
Goat anti-mouse IgG	HRP	1:10.000	Santa Cruz Biotechnology
Goat anti-rabbit IgG	HRP	1:10.000	Santa Cruz Biotechnology

2.6   Antibodies and dyes for immunocytochemistry

Antibody/dye	Target/target species	Raised in	Conjugate	Dilution	Manufacturer
4',6-diamidino-2-phenylindole (DAPI)	DNA	-	-	2µg/ml	Sigma-Aldrich
AlexaFluor® 555 phalloidin	Filamentous actin	-	AlexaFluor® 555	1:50	Invitrogen/Life Technologies
Primary antibody: P-Cofilin	mouse/ human/ rat cofilin	rabbit	-	1:50	Cell Signaling
Secondary antibody: Flourescein goat anti-rabbit IgG	-	goat	FITC	1:200	Invitrogen/Life Technologies

2.7   Cell lines

2.7.1   HEK 293T cells

For the stimulation of classical glioblastoma cells, mouse *Reelin* (mRELN) that was produced by stably transfected HEK 293T cells was used. These cells, originally obtained by ATCC® (American Type Culture Collection), express *Reelin* from the vector pcDNA3 that comprises the complete open reading frame (ORF) of the mRELN gene (D'Arcangelo et al. 1997). As a control, cells that had been stably transfected with a vector encoding for the *green fluorescent protein* (GFP) were used. HEK 293T cells containing the *Reelin* vector, as well as cells transfected with the GFP vector were kindly provided by Prof. Dr. rer. nat. Eckart Förster (Institut für Neuroanatomie, Universitätsklinikum Hamburg-Eppendorf).

2.7.2   Human glioblastoma cells

2.7.2.1   *U87 and U251 glioblastoma cell lines*

For the experiments, the classical glioblastoma cell lines U87 and U251, originally obtained by ATCC®, were modified by transfection to fit the particular needs of research on *Reelin/DAB1* signaling. Both the U87 and the U251 cell line are classified as WHO grade IV astrocytomas with epithelial morphology. U87 cells were collected from a 44 year old male Caucasian, whilst U251 cells are derived from a 75 year old male Caucasian patient. Both patients were diagnosed with primary glioblastoma.

2.7.2.2   *Constructs used for stable cell lines*

In total, three types of stably transfected cells were established for the experiments using the pIRESneo2 vector by Clontech which is depicted in *Figure 9*.
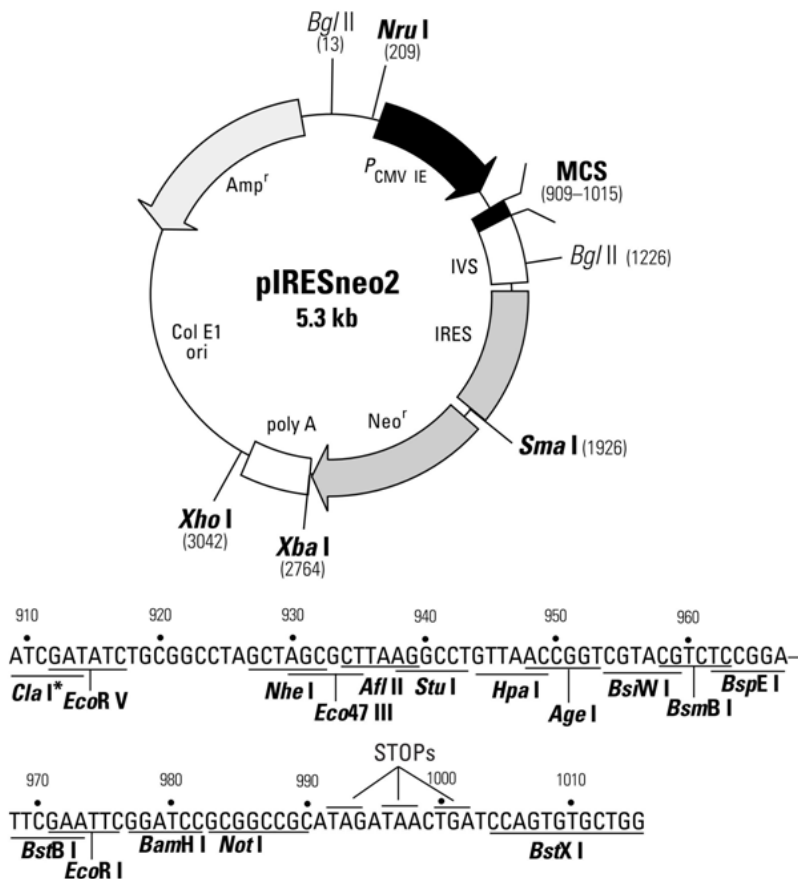
Figure 9: Restriction Map and Multiple Cloning Site of the pIRESneo2 vector by Clontech.
Wildtype *DAB1* or the 5F mutant gene have been cloned into this plasmid using the restriction sites
Nhe I and *Not I*. Taken from (Masonoda) .

First, as a control, cells were transfected with the empty pIRESneo2 vector (EV). Secondly, to analyze the effects of *DAB1* overexpression in U87 and U251 cells, the human *DAB1* gene was cloned into this vector with the restriction enzymes *Nhe I* and *Not I* (DAB1). Finally, as an additional control to investigate on *DAB1*-independent *Reelin* effects, cells that stably express the 5F mutant of *DAB1* were created (5F). This mutant was established by replacing the 5' end of human *DAB1* with the construct of a murine 5F mutant that was kindly provided by Jonathan A. Cooper (Fred Hutchinson Cancer Research Center, Seattle). Therefore, the restriction site *Afl III* was used. As the preceding amino-acid sequence until *Afl III* is completely conserved in murine and human *DAB1*, the resulting construct is encoding for a human 5F mutant protein as the amino-acid alignment (see *Figure 10*) proves. In total, three different stably transfected cell lines were generated from each classical glioblastoma cell line: the empty vector cells (hereafter named U87/U251 EV), cells with *DAB1* overexpression (hereafter named U87/U251 DAB1) and cells expressing the 5F *DAB1* mutant (hereafter named U87/U251 5F).

```
DAB1   1    MSTETELQVAVKTSAKKDSRKKGQDRSEATLIKRFKGEGVRYKAKLIGIDEVSAARGDKL   60
            MSTETELQVAVKTSAKKDSRKKGQDRSEATLIKRFKGEGVRYKAKLIGIDEVSAARGDKL
5F     1    MSTETELQVAVKTSAKKDSRKKGQDRSEATLIKRFKGEGVRYKAKLIGIDEVSAARGDKL   60

Query  61   CQDSMMKLKGVVAGARSKGEHKQKIFLTISFGGIKIFDEKTGALQHHHAVHEISYIAKDI   120
            CQDSMMKLKGVVAGARSKGEHKQKIFLTISFGGIKIFDEKTGALQHHHAVHEISYIAKDI
Sbjct  61   CQDSMMKLKGVVAGARSKGEHKQKIFLTISFGGIKIFDEKTGALQHHHAVHEISYIAKDI   120

Query  121  TDHRAFGYVCGKEGNHRFVAIKTAQAAEPVILDLRDLFQLIYELKQREELEKKAQKDKQC   180
            TDHRAFGYVCGKEGNHRFVAIKTAQAAEPVILDLRDLFQLIYELKQREELEKKAQKDKQC
Sbjct  121  TDHRAFGYVCGKEGNHRFVAIKTAQAAEPVILDLRDLFQLIYELKQREELEKKAQKDKQC   180

Query  181  EQAVYQTILEEDVEDPVYQYIVFEAGHEPIRDPETEENIYQVPTSQKKEGVYDVPKSQPV   240
            EQAV+QTILEEDVEDPV+Q+IVFEAGHEPIRDPETEENI+QVPTSQKKEGV+DVPKSQPV
Sbjct  181  EQAVFQTILEEDVEDPVFQFIVFEAGHEPIRDPETEENIFQVPTSQKKEGVFDVPKSQPV   240

Query  241  SAVTQLELFGDMSTPPDITSPPTPATPGDAFIPSSSQTLPASADVFSSVPFGTAAVPSGY   300
            SAVTQLELFGDMSTPPDITSPPTPATPGDAFIPSSSQTLPASADVFSSVPFGTAAVPSGY
Sbjct  241  SAVTQLELFGDMSTPPDITSPPTPATPGDAFIPSSSQTLPASADVFSSVPFGTAAVPSGY   300

Query  301  VAMGAVLPSFWGQQPLVQQQMVMGAQPPVAQVMPGAQPIAWGQPGLFPATQQPWPTVAGQ   360
            VAMGAVLPSFWGQQPLVQQQMVMGAQPPVAQVMPGAQPIAWGQPGLFPATQQPWPTVAGQ
Sbjct  301  VAMGAVLPSFWGQQPLVQQQMVMGAQPPVAQVMPGAQPIAWGQPGLFPATQQPWPTVAGQ   360

Query  361  FPPAAFMPTQTVMPLPAAMFQGPLTPLATVPGTSDSTRSSPQTDKPRQKMGKETFKDFQM   420
            FPPAAFMPTQTVMPLPAAMFQGPLTPLATVPGTSDSTRSSPQTDKPRQKMGKETFKDFQM
Sbjct  361  FPPAAFMPTQTVMPLPAAMFQGPLTPLATVPGTSDSTRSSPQTDKPRQKMGKETFKDFQM   420

Query  421  AQPPPVPSRKPDQPSLTCTSEAFSSYFNKVGVAQDTDDCDDFDISQLNLTPVTSTTPSTN   480
            AQPPPVPSRKPDQPSLTCTSEAFSSYFNKVGVAQDTDDCDDFDISQLNLTPVTSTTPSTN
Sbjct  421  AQPPPVPSRKPDQPSLTCTSEAFSSYFNKVGVAQDTDDCDDFDISQLNLTPVTSTTPSTN   480

Query  481  SPPTPAPRQSSPSKSSASHASDPTTDDIFEEGFESPSKSEEQEAPDGSQASSNSDPFGEP   540
            SPPTPAPRQSSPSKSSASHASDPTTDDIFEEGFESPSKSEEQEAPDGSQASSNSDPFGEP
Sbjct  481  SPPTPAPRQSSPSKSSASHASDPTTDDIFEEGFESPSKSEEQEAPDGSQASSNSDPFGEP   540

Query  541  SGEPSGDNISPQAGS   555
            SGEPSGDNISPQAGS
Sbjct  541  SGEPSGDNISPQAGS   555
```

Figure 10: Protein sequence alignment of wildtype DAB1 (Query) and 5F mutant (Sbjct).
The five tyrosines (Y) which are changed into phenylalanine (F) in the 5F mutant are highlighted yellow.
Kindly provided by Markus Schulze.

2.7.2.3 Establishment of stable cell lines

Transfection of the cells was performed according to the following protocol:

First, 8×10^5 cells were precultured in complete Dulbecco´s modified Eagle´s medium (cDMEM) (see *chapter 2.12.1*) into Ø 100 mm culture dishes for 24 h and then incubated with 12 ml of prewarmed Opti-MEM. Then a mix of 250 µl of Opti-MEM and 1.5 µg of the indicated RNA or DNA concentration, as well as a mix of 250 µl of Opti-MEM and 12 µl of the transfection reagent Lipofectamine 2000, was prepared and kept for 5' at room temperature (RT) in polystyrene tubes. Afterwards, these solutions were mixed and incubated for another 20' in order to achieve formation of transfection complexes. This mixture was applied to the cultured cells in a dropwise fashion and then incubated for 4 hours. Finally, the Opti-MEM medium containing the transfection complexes was exchanged by complete

medium. For the establishment of stably transfected cells the antibiotic G418 was added to the complete medium in a concentration of 0.2 mg/ml for U87 respectively 0.4 mg/ml for U251 after 24 hours and the cells were cultured for another two weeks until resistant and stably proliferating cells emerged. Only transfected cells containing the G418 resistance gene and therefore also a transfection vector are able to survive this selection pressure.

The transfected cells for this research were kindly provided by Dr. Markus Schulze of the Department for Neuropathology, Universität Regensburg.

2.8   Devices

Device	Manufacturer	Application
AF-6000 LX Life Cell Imaging System	Leica Microsystems	Live cell imaging/high magnification images
Balance PBJ6200-2M	Kern	Buffer preparation
BX61 microscope	Olympus	Quantitative immunocytochemistry
Casting Stand	Bio-Rad	SDS-PAGE gel casting
Fastblot B44	Biometra	SDS-PAGE gel blotting
FE20 – FiveEasy™	Mettler Toledo	pH measurement
Heracell™	Heraeus	CO_2 incubator
Heracell™ 240i	Thermo Scientific	CO_2 incubator
HERAsafe laminar flow	Heraeus	Cell culture
HERAsafe laminar flow	Thermo Scientific	Cell culture
ImageQuant LAS 4000 mini	GE Healthcare Life Sciences	Processing of western blots
IX81 microscope	Olympus	Image acquisition for transwell assay
MIKRO 200R	Hettich Zentrifugen	Sample centrifugation
Mini Protean® Tetra System	Bio-Rad	SDS gel electrophoresis
NanoDrop2000	Thermo Scientific/peqlab	Measurement of DNA/RNA concentrations
PowerPac™ Basic (300 V, 400 mA, 75 W)	Bio-Rad	Power supply
Rotina 420R	Hettich Zentrifugen	Sample centrifugation
Schüttelmaschine LS10	gerhardt	Shaking of western blot membranes
SHAKER DOS-10L	neoLAB®	Shaking of western blot membranes

StepOnePlus	Applied Biosystems	Real-time PCR
T3000	Biometra	Thermocycler
Thermomixer® compact	eppendorf	Sample preparation

2.9   Software

Software	Manufacturer	Application
Cell^P	Olympus	Quantitative immunocytochemistry
CellProfiler 2.1.1	Broad Institute Imaging Platform	Cell image analysis of Actin / P-Cofilin stainings
CellSens Dimension 1.9	Olympus	Image acquisition for transwell assay
Chemotaxis and Migration Tool V2.0	ibidi®	Tracking of cell migration
Excel 2007	Microsoft Office	Data analysis
GraphPad Prism 4	GraphPad Software	Statistical analysis
Image Quant TL 8.1	GE Healthcare Life Sciences	Quantification of western blotting
ImageJ 1.48v	NIH Image	Quantification of cell invasion
Leica Application Suite LAS X 1.x	Leica Microsystems	Live cell imaging/high magnification images

2.10   Kits

Kit	Manufacturer
RNeasy Mini Kit	Qiagen
SuperScript™ II Reverse Transcriptase	Invitrogen/life technologies
SuperSignal West Pico Substrate	Thermo Fisher Scientific
SuperSignal West Femto Maximum Sensitivity Substrate	Thermo Fisher Scientific

2.11   Other materials

Material	Manufacturer
Bottle-Top Vacuum Filter Systems	Corning®
Chemical pipettes 0.5-10, 2-20, 20-200, 100-1000 µl	eppendorf
Chemical pipettes 1-10, 2-20, 20-100, 50-200, 200-1000 µl	Gilson
Cover slips 18x18 mm, 24x50 mm	Roth
Disposable Scalpel No. 10	Feather
Fluoromount-G	SouthernBiotech
MagicMark[TM] Western Protein Standard (20-220 kDa)	Life Technologies
Microscope slides	Marienfeld
Needle 20G x 1.5''	Becton Dickinson
SafeSeal microtubes 0.5 ml, 1.5 ml, 2 ml	Sarstedt
Syringe 1 ml	Becton Dickinson

2.12   Solutions, buffers and media

2.12.1   Cell culture

Solutions, buffers, media	Composition	
Complete medium for HEK293T	In DMEM 4.5 g/l glucose	
	Fetal calf serum	10% (v/v)
	L-glutamine	2 mM
	Penicillin	100 U/ml
	Streptomycin	100 µg/ml
Complete medium for U87	In DMEM 4.5 g/l glucose	
	Fetal calf serum	10% (v/v)
	L-glutamine	2 mM
	Penicillin	100 U/ml
	Streptomycin	100 µg/ml
	G418	0.2 mg/ml
Complete medium for U251	In DMEM 4.5 g/l glucose	
	Fetal calf serum	10% (v/v)
	L-glutamine	2 mM

	Penicillin	100 U/ml
	Streptomycin	100 μg/ml
	G418	0.4 mg/ml
Freezing medium	In fetal calf serum	
	DMSO	15% (v/v)
Blocking buffer for plate coating	In PBS	
	Bovine serum albumin (BSA)	0.5% (v/v)

2.12.2 Western blotting

Solutions, buffers, media	Composition (in dH$_2$O, unless mentioned otherwise)	
Radio Immuno Precipitation Assay buffer (RIPA) lysis buffer	Sodium chloride	150 mM
	Triton X-100	1.0% (v/v)
	Sodium deoxycholate	0.5% (w/v)
	SDS	0.1% (w/v)
	Tris base, pH 8.0	50 mM
Running gel (lower gel) buffer	Tris base	1.5 M
	adjust pH to 8.8	
	SDS	0.4%
Stacking Gel (upper gel) buffer	Tris base	0.5 M
	adjust pH to 6.8	
	SDS	0.4%
10 x Running buffer SDS Gels	Tris base	150 mM
	Glycine	2 M
	SDS	1%
Blotto buffer	Non fat dry milk	5.0% (w/v)
	Tris-HCl pH = 8,0	50.0 mM
	NaCl	80.0 mM
	CaCl$_2$	2.0 mM
	NP-40	0.2% (v/v)
Antibody dilution buffer	BSA	1.0% (w/v)
	HEPES	10.0 mM
	NaCl	0.5 M
	NaN$_3$	0.02% (w/v)
	Tween-20	0.2% (v/v)

10x TBS (concentrated Tris-buffered Saline)	Tris base	0.2 M
	NaCl in dH$_2$O	1.5 M
	adjust pH to 7.6 with 12N HCl	
TBS-T	In 1x TBS	
	Tween-20	0.05% (v/v)
Anode I buffer	Tris base	0.3 M
	Methanol	20% (v/v)
Anode II buffer	Tris base	25.0 mM
	Methanol	20% (v/v)
Cathode buffer	Tris base	25.0 mM
	Glycine	40.0 mM
	Methanol	10% (v/v)
	SDS	0.005% (w/v)
10x Towbin buffer	Tris base	250 mM
	Glycine	2 M
1x Towbin buffer	dH$_2$O	700 ml
	10x Towbin buffer	100 ml
	Methanol	200 ml
Phos-tag^{TM} solution D	in dH2O containing 3% methanol (v/v)	
	Phos-tag^{TM}	5 mM
Phos-tag^{TM} solution E	MnCl$_2$	10 mM
4x Laemmli buffer	SDS	8% (w/v)
	β-mercaptoethanol	10% (v/v)
	Glycerol	20% (v/v)
	Bromophenol blue	0.004% (w/v)
	Tris-HCl	0.125 M
	adjust pH to 6.8	
SuperSignal West Pico Substrate	Luminol/Enhancer	2.5 ml
	Stable Peroxide buffer	2.5 ml
SuperSignal West Femto Maximum Sensitivity Substrate	Luminol/Enhancer	2.5 ml
	Stable Peroxide buffer	2.5 ml

2.12.3 2D migration assay

Solutions, buffers, media	Composition	
Complete CO$_2$ independent medium	In CO$_2$ independent Medium	
	Fetal calf serum	5% (v/v)
	L-glutamine	2 mM
	Penicillin	100 U/ml
	Streptomycin	100 μg/ml

2.12.4 Transwell invasion assay

Solutions, buffers, media	Composition	
Paraformaldehyde	In PBS	
	Paraformaldehyde	4% (w/v)
	adjust pH to 7.2	
Complete medium 10% FCS	In DMEM w/o phenolred 4.5 g/l glucose	
	Fetal calf serum	10% (v/v)
	L-glutamine	2 mM
	Penicillin	100 U/ml
	Streptomycin	100 μg/ml
Complete medium 0.5% FCS	In DMEM w/o phenolred 4.5 g/l glucose	
	Fetal calf serum	0.5% (v/v)
	L-glutamine	2 mM
	Penicillin	100 U/ml
	Streptomycin	100 μg/ml

2.12.5 Immunocytochemistry

Solutions, buffers, media	Composition (in PBS, unless mentioned otherwise)	
Complete medium 5% FCS	In DMEM 4.5 g/l glucose	
	Fetal calf serum	5% (v/v)
	L-glutamine	2 mM
	Penicillin	100 U/ml
	Streptomycin	100 μg/ml

Blocking buffer	Normal goat serum	5% (v/v)
	Saponin	0.3% (w/v)
Antibody dilution buffer	Normal goat serum	1.0% (v/v)
	Saponin	0.3% (w/v)
Washing buffer	Saponin	0.3% (w/v)

3 Methods

3.1 Cell biological methods

3.1.1 Cell lines and cell culture conditions

All cells were cultured with sterile equipment and all working steps were performed under a laminar airflow bench. HEK 293T cells, as well as the two glioblastoma cell lines U87 and U251 were cultured in complete DMEM (see *chapter 2.12.1*), in a humidified atmosphere at 37°C and 5% CO_2. Additionally, the medium for the transfected U87 and U251 cell lines contained 0.2 mg/ml respectively 0.4 mg/ml G418.

3.1.1.1 Cell passaging

Cells were cultured to a confluency of 80 - 90% and then splitted. For this purpose, their medium was aspirated and the adherent cells were washed with 5 ml of PBS. After that, 3 ml of trypsin/EDTA were added and 2.5 ml reaspirated leaving the cells covered with 0.5ml of trypsin/EDTA. The cells were allowed to detach for 3' at 37°C and were subsequently resuspended in 9.5 ml complete medium. For a 1:10 dilution, 1 ml of this cell suspension was plated onto a new culture dish. The total volume in the 75 cm^2 culture flask and the Ø 100 mm culture dish was 12.5 ml.

3.1.1.2 Freezing cells

For purposes of long term storage, cells were cryoconserved. Therefore, cells were grown to 80% confluency on 75 cm^2 culture flasks and harvested by trypsinization according to *chapter 3.1.1.1*. Then, the cells were resuspended in 5 ml of complete medium and collected by centrifugation for 5' at 99 x *g*. The cell pellet was resuspended in complete medium containing FCS 20% (v/v) and DMSO 10% (v/v), immediately transferred into a cryo tube and put on ice. Finally, the cells were stored at -80°C overnight and then transferred into liquid nitrogen on the next day.

3.1.1.3 *Thawing cells*

For rethawing, the cells were thawn in a waterbath at 37°C, until only a small ice crystal was left in the cryo tube. The cell suspension from the cryo tube was mixed with 5 ml of complete medium in a 15 ml falcon tube and then the cells were collected by centrifugation at 99 x *g* for 5'. The cells were resuspended in 3 ml of complete medium and then plated on to a 75 cm^2 culture flask in a total volume of 12.5 ml.

3.1.2 Plate coating

For immunocytochemistry and analysis of cell migration, plates were protein-coated to simulate an extracellular matrix. Plate coating was performed in μ-Slide 8 wells ibiTreat and Lab-Tek II Chamber Slide 8 wells. Therefore, these slides were washed with sterile H_2O and then coated with 5 μg/ml fibronectin diluted in PBS or 2 μg/ml laminin diluted in Hank's Buffered salt solution (HBSS) for 60 minutes at RT. Afterwards, the coating solution was removed and the slides were washed with 300 μl of sterile H_2O. The laminin coated plates were allowed to dry for 45' in between at RT. Finally, the plates were incubated with PBS containing 0.5% bovine serum albumin (BSA) for 30' to block uncoated binding sites of the plates and then washed with sterile H_2O again.

Coated plates were stored under sterile conditions at 4°C.

3.1.3 Preparation of Reelin/GFP conditioned medium

For most of the experiments mentioned below, the U87 and U251 cells were stimulated by a conditioned medium that was produced by HEK 293T cells synthesizing either the extracellular protein *Reelin* or the *green fluorescent protein* (GFP) as a control.

For 2D migration assays, 2 x 10^6 HEK 293T cells expressing *Reelin* or GFP were seeded three days prior to the experiment in complete DMEM and incubated overnight in a humidified atmosphere at 37°C and 5% CO_2. The next day, the medium was replaced by complete CO_2 independent medium and cells were incubated for another 48h. On the day of the assay, the supernatant was collected and centrifuged at about 200 x *g* for 4' to remove remaining HEK cells. Then 9 ml of this conditioned medium were collected and used for the assay.

For 3D invasion assays, complete medium 10% FCS w/o phenolred (see *chapter 2.12.4*) was applied instead of the complete CO_2 independent medium. For immunochemistry, complete medium 5% FCS (see *chapter 2.12.5*) was used.

3.2 Molecular biological methods

3.2.1 RNA isolation

To examine the expression of specific genes via polymerase chain reaction (PCR), it is necessary to isolate RNA from the cells that shall be analyzed. Total RNA was isolated using the RNeasy Mini Kit according to the manufacturer's protocol. Therefore an amount of approximately 5 x 10^6 cells was harvested from a plate and lysed in 600 µl of the delivered RLT buffer supplemented with β-mercaptoethanol diluted 1:100. Subsequently, genomic DNA (gDNA) was sheared by centrifugation through a Quiashredder column for 2' at 9500 x *g* and isolated RNA was collected in a tube. Then a mix of RNA and 600 µl of 70% ethanol was prepared, added to a Spin Column and centrifuged for 1' at 9500 x *g*. The flow through was discarded. Then, the RNA was washed by applying 350 µl of RW1 buffer and centrifuging for 1' at 9500 x *g*. After that, remaining DNA was removed by incubation with a mix of 10 µl of DNAse and 70 µl of RDD buffer for 15' and centrifugation with 350 µl of RW1 buffer for 1' at 9500 x *g*. Then, RNA was washed two times with 500 µl of RPE buffer (1' at 9500 x *g*) eluted by applying two times 50 µl of RNAse free water (1' at 9500 x *g*). Finally, the yield and the purity of the collected RNA were measured using a NanoDrop2000.

3.2.2 cDNA synthesis

The following procedure provides the oligonucleotides needed for PCR applications by converting RNA templates into complementary DNA (cDNA). For cDNA synthesis the SuperScript II Kit by Invitrogen was used following the manufacturer's protocol.

For each RNA sample a mix of

Total RNA (1 µg)   x µl
Random Hexamer Primer pd(N) (250 ng/µl)   1 µl

dNTPs (10 mM)	1 µl
RNAse free dH$_2$O	add to a volume of 12 µl

was incubated at a temperature of 65°C for 15 minutes to denature RNA secondary structures. Afterwards, the reaction was chilled on ice.

Then

5 x First Strand buffer	4 µl
0.1 M DTT	1 µl
RNAsin Plus	1 µl

were added, followed by incubation for 2' at RT.

Finally, 1 µl of SuperScript Reverse Transcriptase was added and conversion of RNA into cDNA was performed at 42°C for 50´. The reaction was inactivated by incubating at 70°C for 15'. Eventually, the samples were stored at -20°C.

3.2.3   Real-time quantitative PCR

This method is used to accurately analyze the amount of gene expression via amplifying specific nucleic acid fragments in a sample of cDNA. For this study, the accumulation of the PCR product was measured by quantifying the fluorescence of *SYBR Green I*, a dye capable of intercalating with double-stranded DNA (dsDNA). *SYBR Green I* only shows fluorescence (wavelength 520 nm) after having bound dsDNA and being stimulated by blue light (wavelength 497 nm) (Sigma-Aldrich 2015, Zipper et al. 2004). The master mix reaction per well was composed as shown in *Table 2*. Information on the primers used is given in *Table 3*.

Table 2: Master mix for real-time quantitative PCR.

Reagent	Volume per well
SYBR Green I	12.5 µl
H$_2$O	6 µl
Primer forward (diluted 1:10)	0.75 µl
Primer reverse (diluted 1:10)	0.75 µl

Table 3: Primer sequences used for real-time quantitative PCR.

Target	Primer	Sequences
ARF1	Primer forward	GAC CAC GAT CCT CTA CAA GC
	Primer reverse	TCC CAC ACA GTG AAG CTG ATG
RELN	Primer forward	GGG GAT CCA CTG TGA GAC AA
	Primer reverse	AAA TGT TGT CCA GTG CCC AC

20 µl of the final master mix and 5 µl of 1:20 diluted cDNA were pipetted into a 96 well plate, using three technical replicates per sample. Then expression levels were analyzed by a StepOnePlus Real-time PCR system using the following cycling conditions:

Denaturation	95.0°C	2'	
Denaturation	95.0°C	5''	
Annealing/Elongation	60.0°C	15''	} 40 cycles
+ melt curve			

The StepOnePlus system detects the cycle at which the amount of fluorescence exceeds a certain threshold and plots it logarithmically. This threshold cycle (C_t) correlates to the quantity of cDNA targeted by the primers, as the amount of SYBR Green I bound to dsDNA increases. To measure the relative expression in the samples tested, the $2^{-\Delta\Delta Ct}$ method was applied (Livak & Schmittgen 2001). To calculate the ΔC_t, the C_t of a housekeeping gene, here *ADP ribosylationfactor-1* (*ARF1*; GenBank-Accession-No.: M36340.1), is subtracted from the C_t of the target gene. Afterwards, the relative expression of the target gene is related to a control to define $\Delta\Delta C_t$ of the samples as follows: $\Delta\Delta Ct = \Delta C_{t, sample} - \Delta C_{t, control}$. To inverse the logarithmic values, the formula $2^{-\Delta\Delta Ct}$ was used, resulting in the relative expression of the fold changes of the analyzed target gene.

3.3   Protein biochemistry

3.3.1   Western blotting

3.3.1.1   Cell lysis

For analysis of protein abundance by western blotting, the cultured cells have to be lysed in a suitable buffer. Therefore, approximately 150.000 cells were seeded into a Ø 15 mm tissue culture dish and incubated for 48 h in complete medium for U87 respectively U251 in a humidified atmosphere at 37°C and 5% CO_2. Afterwards, cells were washed with ice cold PBS and lysed by using 150 µl of Radio Immuno Precipitation Assay (RIPA) lysis buffer with added Phospatase and Protease Inhibitor Cocktail and kept strictly on ice. Finally, the lysed cells were collected in a tube and stored at -80°C. The lysates were processed as fast as possible in order to keep protein and phosphorylation degradation at a minimum.

3.3.1.2   SDS - Polyacrylamide Gel casting

The following tables show the material composition of separating gels containing 15%, 10% and 8% acrylamide and of the stacking gel. The volumes are adapted for two gels using Bio-Rad casting stands. Gels with a concentration of 15% SDS were used for proteins considered to have a lower molecular weight (~30 kDa); consequently, proteins with a higher molecular weight (~125 kDa) were analyzed on an 8% SDS gel.

Table 4: SDS – Polyacrylamide separating gels.

Chemical/solution	15% Gel	10% Gel	8% Gel
H_2O	2.5 ml	4.17 ml	4.83 ml
Acrylamide	5.0 ml	3.33 ml	2.67 ml
Lower Gel buffer	2.5 ml	2.5 ml	2.5 ml
APS	75 µl	75 µl	75 µl
TEMED	7.5 µl	7.5 µl	7.5 µl

Table 5: SDS – Polyacrylamide stacking gel.

Chemical/solution	Volume
H$_2$O	3.74 ml
Acrylamide	0.78 ml
4x Upper Gel buffer	1.5 ml
APS	30 µl
TEMED	7.5 µl

3.3.1.3 Phos-tag^{TM} SDS - Polyacrylamide Gel casting

Phosphate binding Tag^{TM} (Phos-tag^{TM}) is a molecule capable of capturing phosphomonoester dianions bound to serine, threonine and tyrosine residues. Phosphorylated proteins show slower migration of bands in SDS-Polyacrylamide gel electrophoresis (SDS-PAGE) with polyacrylamide bound Phos-tag^{TM} compared to the corresponding dephosphorylated protein (Kinoshita et al. 2006).

The composition of Phos-tag^{TM} SDS-Polyacrylamide gels is the same as for normal polyacrylamide gels as described above, except for adding 50 µl of each Phos-tag^{TM} D and Phos-tag^{TM} E solution to the mixture of the separating gel.

3.3.1.4 SDS - Polyacrylamide Gel Electrophoresis (SDS-PAGE)

SDS-PAGE is a common tool to separate proteins by their molecular weight and is based on a modified protocol of the Laemmli method (Laemmli 1970).

For SDS-PAGE, 150 µl of the protein lysates (as prepared in *chapter 3.3.1.1*) were diluted in 50 µl of 4x Laemmli-buffer and mixed by using a 1 ml syringe and a 20G x 1.5" needle to remove gDNA. Afterwards, the lysates were kept in a heating block at 70° C for about 3' to denature remaining protein structures and finally, 28 µl of the samples were applied to the gels. As a molecular weight marker, 5 µl of MagicMark^{TM} Western Protein Standard (Life Technologies) were used. Running of the gels was performed at a constant voltage of 80 V for 30' (stacking gel) followed by 140 V for 60'-70' (separating gel), depending on the polyacrylamide concentration of the gels.

Then the protein was transferred onto a nitrocellulose membrane by using a semi-dry or a wet-tank blotting procedure as described below.

3.3.1.5 Semi-dry western blotting

The semi-dry western blotting method was applied for all SDS-PAGE gels, except for Phos-tag^{TM} gels (see below), and performed as follows:

Two whatman papers were soaked with anode I buffer, another one was incubated in anode II buffer and three more in cathode buffer. Before assembling the blotting sandwich as shown in the figure below in a Fastblot B44 (Biometra), the nitrocellulose membrane was wetted with anode II buffer and the gel containing the separated proteins was washed briefly in cathode buffer.
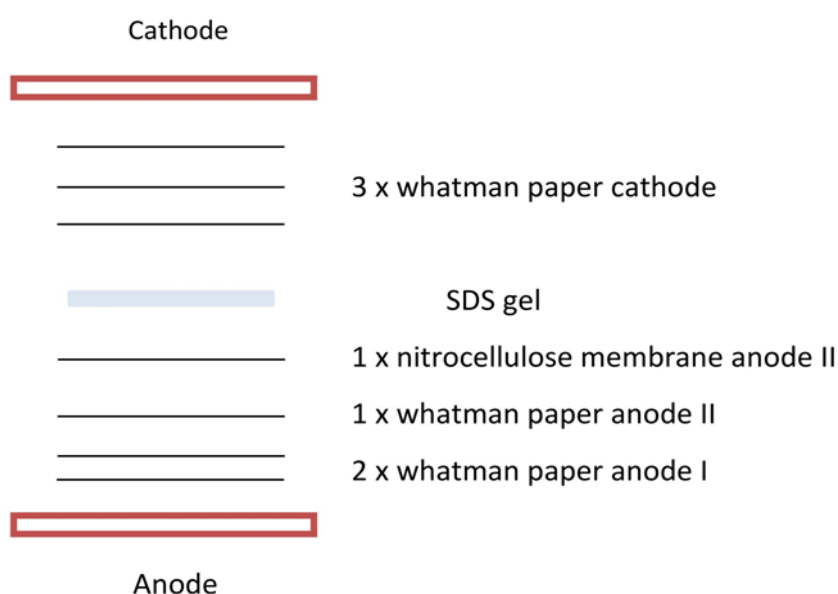
Figure 11: Sandwich for semi-dry western blotting. Taken from (Schulze M 2014).

The proteins were transferred from the gel onto a nitrocellulose membrane using a constant current of 150 mA over a period of 60' and subsequently, the transfer was confirmed with Ponceau S for 5'.

3.3.1.6 Wet-tank transfer

Proteins from Phos-tag^{TM} gels were transferred onto a nitrocellulose membrane according to the subsequent protocol using a wet-tank blotting method:

Directly after gel electrophoresis, the separating gel was washed for 10' in a solution of Towbin containing 10 mM EDTA, being followed by three more washing steps of 4' using

pure Towbin buffer. For blotting, four whatman papers were equilibrated in Towbin buffer and assembled together with a nitrocellulose membrane and the separating gel in a Fastblot B44 (Biometra) as shown in the figure below.
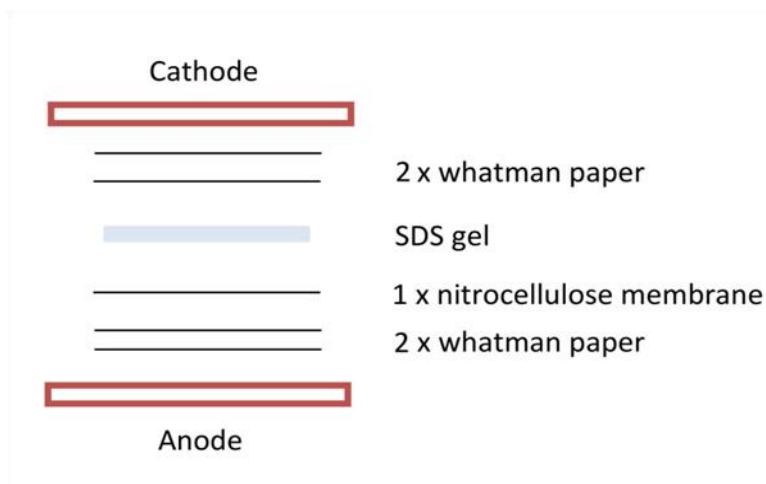
Figure 12: Sandwich for wet-tank protein transfer. Modified from (Schulze M 2014).

The proteins were transferred using a constant current of 150 mA over a period of 60'.

3.3.1.7 *Detection of proteins after western blotting*

After protein transfer to nitrocellulose, the membrane was blocked using Blotto buffer for 60' followed by incubation in primary antibody overnight at 4°C. The primary antibodies were diluted 1:10'000 (Tubulin [Clone DM1A]) or 1:1'000 (all other primary antibodies) using the antibody dilution buffer (see *chapter 2.12*). The next day, the membrane was washed three times in TBS-T for 2' and then the secondary antibody, either anti-rabbit or anti-mouse IgG linked to horseradish peroxidase diluted 1:10,000 in Blotto buffer, was added to the membranes and incubated for 90' at RT.

To visualize the primary antibodies bound to the target protein, the membranes were washed in TBS-T and incubated in horseradish peroxide substrate (HRP) containing luminol and peroxide solution for 2'. Chemiluminescence was detected using the ImageQuant LAS 4000 mini. For standard protein detection the SuperSignal West Pico Substrate was used. To reveal weak bands due to low protein expression (especially P-Kip1/P-p27) the SuperSignal West Femto Maximum Sensitivity Substrate was preferred.

For sequential detection with the same nitrocellulose membrane, HRP activity linked to the secondary antibody was irreversibly inhibited by applying a PBS solution containing 15% of

H$_2$O$_2$ for 30'. After washing with TBS-T for four times, the inactivation was completed and incubation with primary antibodies could be conducted again.

For quantification of protein expression, the signal intensities acquired with the ImageQuant LAS 4000 mini were measured using the ImageQuant TL software. Values were normalized to EV + GFP cells.

For Phos-tag^{TM} western blotting, the phosphorylation ratio is easily calculated by using the intensities of the phosphorylated (P-protein) and unphosphorylated protein as follows:

$$\frac{P - protein}{Total\ protein} = \frac{P - protein}{P - protein + unphosphorylated\ protein}$$

3.3.2 Immunocytochemistry and F-actin staining

Immunocytochemical assays deliver data on cytomorphological changes additionally to information on altered protein expression levels.

Laminin coated Lab-Tek II Chamber Slide 8 wells (see *chapter 3.1.2*) and Reelin/GFP conditioned medium containing 5% FCS for stimulation as prepared under *chapter 3.1.3* were used for the immunocytochemical assays.

3.3.2.1 Cell seeding

Cells were trypsinized as usual, then resuspended in complete medium with 5% FCS and adjusted to 142 cells /µl. Afterwards, the wells of the Lab-Tek Slide were filled with 140 µl of Reelin or GFP conditioned medium containing 5% FCS and about 10,000 cells were seeded by adding 70 µl of the cell suspension. Before starting the staining procedure, cells were allowed to adhere overnight.

3.3.2.2 Staining

After incubation overnight, the cells were washed briefly with PBS and then fixed immediately with 12 ml of prewarmed 4% PFA at room temperature for 15'. Cells were washed again with PBS for 5' and then 12 ml of blocking buffer were applied for 1 h to permeabilize the cell membranes. From this step on, the slides were kept in a wet chamber in

the dark. Then, cells were washed two times with PBS containing 0.3% of the detergent saponin for 5' each and stained overnight using 150 µl of the primary antibody P-Cofilin diluted 1:50 in antibody dilution buffer. The next day, cells were washed three times with PBS + 0.3% saponin and then the secondary antibody Fluorescein anti-rabbit IgG diluted 1:200 and Phalloidin 555 diluted 1:50 for staining of actin filaments were applied for 2 h at room temperature. The slides were washed again two times with PBS containing 0.3% saponin and then counterstained with DAPI at a concentration of 2 µg/ml for 5'. Afterwards, the slides were washed two times with pure PBS and then visualized with the fluorescence microscope Olympus BX61 for quantitative analysis at 40x magnification and with a Leica AF-6000 for high magnification imaging at 63x magnification.

3.3.2.3   *Automated image analysis*

For analysis of immunocytochemistry at least 50 cells per condition (normally about 70) were evaluated in each of three independent experiments using the open-source software CellProfiler (Carpenter et al. 2006).

CellProfiler can accurately identify nuclei and cell edges and is capable of differentiating between crowded cells, thus being an effective tool for image analysis.

For this work, DAPI stained nuclei were used for identification of primary objects and afterwards the outlines of a cell surrounding a nucleus were detected using the P-Cofilin stained fluorescence images. *Figure 13* exemplarily displays the steps taken in CellProfiler to identify the glioblastoma cells. The threshold methods applied for U87 and U251 were identical except for minor adjustments concerning the allowed diameter of objects.

A

B

C

D
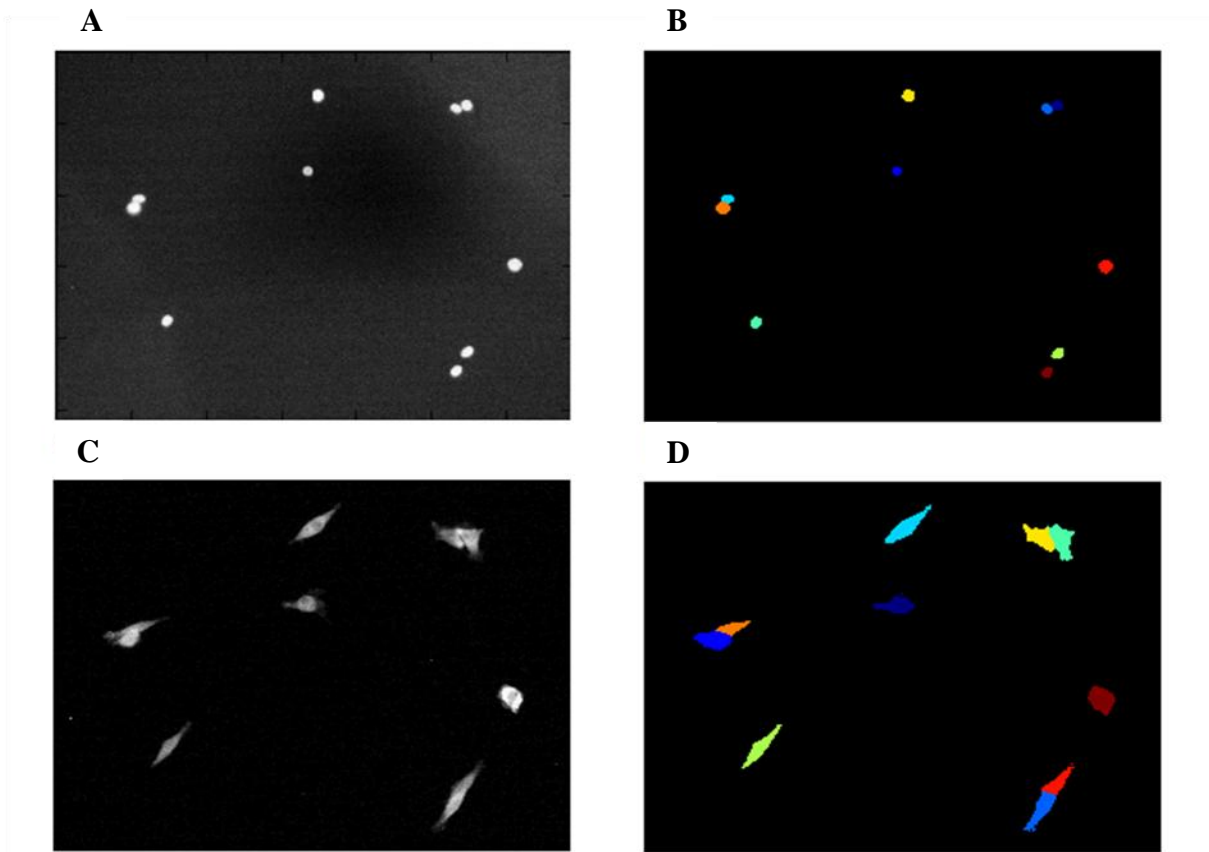
Figure 13: Identification of primary (nuclei) and secondary objects (cells) in CellProfiler. CellProfiler's algorithms are effectively detecting nuclei (B) in the DAPI raw image (A). Once these primary objects are identified, the software can spot cell edges surrounding the nuclei in the P-Cofilin stained raw image (C) and succeeds at distinguishing clumped cells as seen on the left side and in the upper and lower right corners of (D).

Besides cell detection, CellProfiler also delivers numerous ready-to-use modules for quantitative measurements like analysis of fluorescence intensity or evaluation of cell shape and size. In the case of this doctoral thesis, a parameter called ‹Form Factor› was obtained for each cell condition to analyze potential effects that *Reelin* and *DAB1* might have on the morphology of glioblastoma cells. The form factor, also known as shape factor or ‹Circularity›, measures the roundness of objects. This figure is calculated as $\frac{4 \times \pi \times Area}{Perimeter^2}$ and lies between 0 and 1, with 1 describing a perfect circle and values much less than 1 the shape of a star. The perimeter is determined as the length of the boundaries of an identified object.

To investigate further on the expression of the *Reelin/DAB1* signaling downstream targets, the average fluorescence intensities per cell of actin and P-Cofilin were measured for each cell line using another standard module of CellProfiler.

3.4   2D migration assay

The study of cell migration is of great importance to understand features of malignant cancers and can often give further clues towards underlying biological processes.

For the 2D migration assays, 8 well µ-Slide ibiTreat plates with fibronectin- or alternatively laminin-coating were used (see *chapter 3.1.2*). The cancer cells were stimulated with Reelin/GFP conditioned CO_2 independent medium as prepared under *chapter 3.1.3*.

3.4.1   Cell seeding

First, the cells were trypsinized as usual, resuspended in complete CO_2 independent medium and then adjusted to 60 cells per µl, taking care that only single cells were present. Afterwards, 200 µl of Reelin or GFP conditioned medium were filled into each of the wells and finally 100 µl of the cell suspensions containing about 6'000 cells were added and mixed by pipetting. Ahead of starting the time lapse experiment, cells were allowed to adhere for 6 h.

3.4.2   Cell tracking

Cell motility was analyzed using a Leica AF-6000 (Leica Microsystems) microscope and a microscope stage incubator to keep the temperature at 37°C. Pictures were taken every 20' over a period of 12 h.

At least 50 randomly chosen cells from each condition were tracked using *ImageJ* (Schneider et al. 2012) and the *Manual Tracking* plugin (Cordelières F 2011). Immotile cells and cells that divided during the observation period were excluded from tracking. Immotile cells were defined as cells that did not migrate more than one cell perimeter during the observation period.

To analyze these tracks, the *Chemotaxis and Migration Tool* by ibidi® was used. This software measures the accumulated distance *d* and then calculates the two parameters *velocity* and *directionality*. The accumulated distance *d* is the sum of the travelled distances (d_1, d_2, …, d_i) of a cell between the first time t_0 and the last time t_i. The *velocity* is the accumulated distance *d* divided by the total time: *velocity = d/t*. The *directionality* is calculated by dividing the distance from origin *D* through the accumulated distance *d*: *directionality = D/d*. The distance from origin is measured according to *Figure 14*.
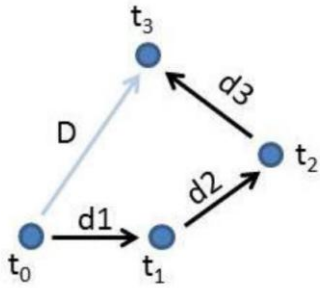
Figure 14: Calculation of the accumulated distance (d1, d2, d3,…) and the distance from origin (D) for cell migration analysis. Taken from (Schulze M 2014)**.**

3.5   Transwell invasion assay

Besides the migration assay (see *chapter 3.4*), a classical invasion assay was used to extend our knowledge on the effects of *Reelin/DAB1* signaling on motility of glioblastoma cells. For this experiment, growth factor reduced matrigel-coated transwell chambers with 8 μm pores were used in a 24-well plate format. As preparation, 600'000 glioblastoma cells were precultured 72 h prior to the assay in Ø 6 cm culture dishes. *Reelin* and GFP conditioned medium was prepared as explained under *chapter 3.1.3* with phenolred-free complete DMEM containing 0.5% FCS.

3.5.1   Cell seeding

On the day of the experiment, the Corning BioCoat™ transwells were thawn for 20' and rehydrated with 500 μl of DMEM w/o phenolred for both the insert and the well over a period of 2 h according to the manufacturer's protocol. For seeding, cells were trypsinized as usual, resuspended in 0.5% FCS complete medium and adjusted to 2×10^5 cells per ml. Then this suspension was further diluted 1:1 using *Reelin* or GFP conditioned medium, resolving in a concentration of 1×10^5 cells per ml. Subsequently, 750 μl of *Reelin* or GFP conditioned medium containing 5% FCS, which was obtained by equally mixing 10% FCS DMEM and conditioned medium with 0.5% FCS, were put into the well. Eventually, 500 μl of the prepared cell suspension, corresponding to about 5×10^4 cells, were pipetted carefully into each matrigel coated transwell chamber using two technical replicates per condition and experiment. Then the seeded cells were incubated at 37°C and 5% CO_2 for 18 h, allowing

them to migrate through the matrigel and the 8 μm pore following the gradient from 0.5% to 5% FCS.

3.5.2   Cell staining and computer-based analysis

After incubation, the non-invading cells were removed from the upper side of the transwell and cells that migrated successfully through the pores were fixed in 4% PFA for 15' at room temperature. Then, nuclei were stained in PBS containing DAPI in a concentration of 2 μg/ml and 0.3% of the detergent Triton X-100 for permeabilization of cell membranes. Finally, the stained cells were washed briefly in pure PBS and the membranes were cut out from the culture inserts and mounted onto microscopy glass slides.

Afterwards, the cells were visualized at 20x magnification using an Olympus IX81 fluorescence microscope. Each membrane was divided into four equal parts of which three were chosen randomly to take a picture of. Finally, the cells were counted automatically for each condition tested applying the built-in method «Analyze Particles…» of ImageJ.

3.6   Data analysis

All graphs and all statistical analysis shown in this doctoral thesis were created with either Microsoft Office Excel 2007 or GraphPad Prism 4 including t-test analyses, calculation of the standard error of the mean (SEM) and the standard deviation as a statistical parameter. The t-test is a statistical hypothesis test that was performed to determine if two sets of data are significantly different from each other, given the null hypothesis that both means are the same and assuming a normal distribution. The p-value is a measure for the probability that this null hypothesis is true. P-values of $< 0.05\%$ (*) and $< 0.01\%$ (**) were considered as statistically significant.

4 Results

4.1 Reelin induced DAB1 phosphorylation in U87 and U251 glioblastoma cell lines

To study the effects of *Reelin* on migration, invasion, cell morphological changes and on protein expression, it was necessary to verify whether *Reelin* is capable of activating *DAB1* in glioblastoma cells. Therefore, the presence of *Reelin/DAB1* signaling in glioblastoma cells was tested by analyzing *DAB1* phosphorylation levels.

As for all the other experiments, *Reelin*, biosynthesized by HEK 293T cells, was used to stimulate U87 and U251 cells, which were transfected with wildtype *DAB1* or an inactive *DAB1* mutant as explained in *chapter 2.7*.

4.1.1 Reelin produced by HEK 293T

As a first step, it was controlled if the HEK 293T cells stably transfected with a vector encoding for the murine *RELN* gene (mRELN) were indeed biosynthesizing *Reelin*. Hence, a real-time polymerase chain reaction (PCR) was performed to analyze the relative expression of *Reelin* in HEK cells transfected with mRELN (HEK + mRELN) compared to control cells treated with a vector containing the *green fluorescent protein* (GFP) gene (HEK + GFP). Primers specific for the murine *RELN* gene were used. As a reference, the housekeeping gene *ARF1* was used. Expression of *Reelin* was barely detectable in HEK + GFP cells whereas the expression of *Reelin* is about 10^7 to 10^8 times higher in HEK + mRELN cells than in control cells (see *Figure 15*).
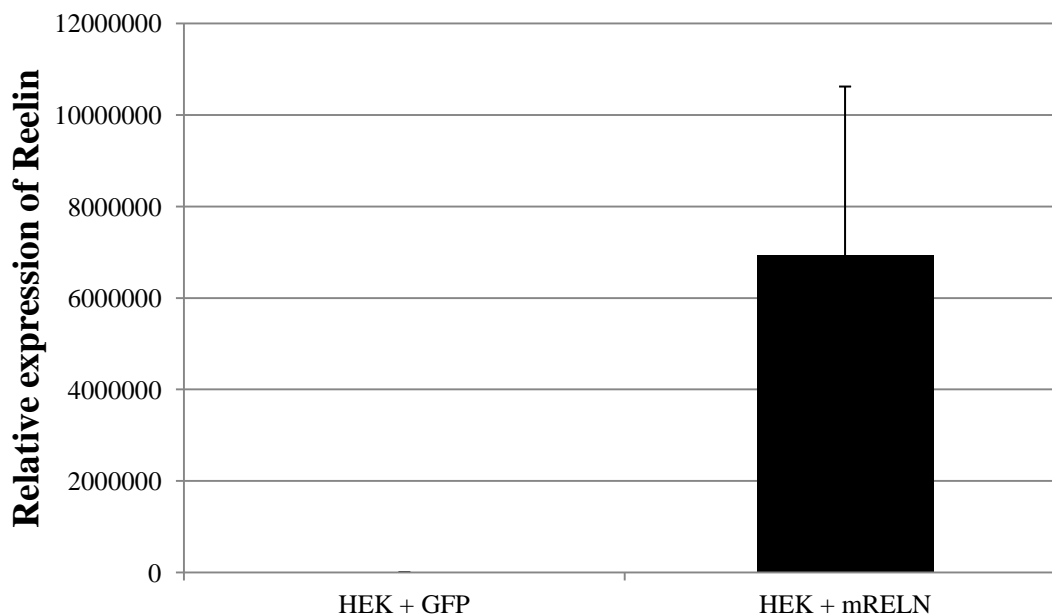
Figure 15: Real-time PCR data of relative expression of *Reelin* in control (HEK + GFP) and transfected HEK cells (HEK + mRELN). As a reference, the housekeeping gene ARF1 was used (n = 2). Shown are arithmetic mean and +/- SEM.
The expression of *Reelin* is about 10^7 to 10^8 times higher in HEK + mRELN cells than in control cells (HEK + GFP).

4.1.2   DAB1 phosphorylation in U87/U251 cells

As described in *chapter 2.7.2*, a set of three different stably transfected glioblastoma cells of the U87 and the U251 cell lines was used for the experiments: Firstly, transfection with an empty vector (U87/U251 EV) was performed to generate control cells that express only endogenous *DAB1*. Secondly, to analyze the effects of *Reelin/DAB1* signaling, cells stably overexpressing *DAB1* (U87/U251 DAB1) were established. Finally, as a second control, cells were transfected with a gene encoding for the *DAB1* 5F (U87/U251 5F) mutant that cannot be phosphorylated through *Reelin* as the typical phosphorylation sites are changed from tyrosine to phenylalanine. To validate *DAB1* expression on protein level, protein lysates of these cells were examined via western blotting using an anti-*DAB1* antibody (see *Figure 16 (A)* for U87 and *(C)* for U251). In U87 glioblastoma cells *(A)*, a main band at approximately 60 kDa can be identified in cells overexpressing *DAB1* (DAB1, lanes 3 and 4) as well as for *DAB1* 5F mutant cells (5F, lanes 5 and 6). In EV cells (lanes 1 and 2) this band cannot be detected.
For the U251 cell line *(C)*, these findings are similar except for the loss of the band at 60 kDa in DAB1 cells (lanes 3 and 4). Instead, a signal at a lower apparent molecular weight of about 45 kDa below and also a signal above at >120 kDa with slower electrophoretic mobility is

found, when compared to EV and 5F cells. These bands are also present in U87 DAB1 cells but are not found in any of the EV or 5F cells.

Besides protein analysis with the anti-*DAB1* antibody, phosphorylated *DAB1* was also detected with anti-Phospho-*DAB1* antibody (P-DAB1) (see *Figure 16 (B)* for U87 and *(D)* for U251). To examine *DAB1* phosphorylation, cells were stimulated with control (GFP) or *Reelin*-containing (mRELN) HEK-cell supernatant and western blots were incubated with an antibody specific for the phosphorylation site Y220 of *DAB1*. The amino-acid Y220 is mutated to phenylalanine in 5F mutant cells. A single band at approximately 60 kDa is found for U87 cells overexpressing *DAB1*, when stimulated with *Reelin* (DAB + mRELN, lane 4). In U251 cells showing overexpression of *DAB1*, a protein at approximately 45 kDa is detected by the anti-Phospho-*DAB1* antibody in both GFP and mRELN stimulated cells. In addition, a less intensive band in DAB1 + mRELN (lane 4) can be detected at about 60 kDa. Furthermore, there is another signal found at 60 kDa with low intensity in U251 for 5F + GFP and mRELN, respectively (lanes 5 and 6).

Further explanation of the observed bands in western blotting can be found in the discussion of this doctoral thesis (see *chapter 5.1*).

A

B

C

D
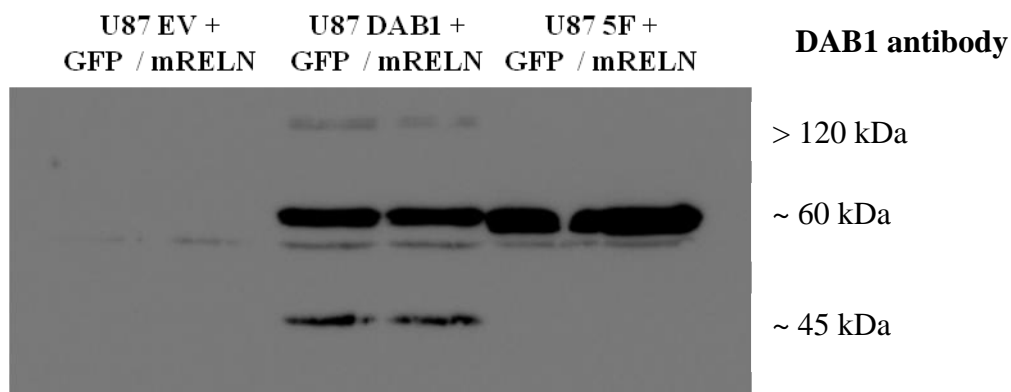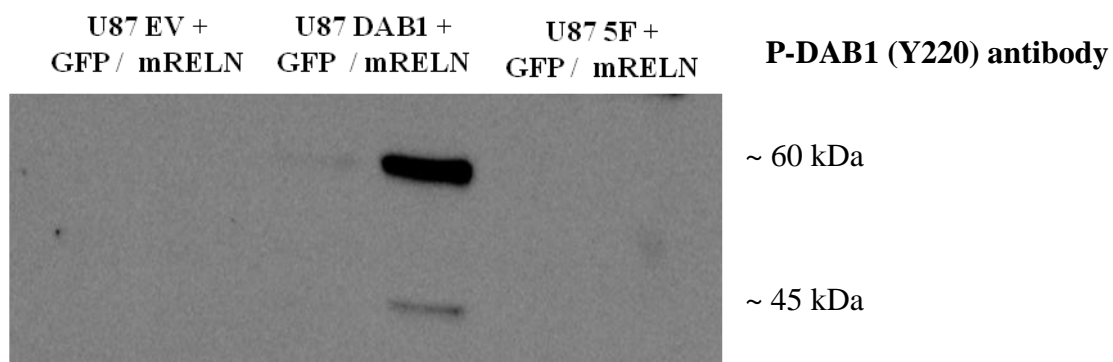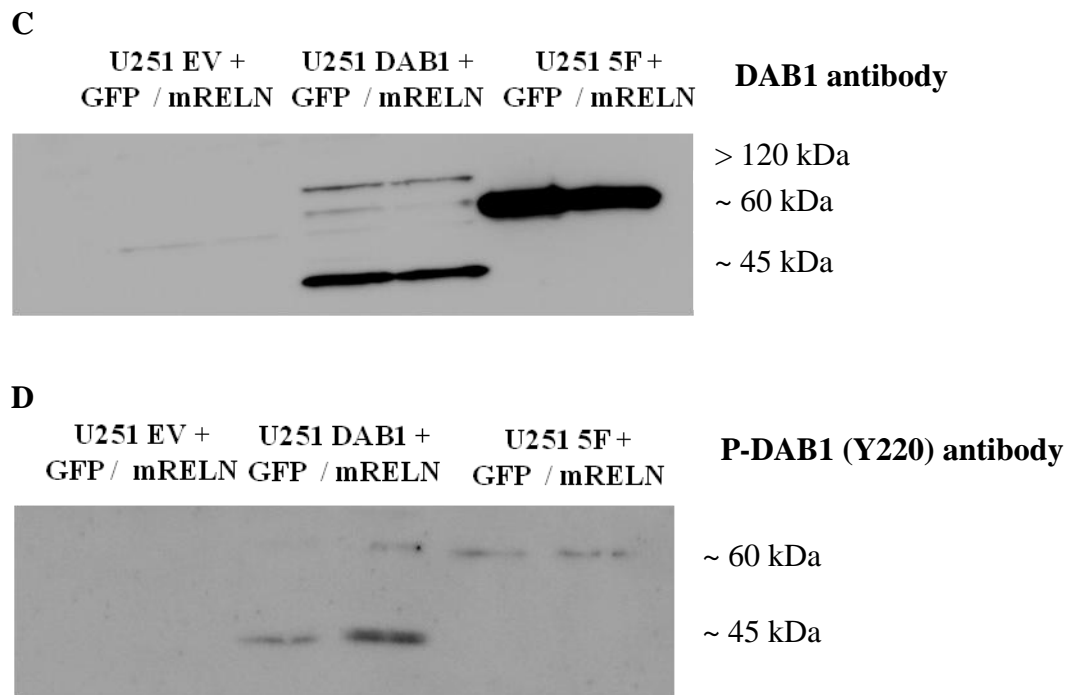
Figure 16: Analysis of *DAB1* (DAB1) and phosphorylated *DAB1* (P-DAB1) by western blotting in human glioblastoma cells. Transfected U87 (A, B) and U251 (C, D) cells were incubated with a control supernatant (GFP) or Reelin-containing supernatant (mRELN). The cell lysates (EV: empty vector, DAB1: overexpression of DAB1 and 5F: DAB1 mutant without phosphorylation sites) show different responses to Reelin stimulation.
(A) U87 cell lysates analyzed with anti-DAB1 antibody: A signal at about 60 kDa is detected for both DAB1 and 5F cells. Additional signals are found at >120 kDa and 45 kDa for the DAB1 cell line.
(B) U87 cell lysates analyzed with anti-Phospho-DAB1 antibody: DAB1 cell lysates that were previously incubated with *Reelin* (DAB1 + mRELN) show a band at about 60 kDa and another less intensive one at approximately 45 kDa.
(C) U251 cell lysates analyzed with anti-DAB1 antibody: DAB1 cells show a signal at about 45 kDa and at >120 kDa. A less intensive band can be detected around 60 kDa. 5F cells exhibit a very strong signal at about 60 kDa.
(D) U251 cell lysates analyzed with anti-Phospho-DAB1 antibody: A band is detected in DAB1 + mRELN at about 45 kDa and less intensive bands can be found in DAB1 + GFP (at approximately 45 kDa) and in 5F cells (at about 60 kDa).

4.2 Analysis of migration under the influence of Reelin/DAB1 signaling

To analyze the migratory phenotype of the glioblastoma lines U87 and U251 after manipulation of the *Reelin/DAB1* signaling pathway, cell motility was measured on both fibronectin and laminin after treatment with either *Reelin* (mRELN) or control supernatant (GFP). For this assay, the same set of transfected cells as for the *DAB1* protein expression analysis was used. Glioblastoma cell motility was evaluated based on the two parameters

velocity and directionality. These values are complemented by an exemplary plot featuring the cell tracks for each condition of one experiment.

Briefly summarized, it is a reoccurring finding throughout this whole series of experiments that cells which are overexpressing *DAB1* and are stimulated by *Reelin* (DAB1 + mRELN) show the lowest velocities compared to all other conditions, whereas the highest velocities are observed in EV + GFP and 5F + GFP cells. As a general difference between both glioblastoma cell lines it can be found that U87 cells show higher velocities with about 0.7 μm/min opposed to U251 cells with 0.3 μm/min at maximum.

The following subchapters will give more detailed information on the results of each experiment.

4.2.1   Fibronectin

Firstly, the migratory behavior of U87 and U251 glioblastoma cells on fibronectin-coated plates was observed via analysis of the parameters velocity and directionality. Additionally, exemplary plots of the corresponding cell tracks are given below (see *Figure 17*).

As can be seen in *(A)* and *(B)*, neither *Reelin* stimulation nor overexpression of wildtype *DAB1* changes the directionality of U87 and U251 cells on fibronectin.

Graphs *(C)* and *(D)*, however, show that velocity is changed due to mRELN stimulation and/or *DAB1* overexpression:

For U87 glioblastoma cells on fibronectin, a significant decrease of velocity can be found in *Reelin* stimulated 5F cells (5F + GFP vs. 5F + mRELN: p = **0.0153**, two-tailed t-test, n = 3) (see *Figure 17 (C)*). Additionally, a nearly significant reduction of speed can be found in control medium stimulated DAB1 cells compared to 5F cells (DAB1 + GFP vs 5F + GFP: p = 0.0531, two-tailed t-test, n = 3). Finally, mRELN stimulated EV and DAB1 cells also show reduced velocities compared to stimulation with GFP, but a statistically significant change cannot be detected for these conditions. Overall, U87 cells overexpressing *DAB1* show the lowest velocities when stimulated with *Reelin* (DAB1 + mRELN).
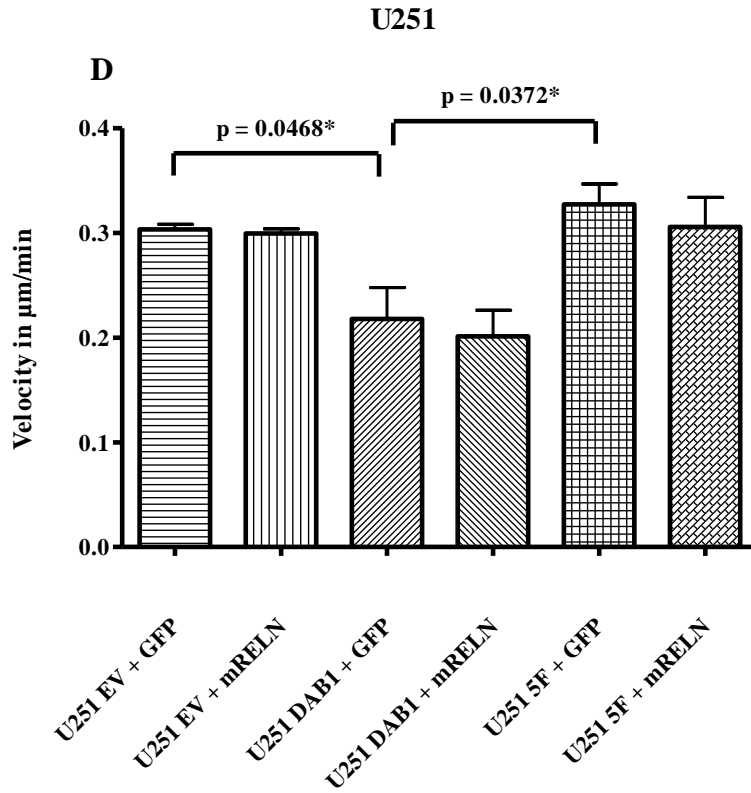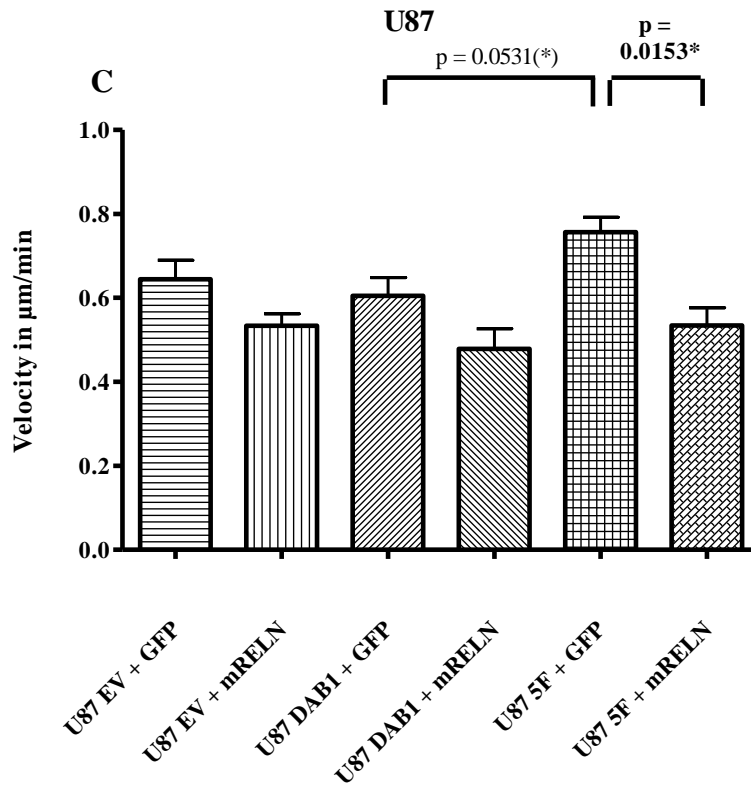
Figure 17 (D) shows that the velocity of U251 cells overexpressing *DAB1* (DAB1 + GFP, DAB1 + mRELN) is significantly lower than in the control cells EV and 5F (DAB1 + GFP vs. EV + GFP: p = **0.0468**, two-tailed t-test, n = 3, DAB1 + GFP vs. 5F + GFP: p = **0.0372**, two-tailed t-test, n = 3). However, there is no major effect of *Reelin* on the velocity in all of the tested cells compared to control medium (GFP).

The exemplary plots in *Figure 17* (*E + F*) are visualizing the results of the analyses above in a different manner. It can be observed that cells are equally migrating to the left (black) and to the right side (red). In accordance with the reduced velocities found in cells overexpressing *DAB1* or being stimulated by mRELN medium, less scattered and more compact tracks can be found in these plots compared to EV or 5F cells that were treated with control medium.
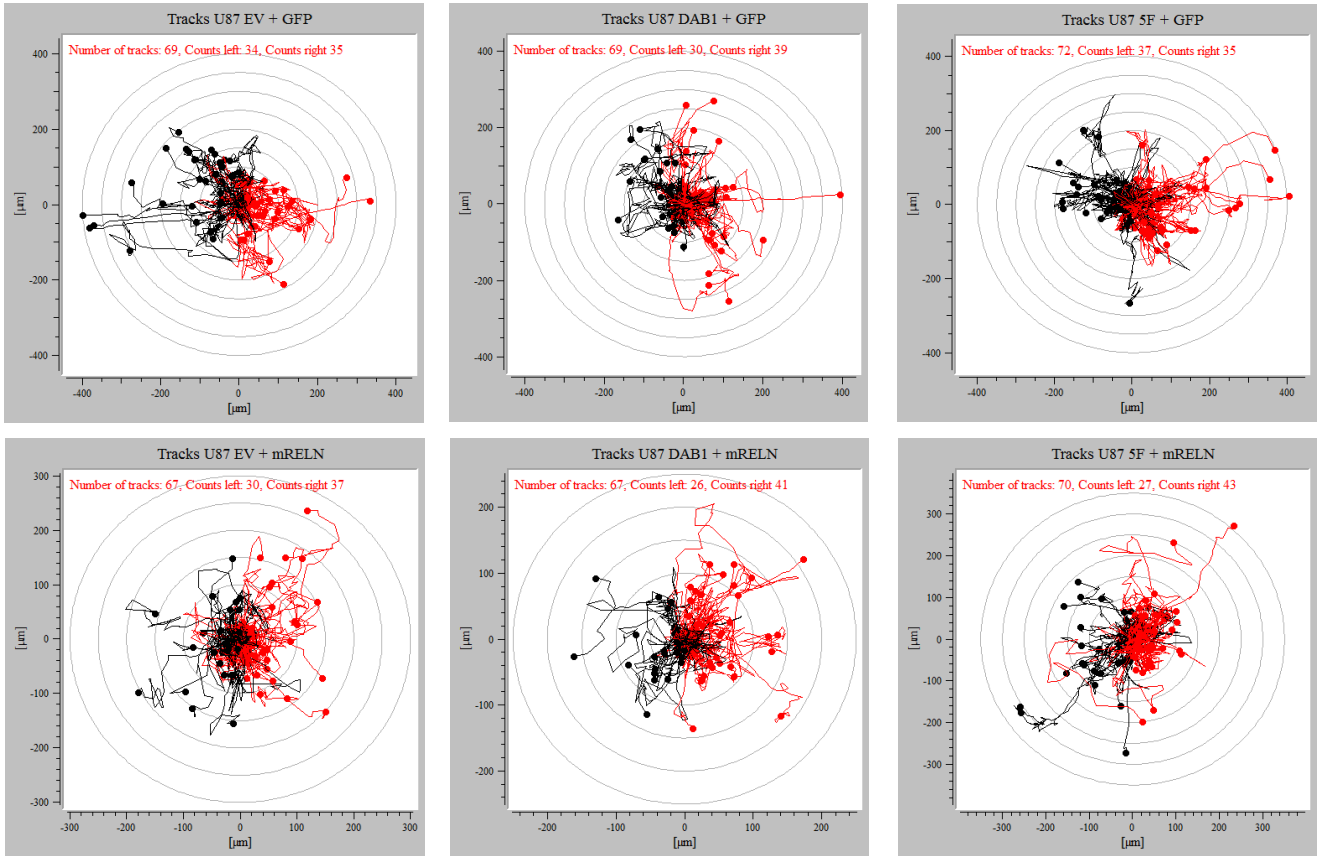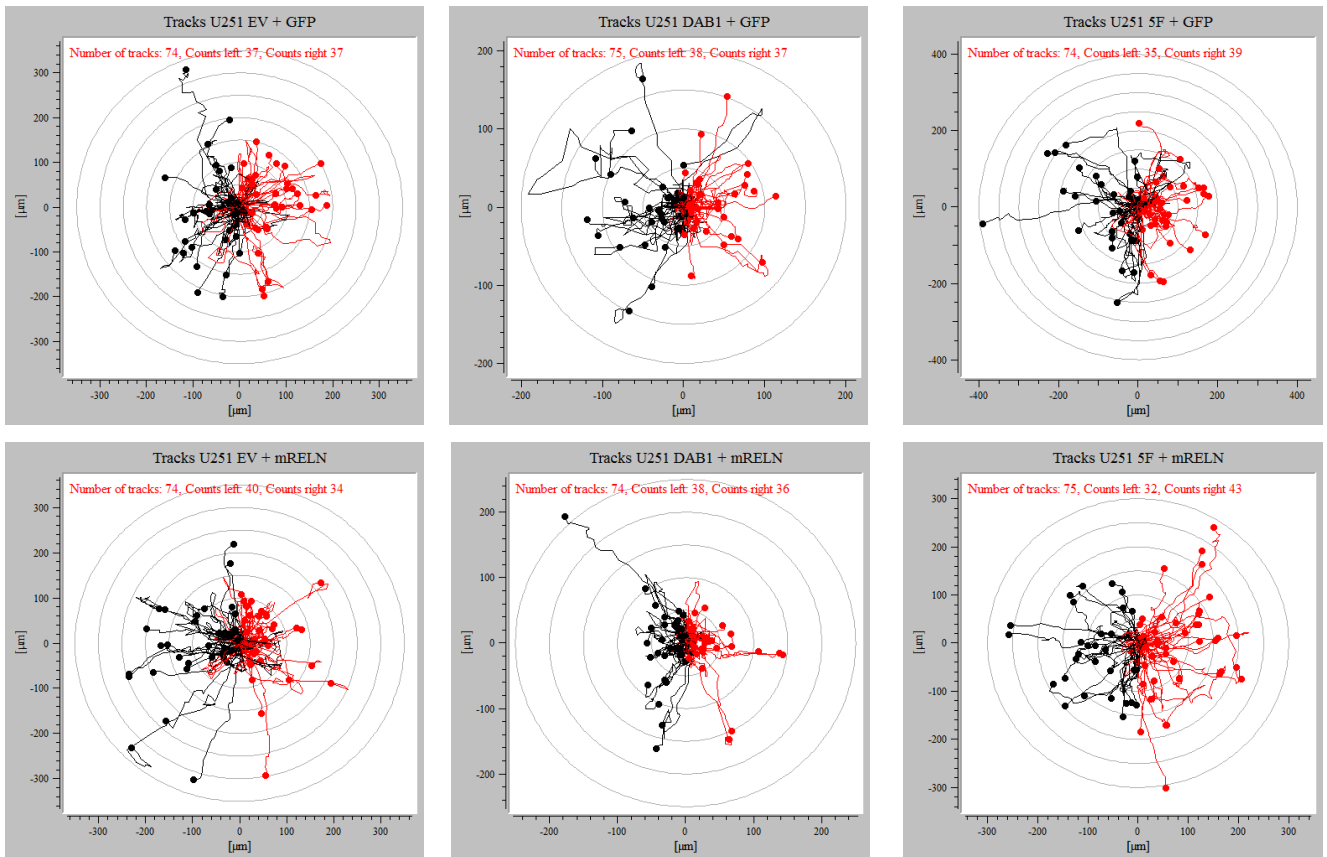
Fibronectin

A   **U87**

B   **U251**

Fibronectin

U87

U251

E: U87

Fibronectin

Tracks U87 EV + GFP
Number of tracks: 69, Counts left: 34, Counts right 35

Tracks U87 DAB1 + GFP
Number of tracks: 69, Counts left: 30, Counts right 39

Tracks U87 5F + GFP
Number of tracks: 72, Counts left: 37, Counts right 35

Tracks U87 EV + mRELN
Number of tracks: 67, Counts left: 30, Counts right 37

Tracks U87 DAB1 + mRELN
Number of tracks: 67, Counts left: 26, Counts right 41

Tracks U87 5F + mRELN
Number of tracks: 70, Counts left: 27, Counts right 43

F: U251

Tracks U251 EV + GFP
Number of tracks: 74, Counts left: 37, Counts right 37

Tracks U251 DAB1 + GFP
Number of tracks: 75, Counts left: 38, Counts right 37

Tracks U251 5F + GFP
Number of tracks: 74, Counts left: 35, Counts right 39

Tracks U251 EV + mRELN
Number of tracks: 74, Counts left: 40, Counts right 34

Tracks U251 DAB1 + mRELN
Number of tracks: 74, Counts left: 38, Counts right 36

Tracks U251 5F + mRELN
Number of tracks: 75, Counts left: 32, Counts right 43

Figure 17: Analysis of glioblastoma cell directionality and velocity on fibronectin for U87 and U251 cells (n = 3). Exemplary tracks of U87 and U251 for each condition. Shown are arithmetic mean and +/- SEM.
(A) Quantification of directionality of U87 cells in a 2D migration experiment on fibronectin: No significant changes were observed after *DAB1* overexpression or *Reelin* stimulation (two-fold t-test).
(B) Quantification of directionality of U251 cells in a 2D migration experiment on fibronectin: No significant changes were observed after *DAB1* overexpression or *Reelin* stimulation (two-fold t-test).
(C) Quantification of velocity of U87 cells in a 2D migration experiment on fibronectin: A significant decrease of velocity can be found for 5F cells under *Reelin* stimulation opposed to control medium (5F + GFP vs. 5F + mRELN: p = **0.0153**, two-fold t-test). A nearly significant reduction is found for control medium stimulated DAB1 cells compared to 5F cells (DAB1 + GFP vs 5F + GFP: p = 0,0531, two-fold t-test). A remarkable, yet not significant, decrease can also be seen for EV and DAB1 cells after *Reelin* stimulation, compared to GFP.
(D) Quantification of velocity of U251 cells in a 2D migration experiment on fibronectin: The velocity of DAB1 cells is significantly reduced compared to EV and 5F cells (DAB1 + GFP vs. EV + GFP: p = **0.0468**, two-fold t-test, DAB1 + GFP vs. 5F + GFP: p = **0.0372**, two-fold t-test). No significant changes can be found for cells after *Reelin* stimulation.
(E) Rose plots for U87 cells in a 2D migration experiment on fibronectin: Cells are equally migrating to the left and to the right. The plot of DAB1 + mRELN shows a more compact configuration than plots of the other conditions.
(F) Rose plots for U251 cells in a 2D migration experiment on fibronectin: Cells are equally migrating to the left and to the right. The plots of DAB1 + GFP respectively DAB1 + mRELN show a more compact configuration than plots of the other conditions.

4.2.2   Laminin

Besides fibronectin, the migratory behavior of U87 and U251 glioblastoma cells was observed on laminin-coating via analysis of the parameters velocity and directionality. Additionally, exemplary plots of the corresponding cell tracks are given below (see *Figure 18*).

As for fibronectin, neither *Reelin* nor *DAB1* are significantly altering the directionality (see *Figure 18 (A)* and *(B)*), but again the diagrams for velocity *(C)* and *(D)* show multiple significant changes in U87 and U251.

For U87 cells on laminin, *Figure 18 (C)*, a highly significant reduction of cell motility, independently of mRELN, is found for cells overexpressing *DAB1*, if compared to EV and 5F cells (DAB1 + GFP vs. EV + GFP: p = **0.0016**, two-tailed t-test, n = 3, DAB1 + GFP vs. 5F + GFP: p = **0.0153**, two-tailed t-test, n = 3). At the same time, a decrease of speed can be found for both EV and *DAB1* mutant 5F cells under stimulation with mRELN (EV + GFP vs. EV + mRELN: p = **0.0166**, two-tailed t-test, n = 3, 5F + GFP vs. 5F + mRELN: p = 0.0555, two-tailed t-test, n = 3). In contrast, *Reelin* treatment of *DAB1* expressing cells (DAB1 + mRELN) does not significantly alter the velocity compared to stimulation with a control supernatant (DAB1 + GFP).

Similar results can be found for U251 glioblastoma cells on laminin as is presented in graph *(D)*. Again, a significant decrease of velocity, which is found independently of *Reelin*, can be seen for DAB1 cells (DAB1 + GFP vs. EV + GFP: p = **0.0214**, two-tailed t-test, n = 3, DAB1 + GFP vs. 5F + GFP: p = **0.0312**, two-tailed t-test, n = 3). Contrary to U87, there is no

significant influence of *Reelin* compared to control supernatant in any of the tested U251 cells, however, small changes of velocity in EV, DAB1 and 5F cells can still be observed.

Figure 18 (E) + (F) display exemplary tracks for all experimental conditions and are combining the results for both directionality and velocity. It can be observed that cells are equally migrating to the left (black) and to the right side (red). In accordance with the reduced velocities found in cells overexpressing *DAB1* (DAB1 + GFP and DAB1 + mRELN), less scattered and more compact tracks can be found in these plots compared to EV or 5F cells that were treated with control medium.

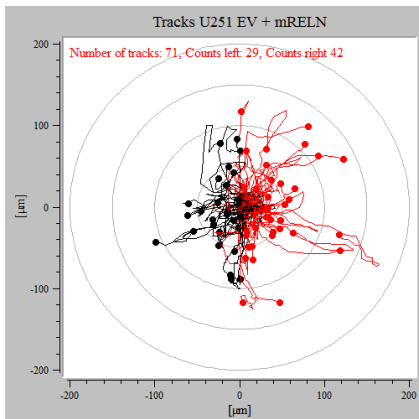**Laminin**

Laminin

U87
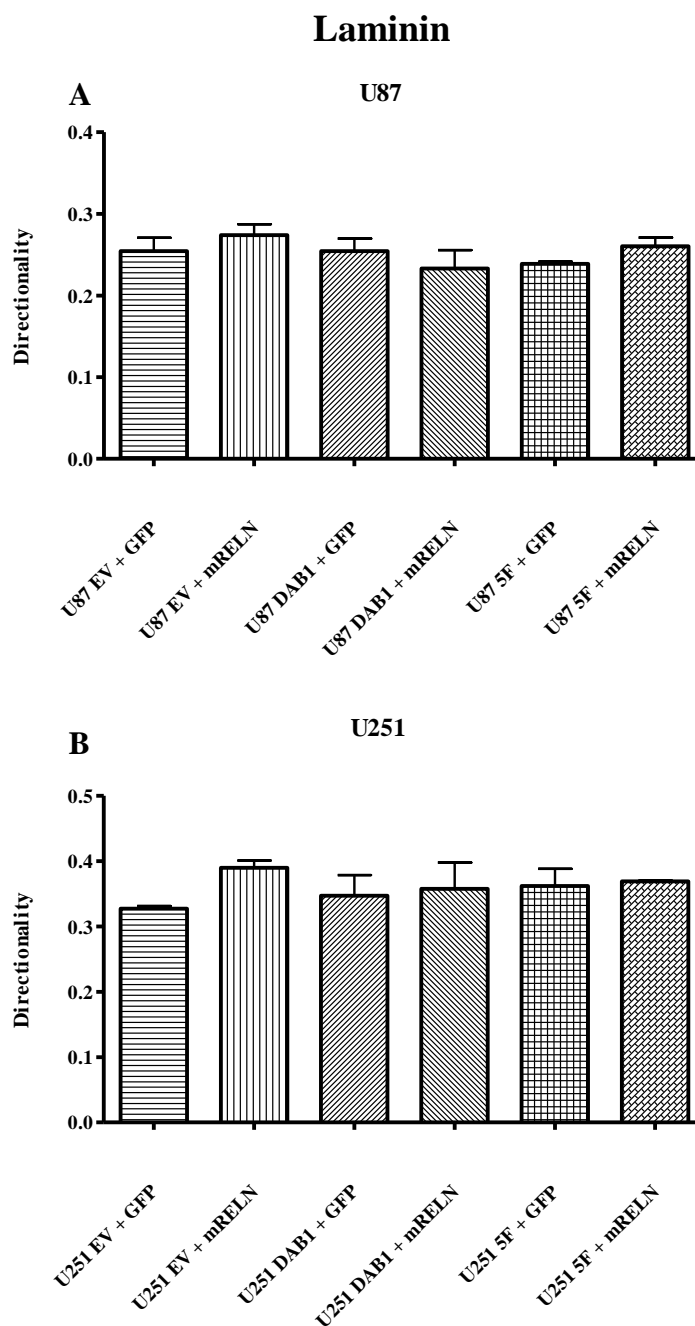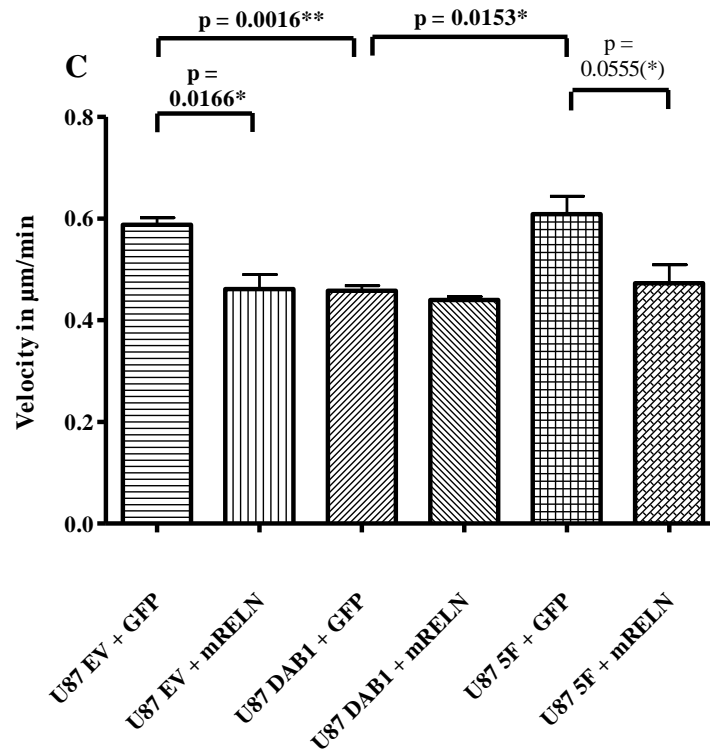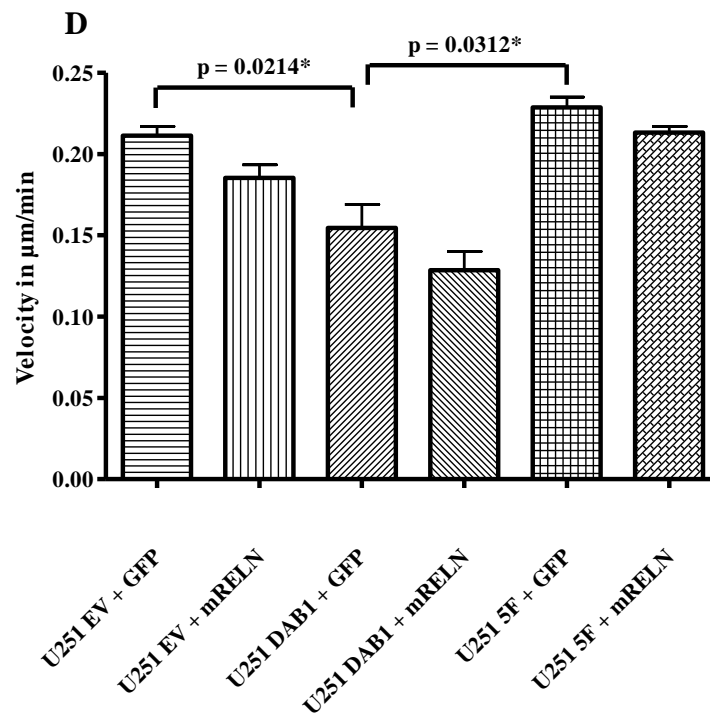
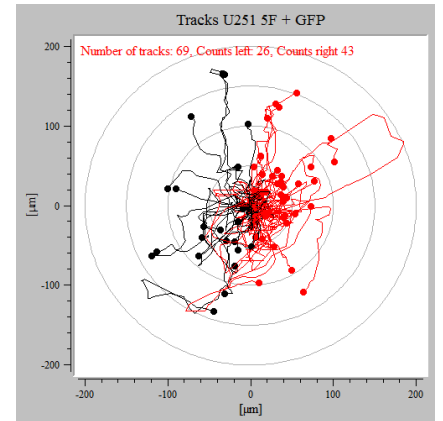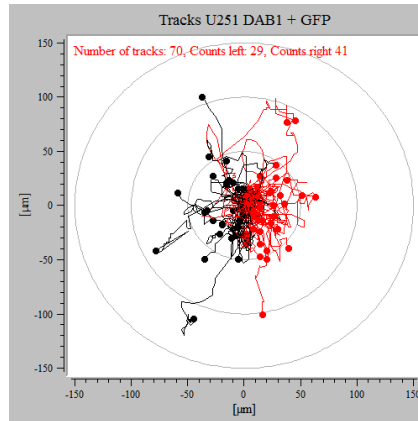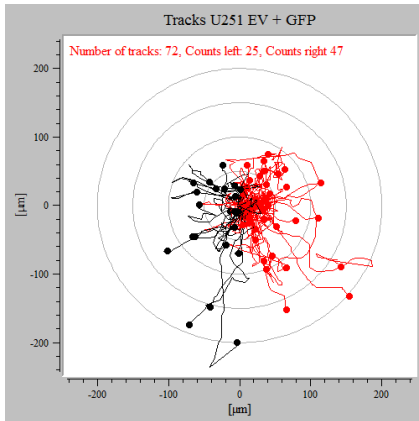

U251

E: U87
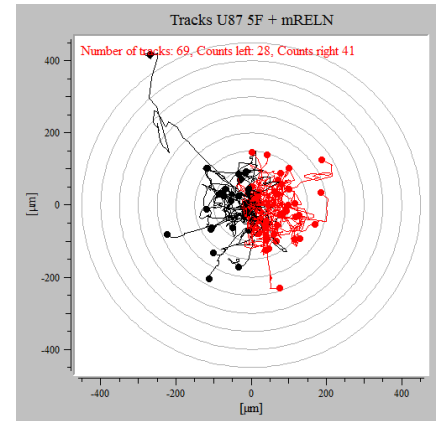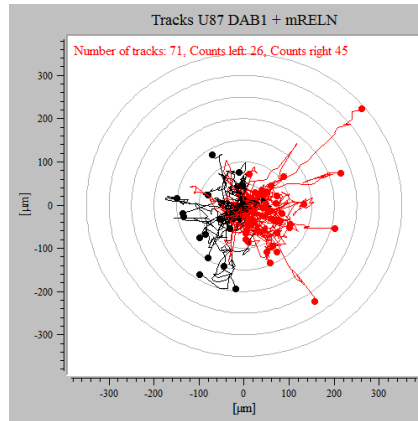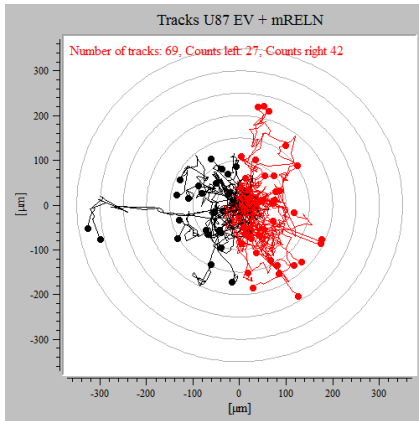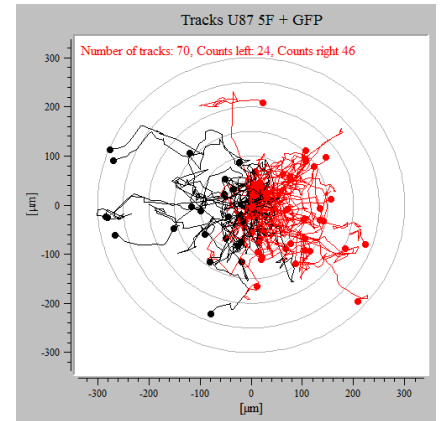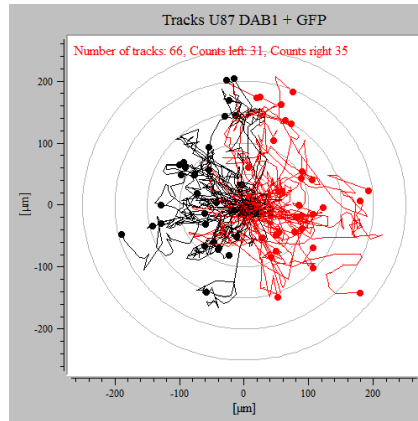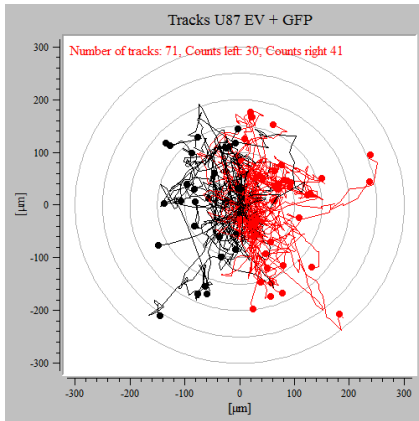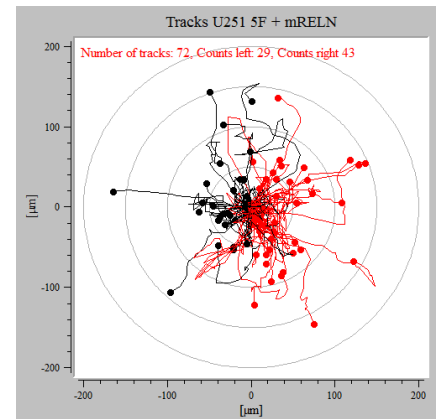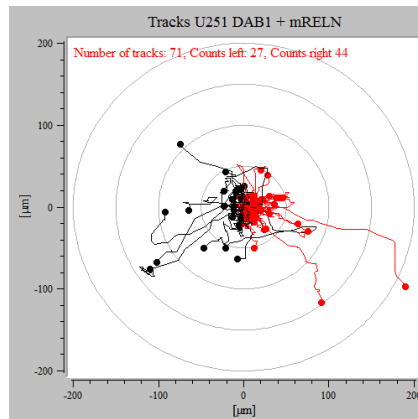
Laminin

Figure 18: Analysis of glioblastoma cell directionality and velocity on laminin for U87 and U251 cells (n = 3). Exemplary tracks of U87 and U251 for each condition. Shown are arithmetic mean and +/- SEM.
(A) Quantification of directionality of U87 cells in a 2D migration experiment on laminin: No significant changes were observed after *DAB1* overexpression or *Reelin* stimulation (two-fold t-test).
(B) Quantification of directionality of U251 cells in a 2D migration experiment on laminin: No significant changes were observed after *DAB1* overexpression or *Reelin* stimulation (two-fold t-test).
(C) Quantification of velocity of U87 cells in a 2D migration experiment on laminin: A highly significant reduction of velocity is observed for cells overexpressing *DAB1*, if compared to the control cells EV and 5F (DAB1 + GFP vs. EV + GFP: p = **0.0016**, two-fold t-test, DAB1 + GFP vs. 5F + GFP: p = **0.0153**, two-fold t-test). Velocity is also significantly decreased in both EV and 5F cells after *Reelin* stimulation (EV + GFP vs. EV + mRELN: p = **0.0166**, two-fold t-test, 5F + GFP vs. 5F + mRELN: p = 0.0555, two-fold t-test), whereas no such alterations can be found for DAB1 cells.
(D) Quantification of velocity of U251 cells in a 2D migration experiment on laminin: A significant decrease of velocity can be seen for DAB1 cells compared to EV and 5F (DAB1 + GFP vs. EV + GFP: p = **0.0214**, two-fold t-test, DAB1 + GFP vs. 5F + GFP: p = **0.0312**, two-fold t-test). However, U251 cells do not show significant changes after stimulation with *Reelin*.
(E) Rose plots for U87 cells in a 2D migration experiment on laminin: Cells are equally migrating to the left and to the right. The plots of DAB1 + GFP and DAB1 + mRELN show a more compact configuration than plots of the other conditions.
(F) Rose plots for U251 cells in a 2D migration experiment on laminin: Cells are equally migrating to the left and to the right. The plots of DAB1 + GFP, respectively DAB1 + mRELN show a more compact configuration than plots of the other conditions.

4.3   Influences of the Reelin/DAB1 pathway on cell invasion

To pursue the findings obtained in the migration assay, the invasive behavior of the same set of cells was examined in a matrigel invasion assay. Matrigel is a protein mixture consisting mainly of structural proteins such as laminin, entactin, collagen and heparan sulfate proteoglycans to simulate a natural cellular environment (Hughes et al. 2010).

The ability to migrate through Matrigel was analyzed for U87 (n = 2) and U251 (n = 1) glioblastoma cells (see *Figure 19*). Empty vector cells stimulated with control medium were used as a reference. As can be seen in *(A)*, U87 cells that are overexpressing *DAB1* show the lowest amount of invading cells when treated with *Reelin* (DAB1 + mRELN), as the number of cells is reduced to about 60% compared to the EV + GFP condition. Additionally, DAB1 cells under stimulation with control medium (DAB1 + GFP) also show a decreased amount of cells to approximately 80%. In contrast, the capability of 5F mutant cells to migrate through Matrigel is increased since the amount of cells was three times higher for 5F + GFP, respectively two times higher for 5F + mRELN, than for EV + GFP cells. Finally, also EV cells stimulated with mRELN medium exhibit a 1.5-fold higher number of cells that migrated through the invasion chambers. None of the alterations described above were statistically significant.

In contrast to U87 cells, U251 cells *(B)* overexpressing the 5F mutant of *DAB1* show the lowest amount of invading cells as the number of cells is reduced to about 30% for both,

stimulation with and without, *Reelin*. Additionally, glioma cells expressing *DAB1* deliver results similar to EV cells and *Reelin* stimulation does not affect the number of cells that migrated through Matrigel in any of the tested conditions.

Table 6 and *Table 7* show the standard deviations as a percentage of the arithmetic mean for each condition of an exemplary experiment. The mean value refers to the number of cells counted on the bottom of the invasion chambers. A variation up to 30 or 40% (below: green, above: red) is generally accepted as a reliable finding for this experiment. As can be seen, these criteria were not always satisfyingly achieved, especially not for U251 5F cells. However, preliminary experiments with self-coated invasion chambers for U251 cells gave results that hinted towards the same direction with a reduced amount of 5F cells that were capable of migrating through Matrigel (data not shown).
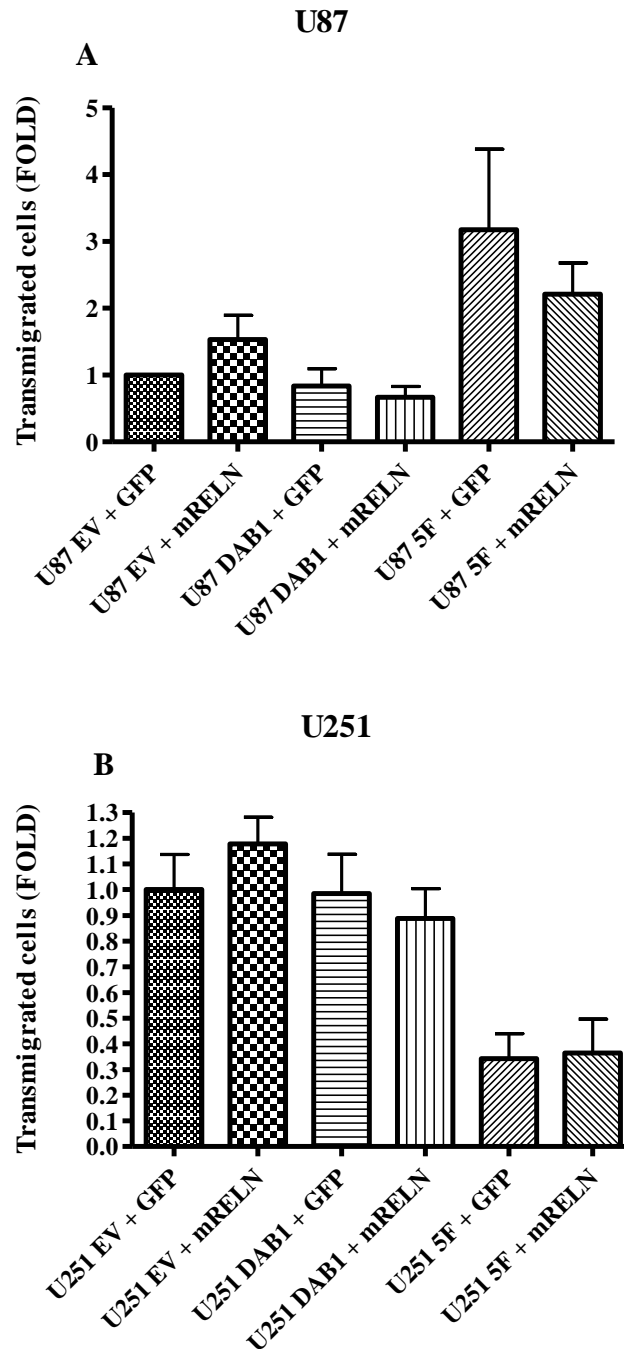
U87

A

U251

B

Figure 19: Matrigel invasion analysis of U87 and U251 cells. The number of cells that were able to migrate through Matrigel is given relatively to that of EV + GFP cells.
(A) U87 Invasion assay (n = 2): The number of cells counted on the bottom of the invasion chambers is reduced to about 80% for DAB1 + GFP and 60% for DAB1 + mRELN. For 5F + GFP and 5F + mRELN the number of cells is threefold, respectively twofold the number of EV + GFP. EV + mRELN cells exhibit a 1.5-fold higher number of cells than EV + GFP. Here, the arithmetic mean and +/- SEM of both experiments are shown. None of these changes are statistically significant.
(B) U251 Invasion assay (n = 1): The ability of 5F cells to migrate through Matrigel is reduced to about 30% compared to that of EV + GFP. DAB1 cells show similar numbers of cells counted on the bottom of the invasion chambers as found for EV cells. Here, the amount of cells normalized to EV + GFP and +/- SEM within this one experiment is given. None of these changes are statistically significant. Preliminary experiments with self-coated chambers showed similar results (data not shown). Therefore only one experiment using factory-coated chambers was performed here.

Table 6: Standard deviations of each experimental condition in U87 cells, presented as a percentage of the arithmetic mean (Sd %). Green: below 40%. Red: above 40%.

U87	EV + GFP	EV + mRELN	DAB1 + GFP	DAB1 + mRELN	5F + GFP	5F + mRELN
Mean	164.83	192.33	95.67	83.67	324.67	286.83
Sd %	56.95	38.28	37.07	29.56	39.88	36.45

Table 7: Standard deviations of each experimental condition in U251 cells, presented as a percentage of the arithmetic mean (Sd %). Green: below 40%. Red: above 40%.

U251	EV + GFP	EV + mRELN	DAB1 + GFP	DAB1 + mRELN	5F + GFP	5F + mRELN
Mean	420.50	495.50	414.17	373.17	144.17	153.50
Sd %	33.62	21.63	38.16	32.41	69.00	88.25

4.4 Analysis of the cytoskeleton under the influence of Reelin/DAB1 signaling

Migrating cells show multiple cellular alterations compared to non-migrating cells of which probably the most crucial ones have implications for the cytoskeleton. As an influence of *Reelin/DAB1* signaling on the actin cytoskeleton has already been published and the own preceding experiments already confirmed an effect of both *Reelin* and *DAB1* on the migratory behavior of glioblastoma cells, an analysis of the actin cytoskeleton via immunocytochemistry was performed on laminin coating. Additionally, the levels of phosphorylated cofilin, a downstream target of *Reelin/DAB1* signaling that is capable of controlling actin conversion (Chai et al. 2009, Kruger et al. 2010), were determined.

Firstly, the total levels of filamentous actin were detected. The signal intensities are given relatively to empty vector cells under treatment with control medium (EV + GFP). Furthermore, the ‹Form Factor› was calculated, a figure between 0 and 1 characterizing the morphology of a cell as rather a star (0) or a perfect circle (1). By the means of high magnification pictures (see *Figure 21* and *Figure* 22), the intracellular array of actin, particularly the formation of stress fibers or the development of membrane ruffling, was analyzed. Stress fibers are contractile actin bundles that play an important role in a number of cellular functions like cell adhesion and motility (Hall 1998). Membrane ruffles, on the other hand, are an indicator of inefficient lamellipodia adhesion and represent compartments of

actin reorganization (Borm et al. 2005). Therefore, alterations in both membrane ruffling and formation of stress fibers are hinting at changes in migratory behavior.

The levels of phosphorylated cofilin (P-Cofilin) were quantified via immunocytochemical detection as well as via protein analysis in western blotting using the Phos-tag[TM] SDS-PAGE method (see *chapter 3.3.1.3*). The findings are given relatively to EV + GFP. Applying this special western blotting technique, a second band showing a lower electrophoretic mobility can be observed. It was shown that this retarded band is cofilin that was phosphorylated at serine3 (Kinoshita et al. 2006, Schulze et al. 2016).

4.4.1 Analysis of the actin cytoskeleton

The immunocytochemical experiments of this doctoral thesis revealed that neither the levels of actin nor the ‹Form Factor› *(B)* and *(D)* is changed in U87 and U251 glioblastoma cells overexpressing *DAB1* compared to EV or 5F cells (see *Figure 20*). In addition, these parameters are not altered after *Reelin* stimulation.

The exemplary high magnification pictures of U87 (*Figure 21*) and U251 (*Figure 22*) are intended to give a further overview on the morphology and especially on the formation of stress fibers and membrane ruffles in these glioblastoma cells. The pseudocolor blue is indicating the DAPI stained nucleus, filamentous actin in turn is stained red via AlexaFluor® 555 phalloidin. Qualitative analysis showed that the ruffling activity is particularly high in U87 cells for all conditions. In contrast, U251 cells present primarily with formation of stress fibers which can be particularly observed in 5F cells, *(E)* and *(F)*, and less pronounced in EV and DAB1 cells, *(A)* to *(D)*. Additionally in U251, the 5F mutant glioblastoma cells are also showing membrane ruffling at several of their cell protrusions, whereas the other cells are barely exhibiting membrane ruffles.
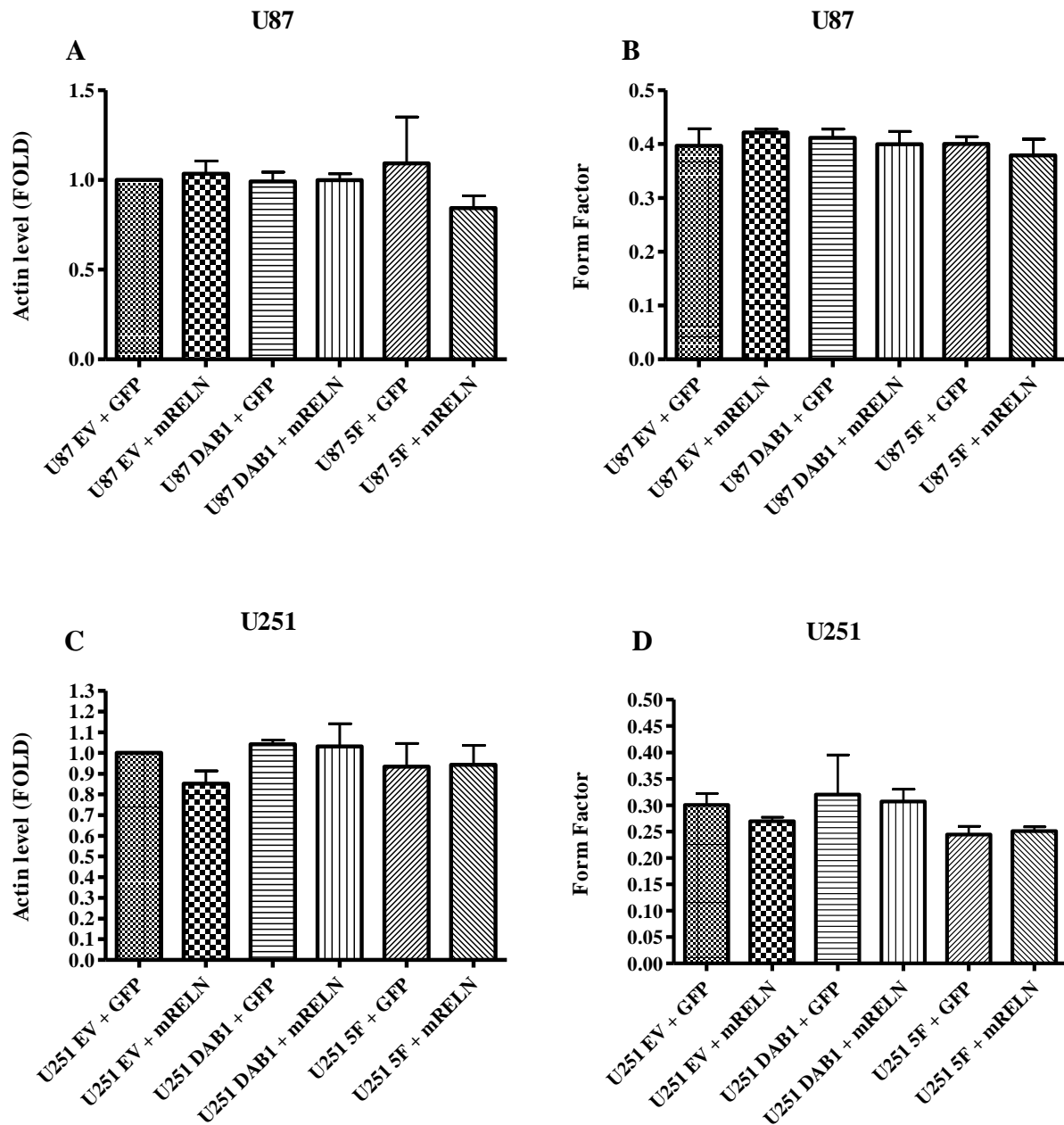
Figure 20: Quantification of actin levels and cell morphology (Form Factor) in glioblastoma cells. The levels of actin are given relatively to the levels measured in EV + GFP cells (n = 3). Shown are arithmetic mean and +/- SEM.
No significant changes were observed after *DAB1* overexpression or *Reelin* stimulation (two-fold t-test).
(A) Quantification of actin levels in U87.
(B) Quantification of the Form Factor in U87.
(C) Quantification of actin levels in U251.
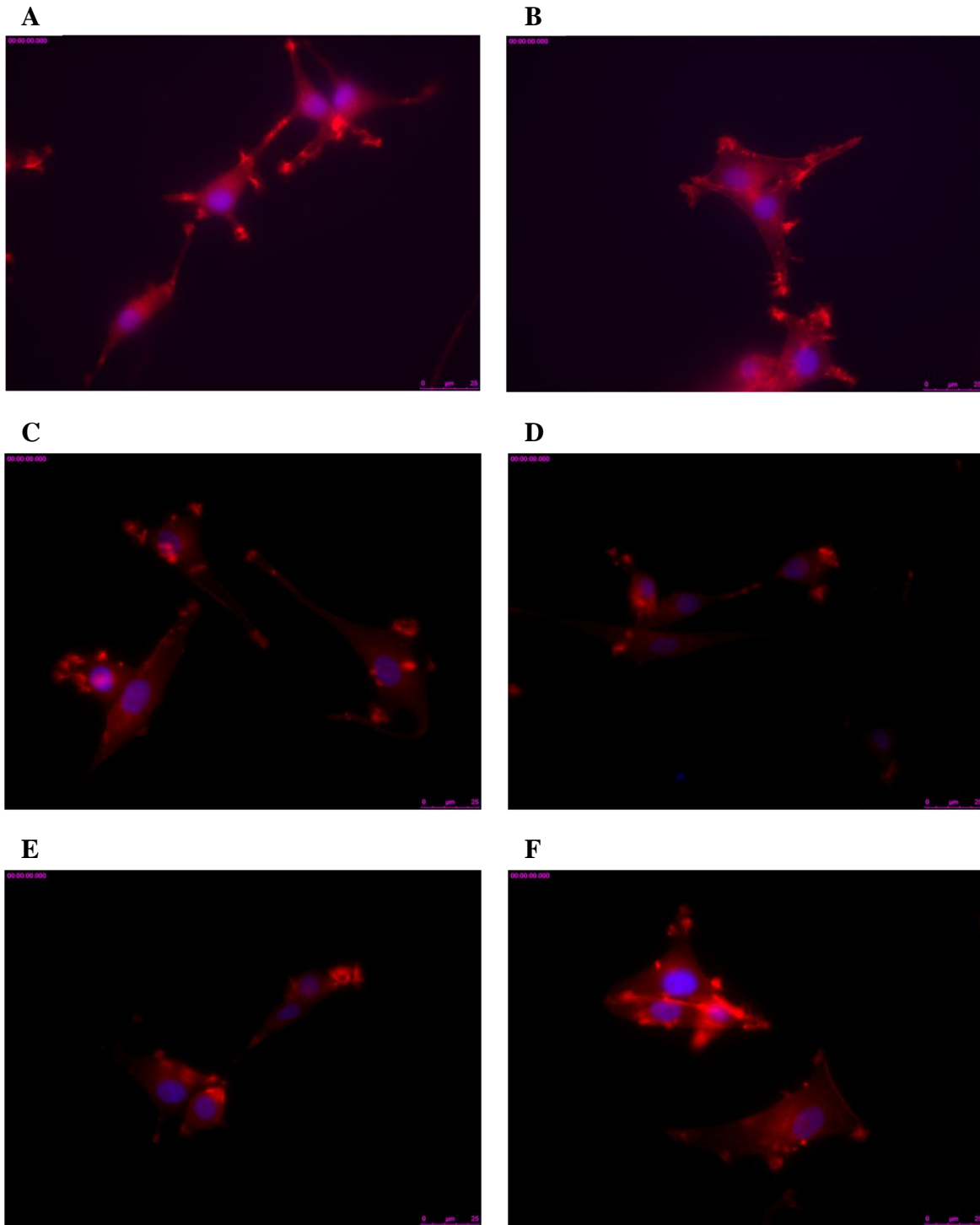**(D) Quantification of the Form Factor in U251.**

U87

Figure 21: U87 high magnification images.
The cellular anatomy of U87 is primarily dominated by membrane ruffling that can be observed throughout all experimental conditions.
(A) EV + GFP.
(B) EV + mRELN.
(C) DAB1 + GFP.
(D) DAB1 + mRELN.
(E) 5F + GFP.
(F) 5F + mRELN.
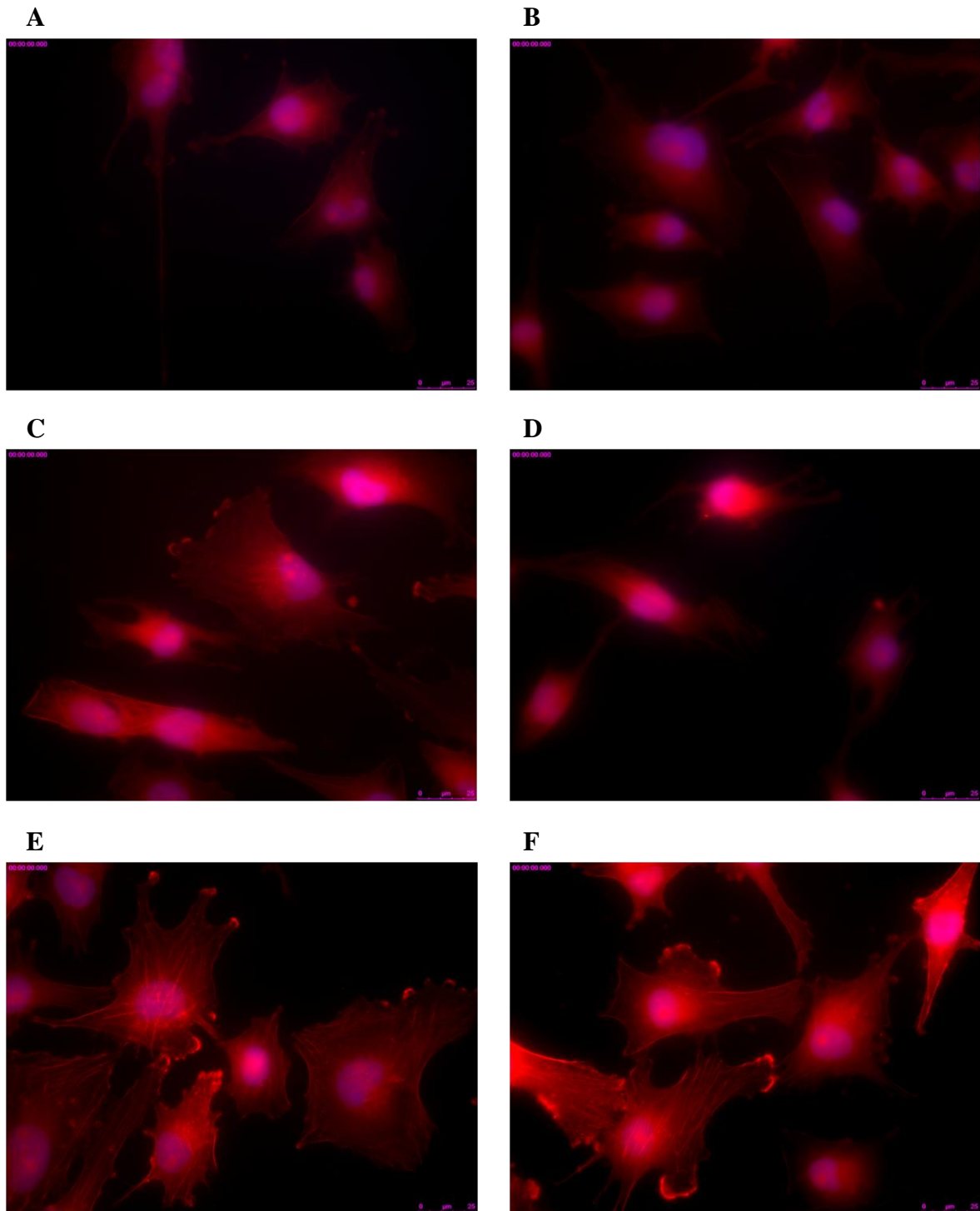
U251

A

B

C

D

E

F

Figure 22: U251 high magnification images.
U251 cells exhibit primarily formation of stress fibers which can be particularly observed in 5F cells (E and F) and less pronounced in EV and DAB1 cells (A – D). Additionally, ruffling of the cell membrane can be seen in 5F cells, whereas the other cells do barely show membrane ruffles.
(A) EV + GFP.
(B) EV + mRELN.
(C) DAB1 + GFP.
(D) DAB1 + mRELN.
(E) 5F + GFP.
(F) 5F + mRELN.

4.4.2 Analysis of the P-Cofilin to Cofilin ratio

The levels of phosphorylated cofilin were analyzed for U87 and U251 cells in an immunocytochemical assay using an anti-P-Cofilin antibody and in western blotting using an anti-Cofilin antibody detecting phosphorylation via Phos-tag^{TM}. Additionally, two exemplary blots of both U87 and U251 are given (see *Figure 23*). The upper band in these blots is phosphorylated cofilin (P-Cofilin), exhibiting slower electrophoretic mobility, whereas unphosphorylated cofilin is found at a lower apparent molecular weight, showing enhanced electrophoretic mobility. The P-Cofilin to Cofilin ratio is easily calculated by using the intensities of phosphorylated and unphosphorylated cofilin as follows:

$$\frac{P - Cofilin}{Total\ Cofilin} = \frac{P - Cofilin}{P - Cofilin + unphosphorylated\ cofilin}$$

A statistically significant effect could be found for U87 DAB1 cells after *Reelin* stimulation in the immunocytochemical experiment, as Phospho-Cofilin levels are about 20% higher than when compared to stimulation with control medium (DAB1 + GFP vs. DAB1 + mRELN: p = **0.0296**, two-fold t-test, n = 3) or compared to EV and 5F cells. There was no statistically significant difference between U251 glioblastoma cells in this assay *(B)*, but the levels of phosphorylated cofilin are increased to about 25% (DAB1 + GFP) and approximately 15% (DAB1 + mRELN) above those of EV and 5F cells.

In Phos-tag^{TM} western blotting, no changes could be detected in the lysates of neither U87 nor U251 as the graphs *(C)* and *(D)* show.

U87

A

p = 0.0296*

B   **U251**

U87

C

U251

D

E

U87 EV   U87 DAB1   U87 5F
GFP/mRELN   GFP/mRELN   GFP/mRELN

P-Cofilin

Total Cofilin

F

U251 EV   U251 DAB1   U251 5F
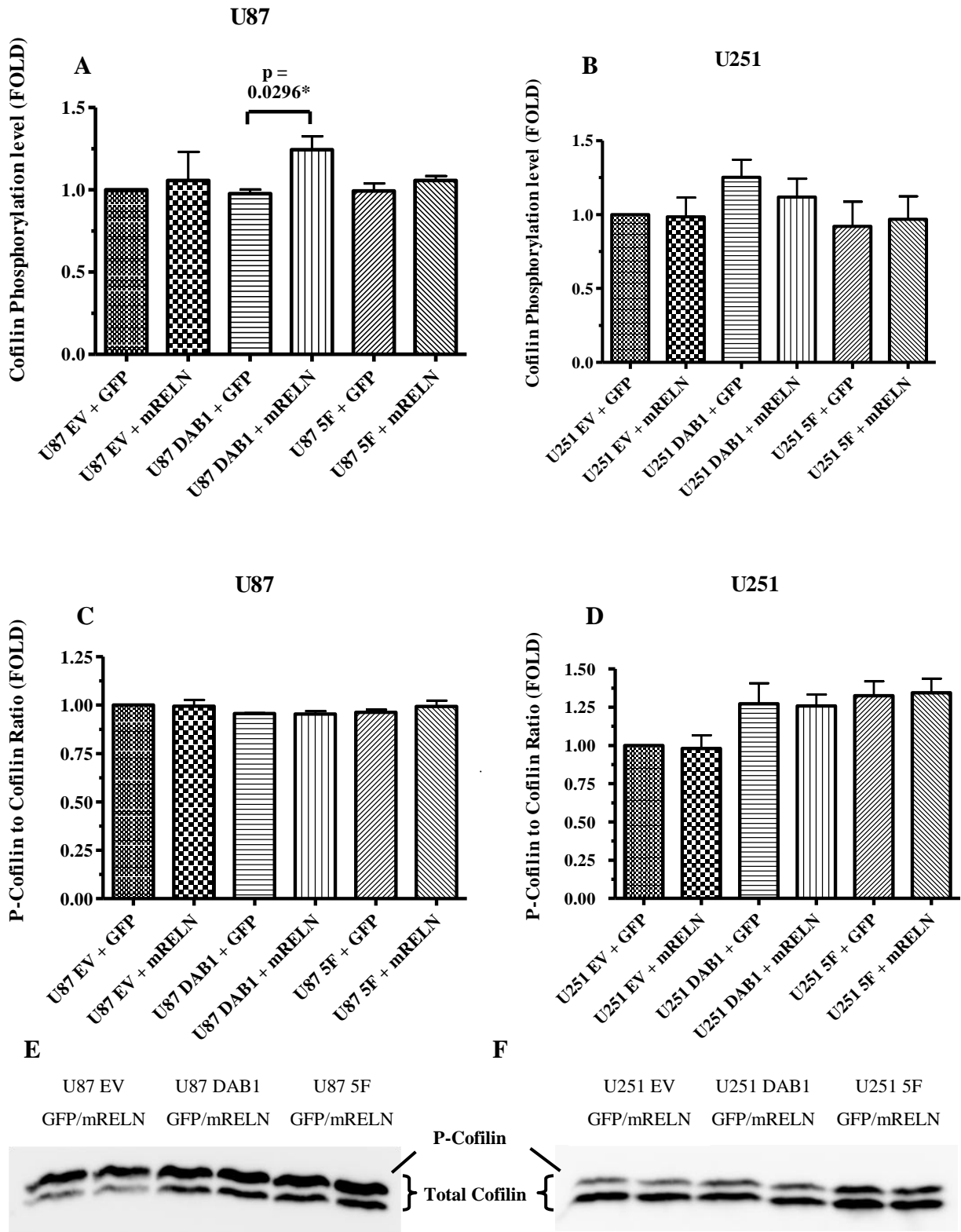GFP/mRELN   GFP/mRELN   GFP/mRELN

Figure 23: Analysis of P-Cofilin to Cofilin ratio via immunocytochemistry and via Phos-tag^{TM} western blotting in U87 and U251 (n = 3). Shown are arithmetic mean and +/- SEM.
(A) Quantification of P-Cofilin levels in U87 cells via immunocytochemistry: Cells overexpressing *DAB1* show statistically significant changes of phosphorylated cofilin after *Reelin* stimulation (U87 DAB1 + mRELN vs. U87 DAB1 + GFP*:* p = **0.0296**, two-fold t-test).
(B) Quantification of P-Cofilin levels in U251 cells via immunocytochemistry: No statistically significant changes can be observed (two-fold t-test), but elevated levels of phosphorylated cofilin are observed independently of *Reelin* stimulation for cells overexpressing wildtype *DAB1*.
(C) Quantification of P-Cofilin levels in U87 cells via Phos-tag^{TM} western blotting: No statistically significant changes can be observed (two-fold t-test).
(D) Quantification of P-Cofilin levels in U251 cells via Phos-tag^{TM} western blotting: No statistically significant changes can be observed (two-fold t-test).
(E) and (F) Representative Phos-tag^{TM} western blots of U87 and U251 lysates with anti-Cofilin antibody: The upper band is corresponding to phosphorylated cofilin (P-Cofilin) and the lower band to unphosphorylated cofilin. P-Cofilin and unphosphorylated cofilin are equivalent to total cofilin levels.

4.5   Analysis of downstream targets in Reelin/DAB1 signaling

Another aim of this doctoral thesis was to discover further downstream targets of *Reelin/DAB1* signaling in glioblastoma cells that might mediate the migratory phenotype found in the other experiments.

Prior to the experiments of this doctoral thesis, U87 cells were screened for potential downstream targets of *Reelin/DAB1* signaling by performing a proteome profiler array of *Reelin* stimulated DAB1 cells that provided multiple phosphoproteins of which Kip1 (also known as p27) and STAT3 (Signal Transducer and Activator of Transcription 3) appeared as potential targets. To verify this finding, western blot analysis of these proteins was performed. For both proteins, Kip1 and STAT3, the levels of the phosphorylated form (T198 for Kip1 and Y705 for STAT3) and the total levels of this protein were measured allowing detection of altered protein expression or degradation (see *Figure 24* and *Figure 25*).

Furthermore, the phosphorylation of the focal adhesion kinase (FAK) was analyzed. This protein is commonly modulated in migrating cells including glioblastoma cells due to its important role in cell-matrix interaction (Riemenschneider et al. 2005). Only levels of phosphorylated FAK were quantified here.

Finally, the levels of total tyrosine phosphorylation were measured using the 4G10 antibody.

However, none of the phosphoproteins analyzed showed significant and reproducible changes in response to *Reelin* or *DAB1* (see *Figure 24* to *Figure 27*). The values of intensity presented are given relatively to empty vector cells treated with control medium (EV + GFP).

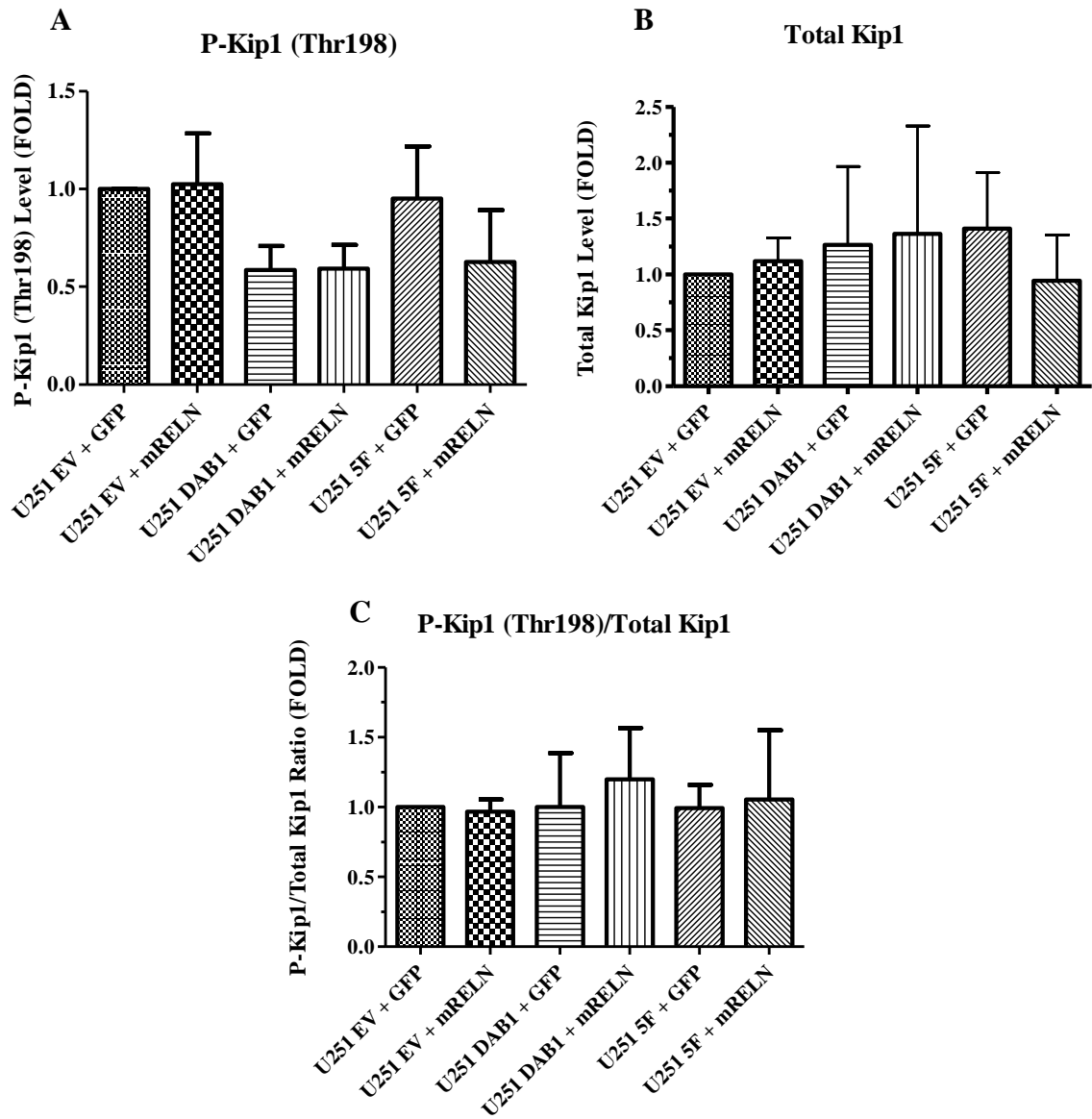No statistically significant changes in any of the experiments described above were found.

A

P-Kip1 (Thr198)

B

Total Kip1

C

P-Kip1 (Thr198)/Total Kip1

Figure 24: P-Kip1 (P-p27) (A), total level of Kip1 (p27) (B) and P-Kip1 to Total Kip1 Ratio (C) in U251 cells (n = 3).
Shown are arithmetic mean and +/- SEM.
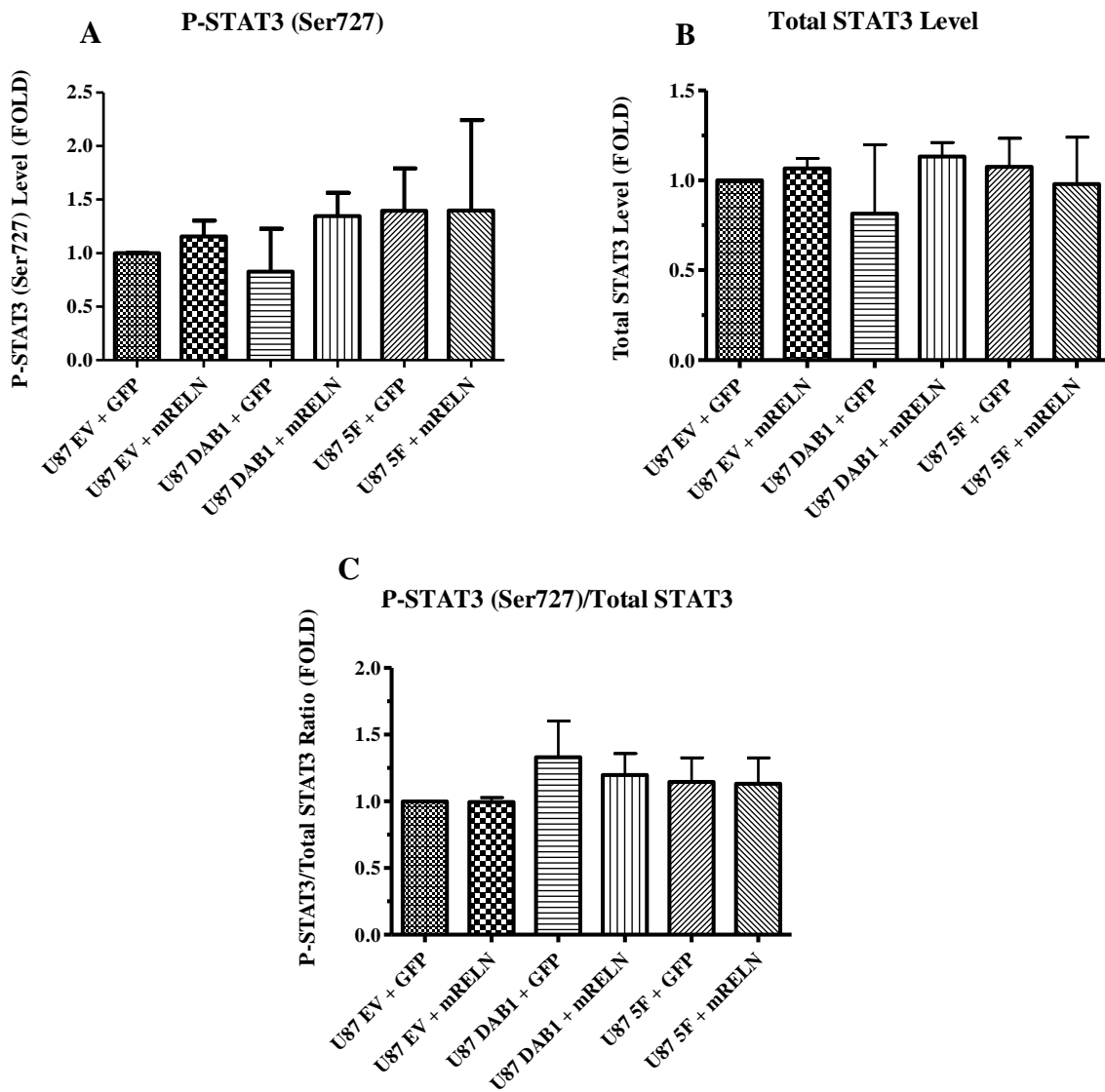No statistically significant changes can be observed (two-fold t-test).

A P-STAT3 (Ser727)

B Total STAT3 Level

C P-STAT3 (Ser727)/Total STAT3

Figure 25: P-STAT3 (A), total level of STAT3 (B) and P-STAT3 to total STAT3 Ratio (C) in U87 cells (n = 3). Shown are arithmetic mean and +/- SEM.
No statistically significant changes can be observed (two-fold t-test).
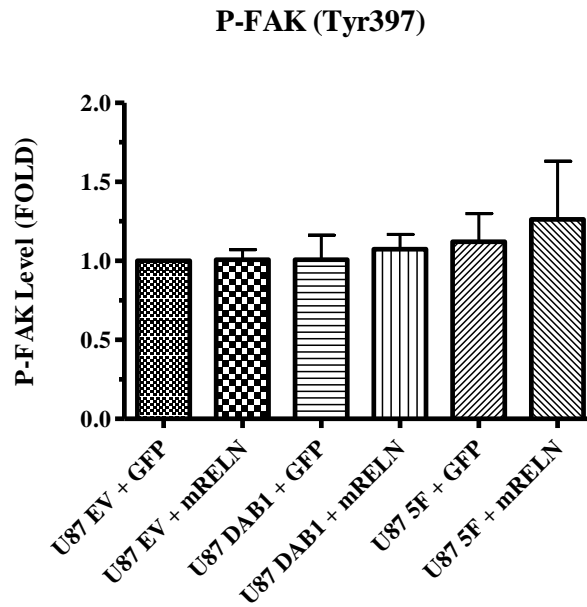
P-FAK (Tyr397)

Figure 26: Phosphorylation level of the focal adhesion kinase (FAK) in U87 (n = 2).
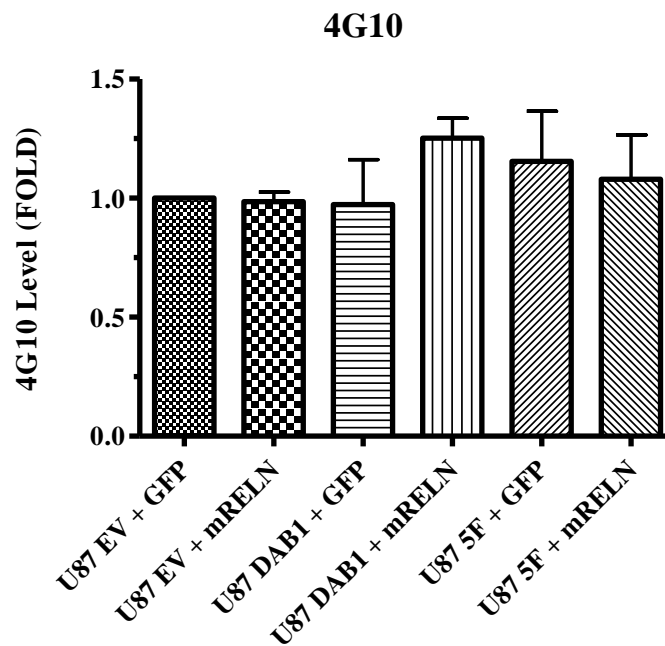No statistically significant changes can be observed (two-fold t-test).

4G10

Figure 27: Total tyrosine phosphorylation level (4G10) in U87 (n = 2).
No statistically significant changes can be observed (two-fold t-test).

5   Discussion

Reelin/DAB1 signaling is known as a crucial regulator for brain development during embryogenesis by preventing neuronal migration in the neocortex (Honda et al. 2011). Moreover, *Reelin* and *DAB1* also act as tumor suppressors in various human cancers e.g. hepatocellular carcinoma, breast cancer, pancreatic cancer or esophageal cancer (Okamura et al. 2011, Sato et al. 2006, Stein et al. 2010, Yuan et al. 2012). However, the relevance of *Reelin/DAB1* signaling in diffusely infiltrating astrocytic gliomas like the glioblastoma (WHO grade IV) was largely unknown until now. From the experiments of this doctoral thesis it can be concluded that *Reelin* and *DAB1* both influence glioma cell migration and might bear tumor suppressive functions in gliomas.

Reelin and *DAB1* are up to date known for a large number of physiological molecular interactions. Furthermore, data indicates that influence of *Reelin/DAB1* signaling on integrins might have an important role in glioblastomas. Among others, α3β1 integrin (also known as laminin receptor) and α5β1 integrin (also called fibronectin receptor) might be of importance for the results found in the experiments of this work. It is known that binding of *Reelin* to α3β1 integrin can lead to inhibition of neuronal migration during brain development and is capable of modulating intracellular levels of *DAB1* (Dulabon et al. 2000). Furthermore, *Reelin* can activate α5β1 integrin through an inside-out signaling mechanism that includes *DAB1*. This pathway improves neuronal adhesion to fibronectin (Sekine et al. 2012). Results of this doctoral thesis show that both *Reelin* and *DAB1* are significantly influencing the migratory behavior of U87 and U251 cells on fibronectin and on laminin in a tumor suppressive manner. More interestingly, it was also possible to differentiate between *DAB1*-dependent and -independent effects that *Reelin* had on glioblastoma cells, which will be further explained below.

In addition, reorganization of the cytoskeleton via phosphorylation of cofilin (Chai et al. 2009, Kruger et al. 2010) or modulation of N-WASP (Suetsugu et al. 2004) might serve as downstream targets that may mediate inhibition of tumor cell migration found after activation of *Reelin/DAB1* signaling.

In summary, the results of this doctoral thesis strongly suggest tumor suppressive functions of *Reelin/DAB1* signaling in high-grade gliomas. The executed experiments of this work have

definitely identified *Reelin* and *DAB1* as novel players in the regulation of glioblastoma cell migration (see *chapter 5.2.1* for more detailed information).

5.1 Reelin stimulation induces DAB1 phosphorylation in glioblastoma cells

For almost all the experiments of this doctoral thesis, the two cell lines U87 and U251, derived from primary glioblastoma tumor patients, were used. Both of these cell lines are well established for transfection and functional analyses as performed for this work. Despite their origin and classification as WHO grade IV tumors (Beckman et al. 1971, Torsvik et al. 2014), these cell lines behaved very differently under certain conditions, due to their unique genetic aberrations and their distinctive protein expression.

5.1.1 DAB1 levels in glioblastoma cell lines U87 and U251

The analyses of the *DAB1* protein levels in U87 and U251 (see *chapter 4.1.2*) show that *Reelin* is capable of properly phosphorylating *DAB1* in these glioblastoma cell lines.

Cells that were transfected with an empty vector (EV) did not show any detectable *DAB1* band as the endogenous protein expression of *DAB1* is rather low in both U87 and U251 cells. Cells transfected with *DAB1* or 5F mutant *DAB1*, by contrast, showed a signal at the expected molecular weight of *DAB1* around 65 kDa. In U87 cells overexpressing *DAB1*, additional bands at 45 kDa and at >120 kDa can be found, which seem to be most likely a degradation product of *DAB1* or, respectively, polyubiquitinated *DAB1*. Both of these modified proteins can still be bound by the anti-*DAB1* antibody. Detection of these proteins indicates that in these cells *DAB1* is successfully phosphorylated which leads to proteasomal degradation (Arnaud et al. 2003). Since no such protein bands could be found in 5F cells, evidence is given that this mutant cannot be phosphorylated and also cannot be activated.

Interestingly, the pattern of bands appears differently in U251 cells that are overexpressing *DAB1* compared to the ones of U87 cells. The band at 65 kDa, which is supposed to be the full length *DAB1* protein, was much weaker than in U87, but enhanced signals were found for the potential degradation product of *DAB1* and for polyubiquitinated *DAB1*. As this could be observed independently of *Reelin* stimulation, these findings suggest that a large amount of

DAB1 protein is already phosphorylated through alternative signaling mechanisms in U251 leading very likely to a higher basal activation level of *DAB1*. The transmembrane proteins VLDLR and ApoER2 (upstream of *DAB1*) are not only bound by *Reelin* but are receptors for a large amount of ligands. Among others, the ligand *Thrombospondin-1* (*THBS1*, HGNC ID: 11785), a glycoprotein that influences tumorigenesis via mediating cell-cell and cell-matrix interactions, might explain these results observed in U251 glioblastoma cells. It was shown that *Thrombospondin-1* leads to phosphorylation of *DAB1* in neurons (Blake et al. 2008) and, additionally, previous work of our laboratory revealed that *Thrombospondin-1* is expressed in U251 but not in U87 cells (Data raised by Sabine Hoja). Besides all this, a cell type specific activation of *DAB1* through SRC family tyrosine kinases (Bock & Herz 2003), through other still unknown tyrosine kinases or due to tumor specific aberrations of the U251 genome may also provide possible explanations found for this phenotype.

5.1.2   Reelin induced DAB1 activation levels in U87 and U251

It is known that extracellular *Reelin* is capable of inducing *DAB1* phosphorylation in neurons during embryogenesis by binding to the VLDL receptor or the ApoE lipoprotein receptor 2 (Hiesberger et al. 1999). Data of this work clearly proves that *Reelin* is also inducing this cascade in U87 and U251 cells (see *chapter 4.1.2*). In U87, only cells that show overexpression of *DAB1* respond to stimulation with *Reelin*-containing medium in terms of revealing elevated levels of Tyr220 phosphorylated *DAB1*. Likewise, U251 cells that are transfected with *DAB1* and stimulated by *Reelin* exhibit highest levels of activated *DAB1*, but in contrast, remarkable levels of phosphorylated *DAB1* can also be observed without *Reelin*. This finding supports again the hypothesis that *DAB1* could already be phosphorylated otherwisely, leading to constitutively active *Reelin/DAB1* signaling in U251 as opposed to U87.

In western blots of U251 cells that were performed with anti-Phospho-*DAB1* antibody (Y220), very slight bands around 65 kDa can be found in 5F cells, although the mutant *DAB1* protein in these cells should not be able to be phosphorylated per definition. As there are no other signals detected in 5F cells, particularly no bands that correspond to polyubiquitinated or degraded *DAB1*, these signals are most likely due to only minor unspecific binding of the antibody. It is rather improbable that these bands might correspond to endogenous *DAB1* as no similar signal was detected in EV cells.

5.2 Reelin/DAB1 preferentially reduces cell migration in glioblastoma cells

The test design of six conditions (EV + GFP, EV + mRELN, DAB1 + GFP, DAB1 + mRELN, 5F + GFP, 5F + mRELN) used for the experiments of this doctoral thesis made it possible to efficiently distinguish between the effects of *Reelin* and *DAB1* on glioblastoma cells. A distinction can be made between cellular phenotypes that are mediated through *DAB1* independently of *Reelin* (DAB1 + GFP), characteristics that are communicated by *Reelin* independently of *DAB1* (EV + mRELN and 5F + mRELN) and between effects that are a combination caused by interaction of both proteins in terms of direct activation of *DAB1* through *Reelin* (DAB1 + mRELN).

5.2.1 Cell migration

The results of the cell migration assay presented in *chapter 4.2* clearly show that *Reelin/DAB1* signaling has a significant impact on the motility of both U87 and U251 cells. These results also suggest that the activation of *DAB1* through *Reelin* is rather less important compared to the effects that each of these proteins itself exerts on reduction of cell migration. Furthermore, experiments proved that the results obtained here are clearly dependent on the cell type and, to a lesser extent, also dependent on the extracellular environment (fibronectin or laminin).

Considered more specifically, for U87 on fibronectin, a significant effect on cellular motility is observed in cells that express the 5F *DAB1* mutant when treated with *Reelin*, suggesting a strong influence of *Reelin* independently of *DAB1* on cell migration. Nonetheless, data also shows that *DAB1* independently of *Reelin* is reducing cell motility to values that are nearly significant. However, cells that are treated with *Reelin* and are overexpressing *DAB1*, only show little reduction of cell migration, proposing that *Reelin/DAB1* interaction has a rather minor role compared to *Reelin* and *DAB1* themselves.

For U87 cells on laminin, nearly similar results as on fibronectin can be found. Again, an effect of *Reelin* independently of *DAB1* but also influences of *DAB1* independently of *Reelin*

were observed in the assays. Furthermore, interplay of *Reelin* and *DAB1* did not have any effect on migration of U87 cells.

In the U251 cell line, significant changes can only be found for *DAB1* independently of *Reelin* on both fibronectin and laminin. Neither *Reelin* alone nor the interaction of *Reelin* and *DAB1* are significantly reducing migration in these cells. As mentioned above, the VLDLR and ApoER2 ligand *Thrombospondin-1*, expressed only by U251 and not by U87 cells, might cause this finding. However, other alternative molecular interactions leading to elevated levels of phosphorylated *DAB1* might serve as a possible explanation for results found in this assay. Since *Reelin* barely effects the migration of these cells, but, on the other hand, a significant change of cell motility is observed in cells overexpressing the *DAB1* protein, it appears plausible that *DAB1* is already activated in U251 cells. These findings are in accordance with the results obtained in western blotting with anti-*DAB1* and anti-Phospho-*DAB1* antibodies as explained in *chapter 5.1*. Nonetheless, it remains unclear which biochemical mechanisms cause constitutive activation of *DAB1* in U251, but by identifying an upregulated expression of *Thrombospondin-1* in these cells a reasonable explanation was found.

Besides *Reelin* and *Thrombospondin-1*, other ligands of the VLDLR and ApoER2, e.g. clusterin and ApoE might influence the changes of migratory behavior observed here. Clusterin, also known as apolipoprotein J, is a glycoprotein with broad tissue distribution and capable of triggering *Reelin*-like signaling via phosphorylation of *DAB1* in neurons (Leeb et al. 2014). In addition, Apolipoprotein E, which is carrying cholesterol and phospholipids is a very common ligand for lipoprotein receptors like VLDLR and ApoER2 and is important for neuronal synaptogenesis. Apart from this, Apolipoprotein E might also be influencing *Reelin/DAB1* signaling due to its receptor affinity (Boyles et al. 1989, Herz & Chen 2006).

Analysis of U251 cells on laminin (see *chapter 4.2.2, Figure 18*), revealed that there was a tendency to decreased cell migration for all tested cells (EV, DAB1 and 5F) after *Reelin* treatment that might be obscured by the influences of *DAB1*. Modulation of the laminin receptor ($\alpha3\beta1$ integrin) and inhibition of neuronal migration via *Reelin* independently of *DAB1* phosphorylation might be a plausible explanation here (Dulabon et al. 2000). Furthermore, a significant effect of *Reelin* independently of *DAB1* was also found in U87 cells on laminin. It therefore appears possible that the direct interaction of *Reelin* and $\alpha3\beta1$ integrin might be of importance for glioma cell migration.

With regards to the migration assay of U87 and U251 cells on fibronectin, latest research revealed that *Reelin* can activate the fibronectin receptor ($\alpha5\beta1$ integrin) via an intracellular pathway that involves *DAB1* as a signaling molecule leading to activation of neuronal adhesion (Sekine et al. 2012). The data raised in this doctoral thesis underlines that this signaling cascade might also play a role in gliomas, as U87 cells and U251 cells overexpressing *DAB1*, exhibited the lowest migratory velocities after *Reelin* treatment (see *chapter 4.2.1, Figure 17* and *Figure 18*). The influences of *Reelin* via this pathway might be obscured due to the strong effect of *DAB1* alone, especially in U251.

In conclusion, it must be stated that the relationships in *Reelin/DAB1* signaling are complex. They may be influenced by alternative ligand binding, extracellular matrix molecules and integrin receptors and other additional molecular factors yet unknown.

Figure 28 is presenting the hypothetical pathways of *Reelin/DAB1* signaling including $\alpha3\beta1$ and $\alpha5\beta1$ integrin. Results of this work suggest that these molecular interactions are of notable importance for glioblastoma cell migration.
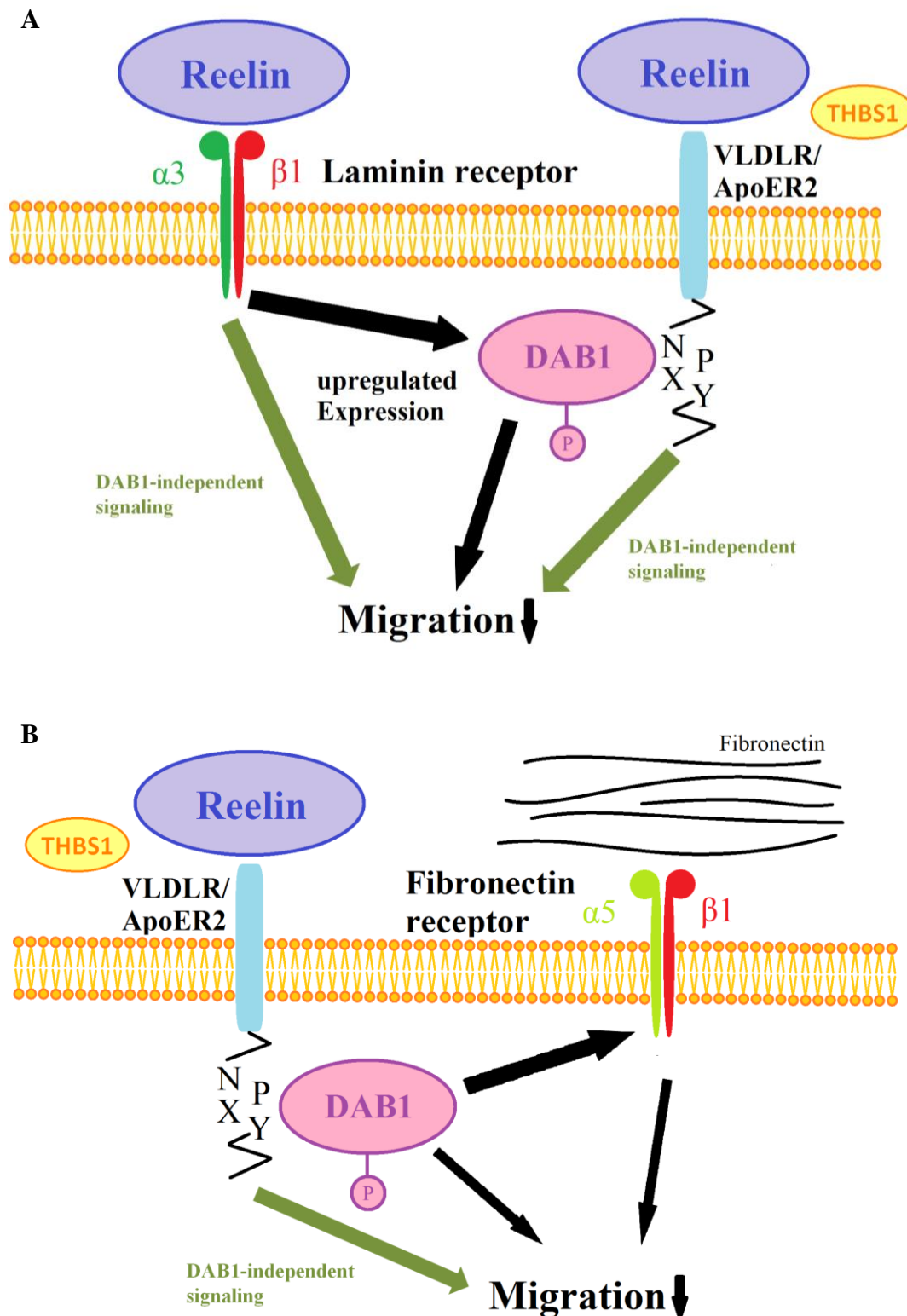
Figure 28: Hypothetical pathway of Reelin interacting with the laminin receptor (α3β1) (A) and of modulating the fibronectin receptor (α5β1) (B) in glioblastoma cells leading to decreased migration. Apart from *Reelin*, other ligands of the VLDL lipoprotein receptor (VLDLR) and the Apolipoprotein E receptor 2 (ApoER2), like Thromobospondin-1 (THBS1), might influence this signaling pathway.
(A) Laminin receptor (α3β1): *Reelin* is known to bind α3β1 integrin leading to upregulated expression of *DAB1* in neurons (Dulabon et al. 2000). Data of this work suggests that similar mechanisms might cause inhibition of migration due to *Reelin/DAB1* signaling in glioblastomas.
(B) Fibronectin receptor (α5β1): It is known that *Reelin* can activate α5β1 integrin via intracellular phosphorylation of *DAB1* in neurons (Sekine et al. 2012). Similar interactions might also lead to reduced cell migration in glioblastoma cells in response to *Reelin/DAB1* signaling.

Briefly summarized, the migration assays showed that *Reelin*/*DAB1* signaling is reducing migration indicating tumor suppressive functions for glioblastoma cells. However, data reveals that it is not necessarily a direct activation of *DAB1* through *Reelin* that exerts the strongest influence on the phenotypes observed here. It is much more probable that both proteins exert individual and partly independent effects on cell motility that might include *Reelin* interactions with α3β1 and α5β1 integrins on the one hand and *DAB1* activation through alternative ligand binding on the other hand.

5.2.2   Matrigel invasion assay

To pursue the promising results found for glioma cell migration on laminin and fibronectin, a Matrigel invasion assay was performed to study the behavior of U87 and U251 cells in a 3D environment after activation of the *Reelin/DAB1* signaling pathway. However, opposed to the migration assay, only cell line specific effects could be observed in this assay.

Chapter 4.3 and *Figure 19* clearly show that *Reelin* and *DAB1* have tumor suppressive functions for U87 in terms of reduced migration through matrigel. Here, the lowest amount of cells was counted for *DAB1*-overexpressing cells after *Reelin* treatment (DAB1 + mRELN). However, *DAB1* alone without *Reelin* stimulation (DAB1 + GFP) already has nearly the same effect on U87 cells opposed to control cells, suggesting primarily an influence of *DAB1* independently of *Reelin* on cell invasion. The fact, that cells overexpressing the 5F mutant of *DAB1* show values that are much higher than in DAB1 or EV cells, affirms this hypothesis. All of these results support the theory of *Reelin/DAB1* being able to reduce invasion of U87 glioblastoma cells. However, it can not be explained why *Reelin* seems to have some minor pro-invasive capabilities in empty vector cells as invasion was increased after *Reelin* stimulation (EV + mRELN).

Opposed to U87 cells, the invasion assay for U251 shows a completely different result: Cells overexpressing the 5F mutant of *DAB1* show drastically reduced invasive properties compared to EV and DAB1 cells. Additionally, preliminary experiments for U251 with self-coated invasion chambers gave results that hinted towards the same direction exhibiting a reduced amount of 5F cells that were capable of migrating through Matrigel. If *Reelin* and *DAB1* had the same tumor suppressive functions in U251 as for U87 cells, one would rather

expect decreased invasion for cells overexpressing the wildtype *DAB1* than the inactive 5F mutant.

A possible explanation for this finding might be that the complex protein mixture of Matrigel, containing mainly the structural proteins laminin, entactin, collagen and heparan sulfate proteoglycans (Hughes et al. 2010), is additionally triggering unknown signaling pathways in U251, other than in U87, causing the pro-invasive phenotype observed in 5F mutants.

However, as mentioned before, the data raised for U251 has to be interpreted with caution as the standard deviations presented in *Table 6* and *Table 7* of *chapter 4.3* are varying up to 88% especially in 5F cells whereas standard deviations up to only 30 or 40% are generally accepted as reliable. It appears that these glioblastoma cells might not be suitable for this kind of invasion assay or that further, very time-consuming adaptations of the protocol would be necessary to generate trustworthy results.

Generally spoken, the extremely high standard deviations of this invasion assay are casting doubts upon the reliability of these experiments. In conclusion, a clear statement cannot be made whether *Reelin/DAB1* signaling is reducing invasiveness of glioblastoma cells in general and further research is needed. However, at least for U87 cells, the invasion assay seems to point in a similar direction as the migration assays. Further research, implying other invasion assays or adaptations to the existing protocol are still necessary to accurately evaluate what kind of effects *Reelin/DAB1* signaling has on glioblastoma cell invasion.

5.2.3 Cofilin, actin cytoskeleton and other downstream targets

As the results found in the migration assay suggest tumor suppressive functions of *Reelin* and *DAB1*, potential downstream targets that might mediate the effects of *Reelin* and *DAB1* were examined.

It is already known that *Reelin/DAB1* signaling leads to activation of the *LIM kinases 1* and *2* which convert cofilin into a phosphorylated/inactive form in neurons. This inactive form is no longer capable of disassembling filamentous (F)-actin and is therefore promoting actin polymerization and cytoskeletal stability. As a consequence, actin turnover is suppressed and cell motility reduced (Chai et al. 2009, Kruger et al. 2010).

For this doctoral thesis, the levels of phosphorylated/inactive cofilin were analyzed via both Phos-tag^{TM} western blotting and immunocytochemistry. Data suggests that the mechanism of

cofilin inactivation described above might also be present in glioblastoma cells, because a significant increase of phosphorylated cofilin was observed after *Reelin* stimulation for U87 cells overexpressing *DAB1*. U251 cells overexpressing *DAB1* also exhibited increased, yet not significant levels of inactive cofilin. However, these changes could only be found for the immunocytochemical assay where cells were cultured on laminin. For Phos-tag^{TM} western blotting, cells were cultured on uncoated dishes and no significant changes were detected. Probably, the extracellular matrix – in this case laminin – plays an important role as trigger for such molecular interactions. This finding emphasizes the relevance of integrins, like e.g. α3β1 or α5β1 integrin, for the function of *Reelin/DAB1* signaling as it has already been explained in *chapter 5.2.1*.

Nonetheless, the changes of phosphorylated cofilin observed here are rather minor alterations and do not exceed the values of control cells by more than 20 to 25%. Therefore, it appears probable that *Reelin/DAB1* might also trigger different, unknown pathways which regulate the cytoskeleton and contribute to reduced cell migration. It is already known that *Reelin* is capable of inactivating the neuronal Wiskott-Aldrich syndrome protein (N-WASP) which should also stabilize the actin cytoskeleton and reduce the formation of filopodia (Tang et al. 2013).

Besides cofilin, also actin levels and cell morphology were examined via immunocytochemistry for this doctoral thesis. However, neither analyses of actin levels nor evaluation of cell morphological changes generated data that suggests connections between *Reelin/DAB1* signaling and the actin cytoskeleton as a mediator for cell migration.

These findings might suggest that the influence of *Reelin/DAB1* signaling on cofilin and actin is of rather minor importance for migration of glioblastoma cells. On the other hand, new questions arise about the underlying mechanisms causing the tumor suppressive functions of *Reelin* and *DAB1* in glioblastomas. Possibly, interaction of *Reelin/DAB1* with microtubules through τ-protein might be important (Hiesberger et al. 1999). Additionally, *in vitro* analyses suggested that contraction of myosin II behind the nuclei and endocytosis of adhesion molecules just proximal to the cell somata are involved in neuronal migration (Schaar BT et al. 2005, Shieh JC et al. 2011). Similar molecular interactions might mediate the influences of *Reelin* and *DAB1* on migration of glioblastoma cells, too. Studying such underlying biochemical mechanisms of *Reelin/DAB1* signaling exceeded the scope of this doctoral thesis, thus further research is needed.

As far as the other analyzed downstream targets are concerned (Kip1/p27, STAT3, focal adhesion kinase and the overall tyrosine phosphorylation via the 4G10 antibody), none of these proteins showed significant changes in response to *Reelin* and *DAB1*. All of these western blots were performed using lysates of glioblastoma cells that had been cultured on uncoated dishes. As mentioned earlier, data of this doctoral thesis suggests that the functions of *Reelin* and *DAB1* are linked to cell-matrix interaction. Probably, experiments should be repeated with laminin- or fibronectin-coated culture dishes.

5.3   Conclusions

This doctoral thesis analyzes the in vitro biochemical influences of *Reelin/DAB1* signaling on migration and invasion of highly-malignant astrocytic tumors *in vitro*. The classical glioblastoma cell lines U87 and U251 were used here. This monography also makes a contribution to the understanding of further involved intracellular targets that mediate the effects of these signaling proteins on a molecular level.

To sum up, the data raised within this doctoral thesis clearly demonstrates that *Reelin* and *DAB1* both have tumor suppressive functions in terms of reducing migration of glioblastoma cells. However, results indicate that it is not necessarily only the direct activation of *DAB1* through *Reelin* but that both proteins, independently of each other, are capable of inhibiting migration. Additionally, data suggests that cell-matrix interactions probably via integrins might as well play a crucial role for the tumor suppressive functions of *Reelin* and *DAB1*.

Despite numerous efforts, it remained uncertain through which downstream targets *Reelin/DAB1* signaling mediates the phenotypical changes in glioblastomas observed in this doctoral thesis. Potential follow-up studies on this topic could imply investigation on signaling intermediates on laminin- or fibronectin-coated culture dishes. The research on *Reelin/DAB1* signaling in glioblastomas will be continued by the research lab of the Department of Neuropathology at the University Hospital of Regensburg.

Parts of this work were published in the research acrticle "RELN signaling modulates glioblastoma growth and substrate-dependent migration" in *Brain Pathology* on the 10th of January 2018 (Schulze et al. 2017).

6   Abstract

The proteins *Reelin* and *Disabled-1* (*DAB1*) are known to be key regulators in embryonal development of the central nervous system by controlling neuronal migration. Latest research revealed that *Reelin/DAB1* signaling exhibits tumor suppressive functions in several cancers (e.g. hepatocellular carcinoma, breast cancer, esophageal cancer or pancreatic cancer), but until now, effects of *Reelin* and *DAB1* on brain tumors were mostly unknown. As previous work of our laboratory indicated frequent epigenetic inactivation of *Reelin* in high-grade gliomas, research was pursued by examining the motility of glioblastoma cells in response to *Reelin/DAB1* signaling.

In the present doctoral thesis, migration and invasion of U87 and U251 cells, overexpressing either the intracellular protein *DAB1* or the corresponding inactive 5F mutant, was analyzed after *Reelin* stimulation. Both, U87 and U251 cells, showed significantly reduced migration on fibronectin and laminin under the influence of *Reelin* and *DAB1*. Further data suggests that effects of *DAB1*-independent *Reelin* signaling, as e.g. on integrins ($\alpha3\beta1$ and $\alpha5\beta1$ integrin, for example), might contribute considerably to the tumor suppressive functions of this pathway. Besides this, also *Reelin*-independent *DAB1* effects induced by other upstream mediators might play a major role in regulating glioblastoma invasion. Further experiments comprised matrigel invasion assays as well as the investigation of the underlying downstream targets of *Reelin* and *DAB1*.

Taken together, *Reelin* and *DAB1* were identified as novel players in the regulation of glioblastoma cell migration suggesting tumor suppressive functions of *Reelin/DAB1* signaling in high-grade gliomas.

7 Deutschsprachige Zusammenfassung

Die Proteine *Reelin* und *Disabled-1* (*DAB1*) sind bekannt für ihren bedeutenden Einfluss auf die Migration von Neuronen während der embryonalen Entwicklung des zentralen Nervensystems. Neueste Untersuchungen zeigen, dass der *Reelin/DAB1* Signalweg auch Tumor-supprimierende Wirkungen in zahlreichen Karzinomen, wie beispielsweise dem Mamma-, Ösophagus-, Pankreas- oder heptatozellulären Karzinom, aufweist. Dennoch ist die Bedeutung von *Reelin* und *DAB1* für gliale Tumoren bis dato weitestgehend unbekannt. Da frühere Arbeiten unseres Labors eine epigenetische Inaktivierung von *Reelin* in hochgradig malignen Gliomen ergaben, wurden diese Ergebnisse durch Motilitäts-Analysen von Glioblastomzellen nach Modulation des *Reelin/DAB1* Signalweges weitergehend funktionell untersucht.

Die vorliegende Doktorarbeit untersuchte die Migration und Invasion von U87 und U251 Glioblastomzellen, die entweder das intrazelluläre Protein *DAB1* oder das inaktivierte 5F *DAB1* überexprimierten. Die Experimente erfolgten ohne oder mit Stimulation durch *Reelin*. Sowohl U87, als auch U251 Zellen zeigten hier signifikant verminderte Migration auf Fibronektin und Laminin unter dem Einfluss von *Reelin* und *DAB1*. Darüberhinaus lassen unsere Daten erkennen, dass *Reelin* auch *DAB1*-unabhängige Effekte auf die Migration zeigt (z.B. durch $\alpha3\beta1$ und $\alpha5\beta1$ Integrin vermittelt). Außerdem ergaben sich auch Hinweise auf *Reelin*-unabhängige *DAB1*-Effekte auf die Migration, die z.B. durch alternative vorgeschaltete Mediatoren induziert werden. Weitere Experimente in dieser Doktorarbeit umfassen Matrigel-basierte Invasions-Assays und eine Analyse möglicher nachgeschalteter Moleküle im *Reelin/DAB1*-Signalweg.

Zusammengefasst konnten *Reelin* und *DAB1* im Rahmen dieser Doktorarbeit als neue Regulatoren der Migration in Glioblastomen nachgewiesen werden, was belegt, dass der *Reelin/DAB1* Signalweg in hochgradig malignen Gliomen Tumor-supprimierende Funktionen besitzt.

8 References

Alcantara Llaguno S, Chen J, Kwon C, Jackson EL, Li Y, et al. 2009. Malignant astrocytomas originate from neural stem/progenitor cells in a somatic tumor suppressor mouse model. *Cancer cell* 15 (1):45–56

Arnaout MA, Goodman SL, Xiong J. 2007. Structure and mechanics of integrin-based cell adhesion. *Cell to cell contact and extracellular matrix* 19 (5):495–507

Arnaud L, Ballif BA, Cooper JA. 2003. Regulation of Protein Tyrosine Kinase Signaling by Substrate Degradation during Brain Development. *Molecular and Cellular Biology* 23 (24):9293–302

Becker AJ, Klein H, Baden T, Aigner L, Normann S, et al. 2002. Mutational and expression analysis of the reelin pathway components CDK5 and doublecortin in gangliogliomas. *Acta neuropathologica* 104 (4):403–08

Beckman G, Beckman L, Ponten J, Westermark B. 1971. G-6-PD and PGM phenotypes of 16 continuous human tumor cell lines. Evidence against cross-contamination and contamination by HeLa cells. *Human heredity* 21 (3):238–41

Beffert U, Morfini G, Bock HH, Reyna H, Brady ST, Herz J. 2002. Reelin-mediated signaling locally regulates protein kinase B/Akt and glycogen synthase kinase 3beta. *The Journal of biological chemistry* 277 (51):49958–64

Blake SM, Strasser V, Andrade N, Duit S, Hofbauer R, Schneider WJ, Nimpf J. 2008. Thrombospondin-1 binds to ApoER2 and VLDL receptor and functions in postnatal neuronal migration. *The EMBO journal* 27 (22):3069–80

Bleeker FE, Lamba S, Zanon C, Molenaar RJ, Hulsebos TJM, et al. 2014. Mutational profiling of kinases in glioblastoma. *BMC Cancer* 14 (1):718

Bock HH, Herz J. 2003. Reelin activates SRC family tyrosine kinases in neurons. *Curr. Biol.* 13 (1):18–26

Borm B, Requardt RP, Herzog V, Kirfel G. 2005. Membrane ruffles in cell migration: indicators of inefficient lamellipodia adhesion and compartments of actin filament reorganization. *Experimental cell research* 302 (1):83–95

Boyles JK, Zoellner CD, Anderson LJ, Kosik LM, Pitas RE, et al. 1989. A role for apolipoprotein E, apolipoprotein A-I, and low density lipoprotein receptors in cholesterol

transport during regeneration and remyelination of the rat sciatic nerve. *The Journal of clinical investigation* 83 (3):1015–31

Brennan CW, Verhaak RGW, McKenna A, Campos B, Noushmehr H, et al. 2013. The somatic genomic landscape of glioblastoma. *Cell* 155 (2):462–77

Brunne B, Franco S, Bouché E, Herz J, Howell BW, et al. 2013. Role of the postnatal radial glial scaffold for the development of the dentate gyrus as revealed by Reelin signaling mutant mice. *Glia* 61 (8):1347–63

Cahill DP, Louis DN, Cairncross JG. 2015. Molecular background of oligodendroglioma. 1p/19q, IDH, TERT, CIC and FUBP1. *CNS Oncology* 4 (5):287–94

Cairncross G, Berkey B, Shaw E, Jenkins R, Scheithauer B, et al. 2006. Phase III trial of chemotherapy plus radiotherapy compared with radiotherapy alone for pure and mixed anaplastic oligodendroglioma: Intergroup Radiation Therapy Oncology Group Trial 9402. *Journal of clinical oncology : official journal of the American Society of Clinical Oncology* 24 (18):2707–14

Carpenter AE, Jones TR, Lamprecht MR, Clarke C, Kang IH, et al. 2006. CellProfiler: image analysis software for identifying and quantifying cell phenotypes. *Genome Biol.* 7 (10):R100

Ceccarelli M, Barthel FP, Malta TM, Sabedot TS, Salama SR, et al. 2016. Molecular Profiling Reveals Biologically Discrete Subsets and Pathways of Progression in Diffuse Glioma. *Cell* 164 (3):550–63

Chai X, Forster E, Zhao S, Bock HH, Frotscher M. 2009. Reelin stabilizes the actin cytoskeleton of neuronal processes by inducing n-cofilin phosphorylation at serine3. *J Neurosci* 29 (1):288–99

Chamberlain MC, Glantz MJ, Chalmers L, van Horn A, Sloan AE. 2007. Early necrosis following concurrent Temodar and radiotherapy in patients with glioblastoma. *Journal of neuro-oncology* 82 (1):81–83

CopperKettle. 2013. *Schema_of_the_Reelin_protein_vertical_en.png (PNG-Grafik, 350 × 1280 Pixel) - Skaliert (47%).* URL: https://upload.wikimedia.org/wikipedia/commons/d/d4/Schema_of_the_Reelin_protein_vertical_en.png

Cordelières F. 2011. *Manual Tracking*. URL: http://rsbweb.nih.gov/ij/plugins/track/track.html

Coyle JT. 2006. Glutamate and schizophrenia: beyond the dopamine hypothesis. *Cellular and molecular neurobiology* 26 (4-6):365–84

References

D'Arcangelo G, Miao GG, Chen SC, Soares HD, Morgan JI, Curran T. 1995. A protein related to extracellular matrix proteins deleted in the mouse mutant reeler. *Nature* 374 (6524):719–23

D'Arcangelo G, Nakajima K, Miyata T, Ogawa M, Mikoshiba K, Curran T. 1997. Reelin is a secreted glycoprotein recognized by the CR-50 monoclonal antibody. *The Journal of neuroscience : the official journal of the Society for Neuroscience* 17 (1):23–31

DeSilva U, D'Arcangelo G, Braden VV, Chen J, Miao GG, Curran T, Green ED. 1997. The human reelin gene. Isolation, sequencing, and mapping on chromosome 7. *Genome Research* 7 (2):157–64

Dietmaier W, Lorenz J, Riemenschneider MJ. 2015. Molekulare Diagnostik in der Neuropathologie. *Der Pathologe* 36 (2):171–80

Dulabon L, Olson EC, Taglienti MG, Eisenhuth S, McGrath B, et al. 2000. Reelin binds alpha3beta1 integrin and inhibits neuronal migration. *Neuron* 27 (1):33–44

Falconer DS. 1951. Two new mutants, 'trembler' and 'reeler', with neurological actions in the house mouse (Mus musculus L.). *Journ. of Genetics* 50 (2):192–205

Farrell CJ, Plotkin SR. 2007. Genetic causes of brain tumors: neurofibromatosis, tuberous sclerosis, von Hippel-Lindau, and other syndromes. *Neurologic clinics* 25 (4):925-46, viii

Fatemi SH, Earle JA, McMenomy T. 2000. Reduction in Reelin immunoreactivity in hippocampus of subjects with schizophrenia, bipolar disorder and major depression. *Molecular psychiatry* 5 (6):654-63, 571

Fatemi SH, Snow AV, Stary JM, Araghi-Niknam M, Reutiman TJ, et al. 2005. Reelin signaling is impaired in autism. *Biological psychiatry* 57 (7):777–87

Feinstein Y, Borrell V, Garcia C, Burstyn-Cohen T, Tzarfaty V, et al. 1999. F-spondin and mindin: two structurally and functionally related genes expressed in the hippocampus that promote outgrowth of embryonic hippocampal neurons. *Development (Cambridge, England)* 126 (16):3637–48

Förster E, Tielsch A, Saum B, Weiss KH, Johanssen C, et al. 2002. Reelin, Disabled 1, and beta 1 integrins are required for the formation of the radial glial scaffold in the hippocampus. *Proceedings of the National Academy of Sciences of the United States of America* 99 (20):13178–83

Frappaz D, Mornex F, Saint-Pierre G, Ranchere-Vince D, Jouvet A, et al. 1999. Bone metastasis of glioblastoma multiforme confirmed by fine needle biopsy. *Acta neurochirurgica* 141 (5):551–52

References

Friedmann-Morvinski D, Friedmann-Morvinski D, FBushong EA, Bushong EA, FKe E, et al. 2012. Dedifferentiation of neurons and astrocytes by oncogenes can induce gliomas in mice. *Science (New York, N.Y.)* 338 (6110):1080–84

Goffinet AM. 1984. Events governing organization of postmigratory neurons: studies on brain development in normal and reeler mice. *Brain research* 319 (3):261–96

Haas CA, Dudeck O, Kirsch M, Huszka C, Kann G, et al. 2002. Role for reelin in the development of granule cell dispersion in temporal lobe epilepsy. *The Journal of neuroscience : the official journal of the Society for Neuroscience* 22 (14):5797–802

Hall A. 1998. Rho GTPases and the actin cytoskeleton. *Science* 279 (5350):509–14

Hamada S, Yagi T. 2001. The cadherin-related neuronal receptor family: a novel diversified cadherin family at the synapse. *Neuroscience research* 41 (3):207–15

Hartfuss E, Förster E, Bock HH, Hack MA, Leprince P, et al. 2003. Reelin signaling directly affects radial glia morphology and biochemical maturation. *Development (Cambridge, England)* 130 (19):4597–609

Hegi ME, Diserens A, Gorlia T, Hamou M, Tribolet N de, et al. 2005. MGMT gene silencing and benefit from temozolomide in glioblastoma. *The New England journal of medicine* 352 (10):997–1003

Heinrich C, Nitta N, Flubacher A, Müller M, Fahrner A, et al. 2006. Reelin deficiency and displacement of mature neurons, but not neurogenesis, underlie the formation of granule cell dispersion in the epileptic hippocampus. *The Journal of neuroscience : the official journal of the Society for Neuroscience* 26 (17):4701–13

Herz J, Chen Y. 2006. Reelin, lipoprotein receptors and synaptic plasticity. *Nat. Rev. Neurosci.* 7 (11):850–59

Hiesberger T, Trommsdorff M, Howell BW, Goffinet A, Mumby MC, Cooper JA, Herz J. 1999. Direct binding of Reelin to VLDL receptor and ApoE receptor 2 induces tyrosine phosphorylation of disabled-1 and modulates tau phosphorylation. *Neuron* 24 (2):481–89

Honda T, Kobayashi K, Mikoshiba K, Nakajima K. 2011. Regulation of cortical neuron migration by the Reelin signaling pathway. *Neurochem. Res.* 36 (7):1270–79

Hong SE, Shugart YY, Huang DT, Shahwan SA, Grant PE, et al. 2000. Autosomal recessive lissencephaly with cerebellar hypoplasia is associated with human RELN mutations. *Nature genetics* 26 (1):93–96

Howell BW, Gertler FB, Cooper JA. 1997a. Mouse disabled (mDab1): a Src binding protein implicated in neuronal development. *The EMBO journal* 16 (1):121–32

Howell BW, Hawkes R, Soriano P, Cooper JA. 1997b. Neuronal position in the developing brain is regulated by mouse disabled-1. *Nature* 389 (6652):733–37

Howell BW, Herrick TM, Hildebrand JD, Zhang Y, Cooper JA. 2000. Dab1 tyrosine phosphorylation sites relay positional signals during mouse brain development. *Curr. Biol.* 10 (15):877–85

Hughes CS, Postovit LM, Lajoie GA. 2010. Matrigel: a complex protein mixture required for optimal growth of cell culture. *Proteomics* 10 (9):1886–90

Huse JT, Holland E, DeAngelis LM. 2013. Glioblastoma. Molecular Analysis and Clinical Implications. *Annu. Rev. Med.* 64 (1):59–70

Ikeda Y, Terashima T. 1997. Expression of reelin, the gene responsible for the reeler mutation, in embryonic development and adulthood in the mouse. *Dev. Dyn.* 210 (2):157–72

Jossin Y, Goffinet AM. 2007. Reelin signals through phosphatidylinositol 3-kinase and Akt to control cortical development and through mTor to regulate dendritic growth. *Mol. Cell. Biol.* 27 (20):7113–24

Kaatsch P. 2010. Epidemiology of childhood cancer. *Cancer treatment reviews* 36 (4):277–85

Kam R, Chen J, Blümcke I, Normann S, Fassunke J, et al. 2004. The reelin pathway components disabled-1 and p35 in gangliogliomas--a mutation and expression analysis. *Neuropathology and applied neurobiology* 30 (3):225–32

Keshvara L, Magdaleno S, Benhayon D, Curran T. 2002. Cyclin-dependent kinase 5 phosphorylates disabled 1 independently of Reelin signaling. *J. Neurosci.* 22 (12):4869–77

Kinoshita E, Kinoshita-Kikuta E, Takiyama K, Koike T. 2006. Phosphate-binding tag, a new tool to visualize phosphorylated proteins. *Mol. Cell Proteomics* 5 (4):749–57

Kleihues P, Louis DN, Scheithauer BW, Rorke LB, Reifenberger G, Burger PC, Cavenee WK. 2002. The WHO classification of tumors of the nervous system. *Journal of neuropathology and experimental neurology* 61 (3):215-25; discussion 226-9

Kreidberg JA. 2000. Functions of alpha3beta1 integrin. *Curr. Opin. Cell Biol.* 12 (5):548–53

Kruger MT, Zhao S, Chai X, Brunne B, Bouche E, Bock HH, Frotscher M. 2010. Role for Reelin-induced cofilin phosphorylation in the assembly of sympathetic preganglionic neurons in the murine intermediolateral column. *Eur J Neurosci* 32 (10):1611–17

Lacroix M, Abi-Said D, Fourney DR, Gokaslan ZL, Shi W, et al. 2001. A multivariate analysis of 416 patients with glioblastoma multiforme: prognosis, extent of resection, and survival. *Journal of neurosurgery* 95 (2):190–98

References

Laemmli UK. 1970. Cleavage of structural proteins during the assembly of the head of bacteriophage T4. *Nature* 227 (5259):680–85

Leeb C, Eresheim C, Nimpf J. 2014. Clusterin Is a Ligand for Apolipoprotein E Receptor 2 (ApoER2) and Very Low Density Lipoprotein Receptor (VLDLR) and Signals via the Reelin-signaling Pathway. *J. Biol. Chem.* 289 (7):4161–72

Leemhuis J, Bock HH. 2011. Reelin modulates cytoskeletal organization by regulating Rho GTPases. *Commun Integr Biol* 4 (3):254–57

Libermann TA, Nusbaum HR, Razon N, Kris R, Lax I, et al. 1985. Amplification, enhanced expression and possible rearrangement of EGF receptor gene in primary human brain tumours of glial origin. *Nature* 313 (5998):144–47

Livak KJ, Schmittgen TD. 2001. Analysis of relative gene expression data using real-time quantitative PCR and the 2(-Delta Delta C(T)) Method. *Methods (San Diego, Calif.)* 25 (4):402–08

Louis DN, ed. 2007. *WHO classification of tumours of the central nervous system. [this book reflects the views of a working group that convened for an editorial and consensus conference at the German Cancer Research Center (DKFZ), Heidelberg, November 17 - 18, 2006].* Lyon: Internat. Agency for Research on Cancer. 4. ed.

Louis DN, Ohgaki H, Wiestler OD, Cavenee WK, Burger PC, et al. 2007. The 2007 WHO classification of tumours of the central nervous system. *Acta neuropathologica* 114 (2):97–109

Louis DN, Perry A, Reifenberger G, Deimling A von, Figarella-Branger D, et al. 2016. The 2016 World Health Organization Classification of Tumors of the Central Nervous System: a summary. *Acta neuropathologica* 131 (6):803–20

Lund-Johansen M, Bjerkvig R, Humphrey PA, Bigner SH, Bigner DD, Laerum OD. 1990. Effect of epidermal growth factor on glioma cell growth, migration, and invasion in vitro. *Cancer research* 50 (18):6039–44

Malmstrom A, Gronberg BH, Marosi C, Stupp R, Frappaz D, et al. 2012. Temozolomide versus standard 6-week radiotherapy versus hypofractionated radiotherapy in patients older than 60 years with glioblastoma: the Nordic randomised, phase 3 trial. *The Lancet. Oncology* 13 (9):916–26

Manning BD, Cantley LC. 2007. AKT/PKB signaling: navigating downstream. *Cell* 129 (7):1261–74

Masonoda. *pIRESNeo2 vector.* URL: http://img51.chem17.com/1/20130906/635140635398218871960.pdf

References

Medical Disability Guidelines. 2012. *Astrocytoma.* URL: http://www.mdguidelines.com/astrocytoma

Mori S, Rönnstrand L, Yokote K, Engström A, Courtneidge SA, Claesson-Welsh L, Heldin CH. 1993. Identification of two juxtamembrane autophosphorylation sites in the PDGF beta-receptor; involvement in the interaction with Src family tyrosine kinases. *The EMBO journal* 12 (6):2257–64

Muller PAJ, Vousden KH, Norman JC. 2011. p53 and its mutants in tumor cell migration and invasion. *The Journal of cell biology* 192 (2):209–18

Nakano Y, Kohno T, Hibi T, Kohno S, Baba A, et al. 2007. The extremely conserved C-terminal region of Reelin is not necessary for secretion but is required for efficient activation of downstream signaling. *The Journal of biological chemistry* 282 (28):20544–52

Nikiforova MN, Hamilton RL. 2011. Molecular diagnostics of gliomas. *Archives of pathology & laboratory medicine* 135 (5):558–68

Ohgaki H, Dessen P, Jourde B, Horstmann S, Nishikawa T, et al. 2004. Genetic pathways to glioblastoma: a population-based study. *Cancer research* 64 (19):6892–99

Ohgaki H, Kleihues P. 2005. Epidemiology and etiology of gliomas. *Acta neuropathologica* 109 (1):93–108

Ohkubo N, Lee Y, Morishima A, Terashima T, Kikkawa S, et al. 2003. Apolipoprotein E and Reelin ligands modulate tau phosphorylation through an apolipoprotein E receptor/disabled-1/glycogen synthase kinase-3beta cascade. *FASEB J.* 17 (2):295–97

Okamura Y, Nomoto S, Kanda M, Hayashi M, Nishikawa Y, et al. 2011. Reduced expression of reelin (RELN) gene is associated with high recurrence rate of hepatocellular carcinoma. *Ann. Surg. Oncol.* 18 (2):572–79

Omuro A. 2013. Glioblastoma and Other Malignant Gliomas. *JAMA* 310 (17):1842

Ostrom QT, Gittleman H, Blank PM de, Finlay JL, Gurney JG, et al. 2016. American Brain Tumor Association Adolescent and Young Adult Primary Brain and Central Nervous System Tumors Diagnosed in the United States in 2008-2012. *Neuro-Oncology* 18 (suppl 1):i1-i50

Pasquier B, Pasquier D, N'Golet A, Panh MH, Couderc P. 1980. Extraneural metastases of astrocytomas and glioblastomas: clinicopathological study of two cases and review of literature. *Cancer* 45 (1):112–25

Perrone G, Vincenzi B, Zagami M, Santini D, Panteri R, et al. 2007. Reelin expression in human prostate cancer: a marker of tumor aggressiveness based on correlation with grade.

Modern pathology : an official journal of the United States and Canadian Academy of Pathology, Inc 20 (3):344–51

Pollard TD, Borisy GG. 2003. Cellular motility driven by assembly and disassembly of actin filaments. *Cell* 112 (4):453–65

Riemenschneider MJ, Louis DN, Weller M, Hau P. 2013. Refined brain tumor diagnostics and stratified therapies. The requirement for a multidisciplinary approach. *Acta Neuropathol* 126 (1):21–37

Riemenschneider MJ, Mueller W, Betensky RA, Mohapatra G, Louis DN. 2005. In situ analysis of integrin and growth factor receptor signaling pathways in human glioblastomas suggests overlapping relationships with focal adhesion kinase activation. *The American journal of pathology* 167 (5):1379–87

Riemenschneider MJ, Reifenberger G. 2009. Molecular neuropathology of gliomas. *International journal of molecular sciences* 10 (1):184–212

Sato N, Fukushima N, Chang R, Matsubayashi H, Goggins M. 2006. Differential and epigenetic gene expression profiling identifies frequent disruption of the RELN pathway in pancreatic cancers. *Gastroenterology* 130 (2):548–65

Schaar BT BT, Schaar BT, FMcConnell SK, McConnell SK. 2005. Cytoskeletal coordination during neuronal migration. *Proceedings of the National Academy of Sciences of the United States of America* 102 (38):13652–57

Schlegel J, Merdes A, Stumm G, Albert FK, Forsting M, Hynes N, Kiessling M. 1994. Amplification of the epidermal-growth-factor-receptor gene correlates with different growth behaviour in human glioblastoma. *International journal of cancer. Journal international du cancer* 56 (1):72–77

Schlegel U, Weller M, Westphal M. 2003. *Neuroonkologie.* s.l.: THIEME. 2., erweiterte Auflage

Schneider CA, Rasband WS, Eliceiri KW. 2012. NIH Image to ImageJ. 25 years of image analysis. *Nat Meth* 9 (7):671–75

Schulze M, Fedorchenko O, Zink TG, Knobbe-Thomsen CB, Kraus S, et al. 2016. Chronophin is a glial tumor modifier involved in the regulation of glioblastoma growth and invasiveness. *Oncogene* 35 (24):3163–77

Schulze M, Violonchi C, Swoboda S, Welz T, Kerkhoff E, et al. 2017. RELN signaling modulates glioblastoma growth and substrate-dependent migration. *Brain pathology (Zurich, Switzerland)*

References

Schulze M. 2014. *Role of Chronophin for glioma cell migration and invasion*. *Doctoral thesis for a doctoral degree at the Graduate School of Life Sciences*. Dissertation, Julius-Maximilians-Universität Würzburg, Würzburg

Sekine K, Kawauchi T, Kubo K, Honda T, Herz J, et al. 2012. Reelin controls neuronal positioning by promoting cell-matrix adhesion via inside-out activation of integrin α5β1. *Neuron* 76 (2):353–69

Senzaki K, Ogawa M, Yagi T. 1999. Proteins of the CNR family are multiple receptors for Reelin. *Cell* 99 (6):635–47

Shieh JC JC, Shieh JC, FSchaar BT, Schaar BT, FSrinivasan K, et al. 2011. Endocytosis regulates cell soma translocation and the distribution of adhesion proteins in migrating neurons. *PloS one* 6 (3):e17802

Sigma-Aldrich. 2015. *Universal SYBR Green Quantitative PCR Protocol*. URL: http://www.sigmaaldrich.com/technical-documents/protocols/biology/sybr-green-qpcr.html

Smalheiser NR, Costa E, Guidotti A, Impagnatiello F, Auta J, et al. 2000. Expression of reelin in adult mammalian blood, liver, pituitary pars intermedia, and adrenal chromaffin cells. *Proc. Natl. Acad. Sci. U.S.A.* 97 (3):1281–86

Smirniotopoulos JG, Murphy FM, Rushing EJ, Rees JH, Schroeder JW. 2007. Patterns of contrast enhancement in the brain and meninges. *Radiographics : a review publication of the Radiological Society of North America, Inc* 27 (2):525–51

Sonoshita M, Itatani Y, Kakizaki F, Sakimura K, Terashima T, et al. 2015. Promotion of colorectal cancer invasion and metastasis through activation of NOTCH-DAB1-ABL-RHOGEF protein TRIO. *Cancer Discov* 5 (2):198–211

Stein T, Cosimo E, Yu X, Smith PR, Simon R, et al. 2010. Loss of reelin expression in breast cancer is epigenetically controlled and associated with poor prognosis. *Am. J. Pathol.* 177 (5):2323–33

Strasser V, Fasching D, Hauser C, Mayer H, Bock HH, et al. 2004. Receptor clustering is involved in Reelin signaling. *Molecular and Cellular Biology* 24 (3):1378–86

Stupp R, Mason WP, van den Bent, Martin J, Weller M, Fisher B, et al. 2005. Radiotherapy plus concomitant and adjuvant temozolomide for glioblastoma. *The New England journal of medicine* 352 (10):987–96

Suetsugu S, Tezuka T, Morimura T, Hattori M, Mikoshiba K, Yamamoto T, Takenawa T. 2004. Regulation of actin cytoskeleton by mDab1 through N-WASP and ubiquitination of mDab1. *Biochem. J.* 384 (Pt 1):1–8

Sugawa N, Ekstrand AJ, James CD, Collins VP. 1990. Identical splicing of aberrant epidermal growth factor receptor transcripts from amplified rearranged genes in human glioblastomas. *Proceedings of the National Academy of Sciences of the United States of America* 87 (21):8602–06

Takahara T, Ohsumi T, Kuromitsu J, Shibata K, Sasaki N, et al. 1996. Dysfunction of the Orleans reeler gene arising from exon skipping due to transposition of a full-length copy of an active L1 sequence into the skipped exon. *Human molecular genetics* 5 (7):989–93

Tang H, Li A, Bi J, Veltman DM, Zech T, et al. 2013. Loss of Scar/WAVE complex promotes N-WASP- and FAK-dependent invasion. *Curr. Biol.* 23 (2):107–17

Tonn J, Grossman SA, Rutka JT, Westphal M, eds. 2006. *Neuro-Oncology of CNS Tumors.* Berlin, Heidelberg: Springer-Verlag Berlin Heidelberg

Torsvik A, Stieber D, Enger PO, Golebiewska A, Molven A, et al. 2014. U-251 revisited: genetic drift and phenotypic consequences of long-term cultures of glioblastoma cells. *Cancer medicine* 3 (4):812–24

Tysnes BB, Haugland HK, Bjerkvig R. 1997. Epidermal growth factor and laminin receptors contribute to migratory and invasive properties of gliomas. *Invasion & metastasis* 17 (5):270–80

Violonchi C. 2009. *In situ-Analyse des Reelin-Signalweges in humanen Gliomen. Diplomarbeit zur Erlangung des akademischen Grades eines Diplom-Biologen.* Diplomarbeit, Heinrich-Heine-Universität, Düsseldorf

Walker MD, Alexander E, JR, Hunt WE, MacCarty CS, Mahaley MS, JR, et al. 1978. Evaluation of BCNU and/or radiotherapy in the treatment of anaplastic gliomas. A cooperative clinical trial. *Journal of neurosurgery* 49 (3):333–43

Wang Y, Yang J, Zheng H, Tomasek GJ, Zhang P, et al. 2009. Expression of mutant p53 proteins implicates a lineage relationship between neural stem cells and malignant astrocytic glioma in a murine model. *Cancer cell* 15 (6):514–26

Ware ML, Fox JW, González JL, Davis NM, Lambert de Rouvroit C, et al. 1997. Aberrant splicing of a mouse disabled homolog, mdab1, in the scrambler mouse. *Neuron* 19 (2):239–49

Watanabe T, Katayama Y, Yoshino A, Yachi K, Ohta T, et al. 2007. Aberrant hypermethylation of p14ARF and O6-methylguanine-DNA methyltransferase genes in astrocytoma progression. *Brain pathology (Zurich, Switzerland)* 17 (1):5–10

References

Weeber EJ, Beffert U, Jones C, Christian JM, Forster E, Sweatt JD, Herz J. 2002. Reelin and ApoE receptors cooperate to enhance hippocampal synaptic plasticity and learning. *The Journal of biological chemistry* 277 (42):39944–52

Yan H, Parsons DW, Jin G, McLendon R, Rasheed BA, et al. 2009. IDH1 and IDH2 mutations in gliomas. *The New England journal of medicine* 360 (8):765–73

Yasui N, Nogi T, Kitao T, Nakano Y, Hattori M, Takagi J. 2007. Structure of a receptor-binding fragment of reelin and mutational analysis reveal a recognition mechanism similar to endocytic receptors. *Proceedings of the National Academy of Sciences of the United States of America* 104 (24):9988–93

Yuan Y, Chen H, Ma G, Cao X, Liu Z. 2012. Reelin is involved in transforming growth factor-β1-induced cell migration in esophageal carcinoma cells. *PLoS ONE* 7 (2):e31802

Zhang Z, Morla AO, Vuori K, Bauer JS, Juliano RL, Ruoslahti E. 1993. The alpha v beta 1 integrin functions as a fibronectin receptor but does not support fibronectin matrix assembly and cell migration on fibronectin. *J Cell Biol* 122 (1):235–42

Zipper H, Brunner H, Bernhagen J, Vitzthum F. 2004. Investigations on DNA intercalation and surface binding by SYBR Green I, its structure determination and methodological implications. *Nucleic acids research* 32 (12):e103

9 Acknowledgements

First of all, thanks to the supervisor of my doctoral thesis, Prof. Dr. med. Markus Riemenschneider, for giving me the opportunity to receive my doctoral degree in the Department of Neuropathology at the University Hospital of Regensburg and for letting me work on this challenging but extremely fascinating topic. Thanks for the time invested in supervision, the excellent support during the whole process of this work and especially for the great experiences I was able to gain in this time.

Secondly, I would like to say thanks to Dr. Markus Schulze. He supported and supervised me during the whole time with his ideas and great knowledge. Thanks for all the useful discussions about the theoretical, practical and technical aspects of my work. Whenever I had questions or was faced with problems, I could count on his endless energy, great guidance and helpful advices. Thanks for all the support and and the great time I had working with you.

Furthermore, I would like to thank Prof. Dr. Eugen Kerkhoff and Tobias Welz for all their time spent and their help with my live cell imaging experiments.

Moreover, thanks to PD Dr. Richard Bauer and Anja Pasoldt for introducing me to their microscope that I used for my immunocytochemical experiments and actin-stained cells.

Finally, I would like to say thank you to my family and all of my friends who have helped me throughout the whole progress of this doctoral thesis. Without all their support and encouragement, this work would not have been possible.

10 Curriculum Vitae

Stefan Swoboda

Date of birth:	13.03.1992
Place of birth:	Lauf a. d. Pegnitz
Religion:	Evangelic Lutheran
Nationality:	German

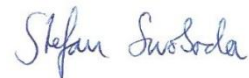## Education

2002 – 2011:	Christoph-Jacob-Treu-Gymnasium Lauf a. d. Pegnitz
04/2011 – 09/2011:	Studies of electrical engineering at the Friedrich-Alexander-University Erlangen
2011 – 2017:	Studies of medicine at the University Regensburg

Research

Co-authorship	**„RELN signaling modulates glioblastoma growth and substrate-dependent migration"** Published in "Brain Pathology", accepted December 2017

11   Eidesstattliche Erklärung

Ich erkläre hiermit, dass ich die vorliegende Arbeit ohne unzulässige Hilfe Dritter und ohne Benutzung anderer als der angegebenen Hilfsmittel angefertigt habe. Die aus anderen Quellen direkt oder indirekt übernommenen Daten und Konzepte sind unter Angabe der Quelle gekennzeichnet. Insbesondere habe ich nicht die entgeltliche Hilfe von Vermittlungs- bzw. Beratungsdiensten (Promotionsberater oder andere Personen) in Anspruch genommen. Niemand hat von mir unmittelbar oder mittelbar geldwerte Leistungen für Arbeit erhalten, die im Zusammenhang mit dem Inhalt der vorgelegten Dissertation stehen. Die Arbeit wurde bisher weder im In- noch im Ausland in gleicher oder ähnlicher Form einer anderen Prüfungsbehörde vorgelegt.

15.01.2019, Regensburg   Stefan Bernd Swoboda

12   Supplement

Parts of this work were published in the research acrticle "RELN signaling modulates glioblastoma growth and substrate-dependent migration" in *Brain Pathology* on the 10th of January 2018 (Schulze et al. 2017).

RESEARCH ARTICLE

RELN signaling modulates glioblastoma growth and substrate-dependent migration

Markus Schulze[1]; Christ Violonchi[2]; Stefan Swoboda[1]; Tobias Welz[3]; Eugen Kerkhoff[3]; Sabine Hoja[1]; Susanne Brüggemann[1]; Johann Simbürger[4]; Jörg Reinders[4]; Markus J. Riemenschneider [1,5]

[1] Department of Neuropathology, Regensburg University Hospital, Regensburg, Germany.
[2] Department of Neuropathology, Heinrich-Heine University, Düsseldorf, Germany.
[3] Molecular Cell Biology Laboratory, Department of Neurology, Regensburg University Hospital, Regensburg, Germany.
[4] Institute of Functional Genomics, University of Regensburg, Regensburg, Germany.
[5] Wilhelm Sander-NeuroOncology Unit, Regensburg University Hospital, Regensburg, Germany.

Abstract

Glioblastoma (GBM) represents the most common and most malignant type of primary brain tumor and significantly contributes to cancer morbidity and mortality. Invasion into the healthy brain parenchyma is a major feature of glioblastoma aggressiveness. Reelin (RELN) is a large secreted extracellular matrix glycoprotein that regulates neuronal migration and positioning in the developing brain and sustains functionality in the adult brain. We here show that both RELN and its main downstream effector DAB1 are silenced in glioblastoma as compared to non-neoplastic tissue and mRNA expression is inversely correlated with malignancy grade. Furthermore, RELN expression is positively correlated with patient survival in two large, independent clinically annotated datasets. RELN silencing occurs via promoter hypermethylation as shown by both database mining and bisulfite sequencing of the *RELN* promoter. Consequently, treatment with 5′-Azacytidine and trichostatin A induced RELN expression *in vitro*. On the functional level, we found RELN to regulate glioblastoma cell migration both in a DAB1 (tyrosine phosphorylation)-dependent and -independent fashion, depending on the substrate provided. Moreover, stimulation of RELN signaling strongly reduced proliferation in glioblastoma cells. This phenotype depends on DAB1 stimulation by RELN, as a mutant that lacks all RELN induced tyrosine phosphorylation sites (DAB1-5F) failed to induce a growth arrest. Proteomic analyzes revealed that these effects are mediated by a reduction in E2F targets and dephosphorylation of ERK1/2. Taken together, our data establish a relevance of RELN signaling in glioblastoma pathology and thereby might unearth novel, yet unrecognized treatment options.

INTRODUCTION

Glioblastoma (GBM) represents the most common and most malignant form of primary brain tumor. Despite an aggressive combination of surgery followed by radiochemotherapy and numerous clinical trials on innovative treatment options, the overall improvements achieved are moderate (45). Thus, the identification of novel molecules and signaling pathways involved in glioblastoma pathology are urgently needed. A hallmark of glioblastoma malignancy is the infiltration of tumor cells into the healthy brain parenchyma that makes complete surgical resection of the tumor impossible. Among others, integrins are believed to play a major role in this context as they mediate the contact of the cells to the extracellular matrix (ECM) (37). However, there are still many unanswered questions regarding the development and regulation of the invasive glioma phenotype.

The large secreted protein reelin (RELN) was discovered as a regulator of neuronal migration in reeler mice. In these mice, cortical neurons fail to reach their normal position in the cortex, resulting in an inside out layering (19). RELN also has been shown to regulate neural precursor cell cycle exit (25) and differentiation (23). It inhibits signaling via integrins by directly disrupting the binding of $\alpha 3\beta 1$ integrin to laminin (14) and the binding of $\alpha 5\beta 1$ integrin to fibronectin in a DAB1-dependent manner (41). In addition, RELN mediates cofilin phosphorylation in neuronal cells (11) with alterations in cofilin activity exerting strong effects on glioma cell invasion (34). In the canonical signaling cascade, APOER2 and VLDLR mediate the tyrosine phosphorylation of the intracellular adaptor protein DAB1 through RELN binding. This phosphorylation event is catalyzed by SRC family kinases and reinforced by phosphorylated DAB1 in a positive feedback loop (19). Importantly, kinases of the SRC family are well known as important players in tumorigenesis and attractive drug targets in glioblastoma (1), connecting RELN signaling and tumorigenesis mechanistically.

Although primarily studied in post-mitotic neurons in the central nervous system (CNS), both RELN and DAB1 are also expressed

in a variety of tissues outside of the CNS (43). In a cancer context, it has been shown that RELN is involved in the regulation of invasion and proliferation of breast cancer (36, 44). Moreover, RELN was found to inhibit both migration and invasion of pancreatic cancer cells (39). Silencing of reelin in these tumors (breast, pancreatic and gastric cancer) occurred via hypermethylation of the CpG island containing the *RELN* promoter (13, 39, 44). Of note, also the *DAB1* gene maps to a site frequently deleted in different cancers (32).

In contrast to epithelial tumors, a role for RELN signaling has not yet been implicated in brain tumors. In a single investigation on gangliogliomas, transcriptional downregulation of DAB1 was observed but the tumors lacked DAB1 mutations (21). Also, the data on neuroblastoma, a peripheral tumor, are controversial (4, 16). Another study reported decreased RELN expression in various tumor types (including glioblastoma) by analyzing TCGA data (9). This prompted us to follow up on the potential tumor suppressive functions of DAB1 and RELN in gliomas. Interestingly, it has been recently suggested that malignant gliomas can also originate from neural progenitors and/or differentiated neurons (2, 17) and DAB1 as well as RELN have been implicated in the regulation of neuronal differentiation (23, 35). Therefore, it seemed likely that crossconnections between RELN signaling and glioma pathology might exist.

MATERIALS AND METHODS

In silico analysis

Prenormalized expression datasets from glioblastoma samples and matched clinical data were obtained from the cancer genome atlas (7) data portal (URL: https://tcga-data.nci.nih.gov). In addition, a second set of gene expression data was obtained from Rembrandt (31) and downloaded via the array express database (URL: http://www.ebi.ac.uk/arrayexpress, accession E-MTAB-3073). The Rembrandt microarrays were RMA normalized and analyzed with R ver. 3.2.1 and the affylmGUI package. Genome wide methylation (22, 46) data as well as the manufacturer's annotation for each CpG probe were obtained from the Gene Expression Omnibus (GEO) Database (URL: http://www.ncbi.nlm.nih.gov/geo, accession GSE36278 and GSE60274, platform GEO accession GPL13534). The GSEAPreranked module v5 for Gene set enrichment analysis (47) was accessed from the gene pattern server (URL: http://genepattern.broadinstitute.org) and GSEA was performed with the fold changes as calculated by DESeq2.

Clinical samples

Thirty-five snap-frozen tumor samples were selected from the tumor tissue collection of the Department of Neuropathology, Heinrich-Heine-University, Duesseldorf, Germany and studied according to protocols approved by the institutional review board. It was confirmed via standard histology that all samples had a tumor content of at least 80%. Included were 12 primary glioblastomas WHO grade IV (pGBM IV), 4 secondary glioblastomas WHO grade IV (sGBM IV), 7 anaplastic astrocytomas WHO grade III (AA III) and 12 diffuse astrocytomas WHO grade II (A II). Classification as secondary glioblastoma was based on the presence of a histologically verified preceding lower grade astrocytic lesion. Non-neoplastic

brain control tissues were derived from four different individuals: one from the temporal lobe of a 66-year-old male, one from the occipital lobe of a 82-year-old female and two from cortex of a 76-year-old male and a 72-year-old female, respectively. All non-neoplastic tissues were surgical specimens (snap-frozen), three with the clinical history of epileptic surgery, one with traumatic brain injury. Extraction of DNA and RNA from frozen tumor tissue was performed as has been described previously (38). The non-neoplastic brain controls used for analysis of the mRNA expression levels in glioma cell lines were commercially available total RNA preparations derived from a 24-year-old male (BioChain, Newark, CA, USA) and a 66-year-old female (Agilent Technologies, Santa Clara, CA, USA).

cDNA synthesis and real-time PCR

cDNA was synthetized from 3 μg total RNA with the super script II reverse transcriptase (Life Technologies, Carlsbad, CA) in a reaction volume of 50 μl. cDNA of 12 ng was then used in a real-time PCR performed with the Platinum SYBR green Kit (Life Technologies) in a StepOne Plus real-time PCR thermocycler (Applied Biosystems, Foster City, CA). Initial incubation was performed at 95°C for 10 minutes followed by 40 cycles of 95°C for 10 s and 60°C for one minute. Relative expression was calculated with the ΔΔCt method (29). All primer sequences used are provided in Supporting Information Table 1.

Bisulfite sequencing

Bisulfite treatment was performed as previously described (38). Bisulfite converted DNA of 100 ng was then amplified using a HotStarTaq (Qiagen, Hilden, Germany) and the primer pairs indicated in Supporting Information Table 1. PCR conditions are available on request. The amplified fragment is provided in Supporting Information Fig. 1. Amplified DNA was purified with the Jet quick kit (Genomed/Thermo Fisher, Waltham, MA) and processed for Sanger sequencing on an ABI PRISM® 377 machine (Applied Biosystems).

Cell culture

Cell lines were cultured, obtained and characterized as has been described previously (18) and cell line identity was confirmed by short tandem repeat analysis of 16 loci by CLS Cell Lines Services (Eppelheim, Germany). After thawing, cells were passaged twelve times or cultured for six weeks, respectively, at maximum. The cells were all tested negatively for mycoplasma contamination by PCR including positive and negative controls as has been described by others (33). HEK293T cells expressing GFP or murine RELN were kindly provided by Prof. Eckart Förster (Ruhr University, Bochum, Germany). Cell culture and 5-Aza-2′-deoxycytidine and trichostatin A treatment of glioblastoma cell lines were performed as previously described (3, 18).

RELN production

HEK-293T cells expressing murine (m)RELN (or GFP as a control) (11) were seeded at a density of ∼26000 cells/cm^2 in complete medium. After overnight incubation, the medium was exchanged to fresh complete medium or starving medium (no FCS, 0.1% BSA).

To remove serum remnants, the cells were washed once with the starving medium. Then, the cells were allowed to grow and secrete RELN for another 48 h. Afterwards, the supernatant was collected and residual cells were removed by centrifugation at $200 \times g$ for 5 minutes. For experiments with the function blocking CR-50 antibody, a mouse isotype control IgG (#5415, clone G3A1; Cell signaling technology, Danver, CO) or the CR-50 antibody (MBL, Nagoya, Japan) were added at a final concentration of 20 µg/ml.

Cloning and generation of stably transfected cells

The ORF of human full length DAB1 in pCMV-Sport6 (Thermo Fisher) was subcloned into the pIRESneo2 vector (Clontech, Palo Alto, CA). As human and mouse DAB1 are identical on the protein level within large parts of their N-terminus, the N-terminal portion containing the murine 5F sequence (20) was cloned into the pIRES-neo2 vector together with the C-terminus of human DAB1. This resulted in a construct that is identical to a human DAB1-5F mutant on protein level. For the establishment of stable cell lines, U87 and U251 cells were seeded at a density of ~7000 cells per cm^2 on Ø10 cm dishes (Sarstedt, Nuembrecht, Germany) and allowed to grow for 48 h. Then, the cells were transfected with 1.5 µg pIRES-neo2 empty vector (EV), hDAB1-WT//pIRES-Neo2 or hDAB1-5F//pIRES-Neo2 with 12 µl of the transfection reagent Lipofect-amine 2000 (Life Technologies). For the establishment of stably transfected cells, G418 (Carl Roth, Karlsruhe, Germany) was added to the medium at a concentration of 200 µg/ml (U87) to 400 µg/ml (U251) and the cells were cultured for two weeks until resistant cells emerged.

Plate coating for live cell imaging

Eight well µ-slides (ibiTreat; Ibidi, Munich, Germany) were coated with 5 µg/ml fibronectin or 2 µg/ml laminin (all from Sigma-Aldrich, St. Louis, Missouri) for 60 minutes. Then, the coating solution was removed and the slides washed with sterile H$_2$O. The laminin coated plates were allowed to dry for 45 minutes at RT. Finally, the plates were blocked with DPBS containing 0.5% bovine serum album (BSA) for 30 minutes.

Two-dimensional-migration assay

Cells were seeded at a density of 6000 cells per cm^2 on laminin or fibronectin coated 8 well µ-slide dishes in CO$_2$-independent medium (Life Technologies) supplemented with 5% FCS, 2 mM L-glutamine, 100 U/ml penicillin and 100 µg/ml streptomycin (Life Technologies). Cells were allowed to adhere for 6 h, two volumes of RELN or GFP conditioned CO$_2$-independent medium were added and afterwards cell motility was analyzed using a Leica AF-6000 (Leica Microsystems, Wetzlar, Germany) microscope and a microscope stage incubator to keep the temperature at 37°C. Pictures were taken every 20 minutes over a period of 12 h. At least 50 randomly chosen cells were tracked using ImageJ 1.47 (40) and the manual tracking plugin. Immotile cells and cells that divided during the observation period were excluded from tracking. To calculate velocity and directionality, we imported the tracking files to the chemotaxis and migration tool (Ibidi).

Proliferation assay

Cells per well of 1500 (U87) or 1000 (U251) were seeded on a 96-well plate in triplicates After 6 h, the medium was changed to starving medium, another 100 µl GFP or RELN conditioned super-natant was added and the cells were incubated at 37°C and 5% CO$_2$. Every 24 h, three wells per condition were labeled with 1 µM (final concentration) Hoechst 33342 for 1 h. Then, four pictures were taken with a low magnification (4×) objective from randomly chosen areas of the triplicate wells and analyzed with an automated cell profiler pipeline (ver. 2.1.1) (8) to count the number of nuclei present.

Cell cycle analysis

Cell cycle analysis was performed via propidium iodide staining. After O/N starvation, cells were trypsinized and counted. Cells of 1×10^6 were fixed in 70% precooled ethanol for 1 h on ice. The cells were washed twice in DPBS, resuspended in staining mix (final concentration 50 µg/ml RNAseA, 40 µg/ml propidium iodide and 0.05% saponin in DPBS) and incubated for 30 minutes at 37°C. Then, the cells were analyzed on a FACS CantoII flow cytometer (Becton Dickinson) and gating as well as quantification was performed with ModFit LT v3.2 (Verity Software House, Topsham, ME, USA).

Western blotting and detection of proteins

Western blotting was performed according to standard protocols. For western blot analysis, 150 000 cells were seeded on Ø1.5 cm tissue culture dishes (Sarstedt) and allowed to grow for 48 h. Primary antibodies used were DAB1 (1:1000, #3328; Cell signaling technology), p(Y220)-DAB1 (1:1000, #3327; Cell signaling technology), caspase-3 and cleaved caspase-3 (1:1000, #14220, clone D3R6Y; Cell signaling technology), p(S491)-DAB1 (ab5776, Abcam, Cambridge, UK) and tubulin as a loading control (1:10 000, clone DM1A; Sigma-Aldrich, St. Louis, MO). Anti-rabbit or anti-mouse IgG linked to horseradish peroxidase (Santa Cruz, Dallas, Texas) were used as secondary antibodies (1:10 000 dilution). After development with picoluminescence sub-strate (Thermo Fisher) quantification was performed on a LAS4000 imaging system (GE healthcare, Munich, Germany) using the ImageQuant TL ver. 7.0 software (GE healthcare). For Reln immu-nohistochemistry, we used the antibody clone E-5 (#sc-25346, Santa Cruz Biotechnology, Dallas, Texas) following a standard protocol (1:50 dilution, overnight incubation, 5 minutes heat-induced antigen retrieval).

Mass spectrometry

Total cellular protein lysates were prepared and subjected to label-free quantification by SWATH-MS as published previously (42). Briefly, 100 µg of protein was subjected to tryptic digestion using the FASP-protocol (50). Six aliquots (1 µg each) of the pooled pro-tein digests were used for generation of the SWATH-library using an 88 minutes-LC-gradient and a TOP40 IDA-method; database searches were conducted with ProteinPilot 4.5 against the Uniprot database (human). SWATH-MS-runs were accomplished with 1 µg of the individual protein digests using the same LC-gradient and SWATH-windows of 15 Da width (total m/z range 400–1000). In

total, 1950 proteins were quantified using PeakView 2.1. Differential abundance of proteins was calculated based on non-normalized protein counts with DESeq2 (30).

Proteome profiler assay

The phosphorylation of 43 different kinases and the amount of two related proteins was detected with the proteome profiler assay (R&D Systems, Minneapolis, MN). Cells were grown and stimulated with GFP or mRELN as described above. The assay was performed according to the manufacturer's instructions. The chemiluminescent signal was detected with a LAS4000 imaging system (GE healthcare).

DuoSet IC ELISA

Commercially available ELISA assays (R&D Systems) for STAT3(Y705) and ERK1(T202/Y204)/ERK2(T185/Y187) were performed according to the manufacturer's instructions. Briefly, 96-well ELISA plates (R&D Systems) were coated with capture antibody (diluted 1:180) in PBS. On the next day, the plates were blocked with BSA in PBS, washed with washing buffer (0.05% Tween-20 in PBS) and cell lysates were incubated for 2 h at RT on the plates. Afterwards, the plates were washed again and detection antibody was added (1:36 diluted). Then, streptavidin-HRP was added for 20 minutes at RT. After washing, a commercially available substrate solution (R&D Systems) was added and the reaction was stopped after 20 minutes with 2N H_2SO_4.

Data analysis

All analyzes were performed with GraphPad Prism 4.0 or higher and R ver. 3.2.1. If not otherwise indicated, two-tailed *t*-tests were used for statistical analysis. We only proceeded with post-tests if the ANOVA or Kruskal-Wallis test indicated significant differences between groups ($P < 0.05$).

RESULTS

RELN pathway gene expression is correlated with glioblastoma subtypes and shorter overall survival

Analysis of agilent gene expression microarrays from the TCGA database (7) revealed that RELN is significantly upregulated in the G-CIMP and neural as compared to the classical and mesenchymal glioblastoma gene expression subtype (49). In line with this finding, RELN was significantly related to *IDH1* mutational status in the TCGA dataset (Bonferroni corrected two-sided Mann-Whitney test, $P = 0.036$) but not to mutations in *EGFR*, *TP53*, *PTEN*, *PIK3CA*, *PIK3R1*, *RB1* or *NF1* (Supporting Information Fig. 1). Of note, *RELN* mutations themselves were also detectable in a significant number of glioblastoma (7.89%), underscoring that RELN is altered in this tumor type. For DAB1, upregulation was only present in the neural subtype (Kruskall-Wallis test followed by Dunn's multiple comparison test, significant changes are indicated; Figure 1A,B). The upregulation of RELN and DAB1 in the neural subtype was confirmed by analysis of another large glioblastoma cohort from Rembrandt (Figure 1E,F) (31).

When the gene expression data were combined with clinical data and patients divided by the median into a low and a high expression subgroup, both high DAB1 and high RELN expression were significantly correlated with increased overall survival in glioblastoma patients in the TCGA dataset (Log-rank (Mantel-Cox) test, $P = 0.0026$ (RELN) and $P = 0.0069$ (DAB1); Figure 1C,D). Importantly, RELN remained significantly ($P < 0.05$) associated with survival in a Cox proportional-hazards regression model that contained G-CIMP status, DAB1 expression as well as age (below or above 50) as variables. Survival correlations could be confirmed in the Rembrandt dataset for RELN. High RELN expression was significantly correlated with longer overall survival (Log-rank (Mantel-Cox) test, $P = 0.0002$; Figure 1G). For DAB1, there was only a trend toward longer overall survival in the high expression subgroup (Figure 1H).

RELN expression in glioblastomas is silenced by promoter methylation

The genomic region around the RELN transcription startsite ($\pm$ 2kb) contains a large ~2kb CpG island as predicted by the CpG island finder software (URL: http://dbcat.cgm.ntu.edu.tw). We designed primers that amplify the part of the CpG island spanning the transcription start site (TSS) (Supporting Information Fig. 2). We analyzed two publicly available datasets that used the Illumina 450k bead array for methylation analysis and additionally contained non-neoplastic brain tissue. We found that the CpGs that are annotated to the RELN gene and that lie within the CpG island (according to the Illumina annotation) are significantly hypermethylated in glioblastoma samples as compared to non-neoplastic brain. In contrast, several CpGs in the gene body (including the first exon and 3-prime UTR according to Illumina annotation) of RELN were hypomethylated (Figure 2A). Own bisulfite sequencing of the region around the transcription start site revealed that RELN is heavily hypermethylated in glioblastoma and that the methylation status is positively correlated with malignancy grade (Supporting Information Table 2). Hypermethylation of the RELN promoter was significantly more often found in glioblastomas as compared to WHO grade II and WHO grade III astrocytomas ($P < 0.001$ and $P < 0.05$, respectively, Fisher's exact test; Figure 2B). The *RELN* promoter was also nearly completely methylated in glioblastoma cell lines *in vitro* and treatment with the demethylating agent 5′-Azacytidine (in combination with trichostatin A) led to a reduction in promoter methylation (Supporting Information Table 3). Consequently, the same treatment regimen led to a strong reexpression of RELN in glioblastoma cell lines (Figure 2C). As such, there is compelling evidence that RELN in glioblastoma tissues and cell lines is silenced epigenetically by promoter hypermethylation.

RELN and DAB1 expression is correlated with malignancy grade in gliomas and tissue expression levels are retained *in vitro*

Real-time PCR analysis of an own panel of astrocytic tumors of different WHO grades showed that both RELN and DAB1 are strongly downregulated on the mRNA level and that the RELN receptors, VLDLR and APOER2, are upregulated as compared to non-neoplastic brain tissue. In addition, both RELN and DAB1 expression were inversely correlated with tumor grade and
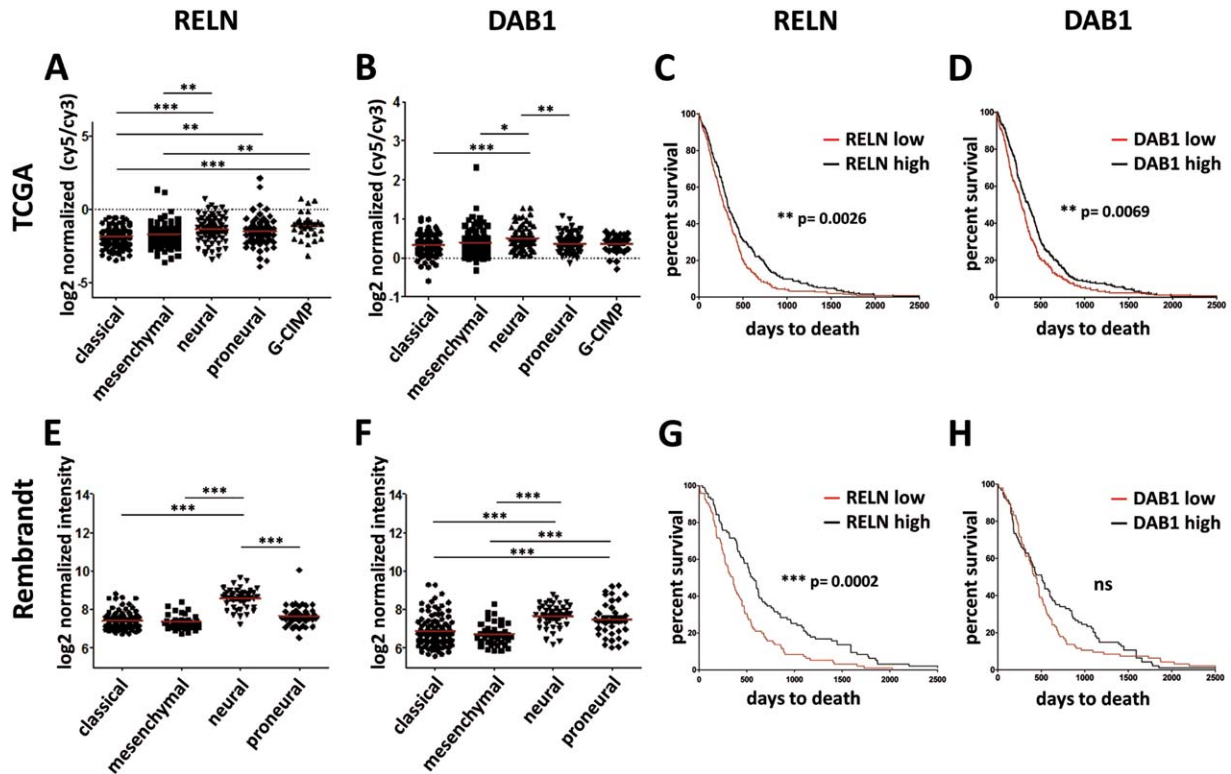
Figure 1. *RELN and DAB1 mRNA expression is correlated with transcriptional subtypes and survival.* **A**, **B**, **C**, **D**. Statistical comparison of expression subtypes was performed by the non-parametric Kruskal-Wallis test followed by Dunn's multiple comparison test. Red lines indicate means. **C**, **D**, **G**, **H**. Survival curves were compared with a log-rank (Mantel-Cox) test. For survival analyzes, samples were divided by the median expression into the low (red line) and high expression (black line) subgroup. Significant changes are indicated (* = $P < 0.05$, ** = $P < 0.01$, *** = $P < 0.001$, **** = $P < 0.0001$). A. RELN expression is low in the mesenchymal and classical subtype and highest in the neural and G-CIMP subtype in the TCGA dataset (Agilent platform). B. DAB1 expression is significantly lower in the mesenchymal and classical subtype than in the neural subtype in the TCGA dataset. C. High RELN expression is correlated with longer overall survival in the TCGA dataset. D. High DAB1 expression is correlated with longer overall survival in the TCGA dataset. E. RELN expression is significantly lower in the mesenchymal and classical subtype than in the neural subtype in the Rembrandt dataset (Affymetrix platform). F. DAB1 expression is low in the mesenchymal and classical subtype and highest in the neural subtype in the Rembrandt dataset (probe set 228329_at). G. High RELN expression is correlated with longer overall survival in the Rembrandt dataset. H. High DAB1 expression (probe set 228329_at) is correlated with longer overall survival in the Rembrandt dataset. Although not significant, there is a strong trend toward longer overall survival in the DAB1 high expression subgroup.

significantly lower in glioblastomas as compared to WHO grade II astrocytomas (Kruskal-Wallis test followed by Dunn's multiple comparison test, significant changes are indicated; Figure 3A). Loss of Reln expression in tumor cells was also confirmed on the protein level by immunohistochemistry although significant intra- as well as intertumoral heterogeneity could be observed (Supporting Information Fig. 3).

To establish a suitable model system for *in vitro* experiments, we screened seven classical glioblastoma cell lines as well as four stem-like cell lines for RELN and DAB1 expression via real-time PCR (Figure 3C,D). Non-neoplastic brain tissues were used as controls. Consistent with the data from the tissue samples (Figure 3A), expression of both genes was absent or low in all glioblastoma cell lines (classical and stem-like cells). We thus decided to make use of the classical cell lines for our further experiments. As classified by ssGSEA, all classical cell lines tested corresponded to either the classical or mesenchymal expression subtype (Figure 3B). Also congruent with the tissue data, the expression of APOER2 was

high in the glioblastoma cell lines as compared to non-neoplastic brain tissue (Figure 3E). The expression of VLDLR was highly variable in glioblastoma cell lines (Figure 3F). We also reanalyzed previously obtained next generation sequencing data of our cell lines (18) to check if any other ligands for the receptors VLDLR and APOER2 were expressed. Indeed, THBS1 and Clusterin were highly expressed (RPKM > 10, Figure 3G).

We then decided to construct an expression system in which DAB1 overexpression was driven from a pCMV promoter followed by an IRES sequence. DAB1 overexpressing cells were selected by adding G418 to the cell culture medium. A DAB1 mutant was used as an additional control. This mutant (5F) has all five tyrosine residues mutated to phenylalanine that are phosphorylated following RELN stimulation (20). Interestingly, we observed varying abundance of DAB1-WT proteins of different length in U251 and U87. While in U87 the predominant band was visible at 60 kDa for both DAB1-WT and 5F, in U251 the predominant band of the DAB1-WT protein was visible at 45 kDa. We checked that
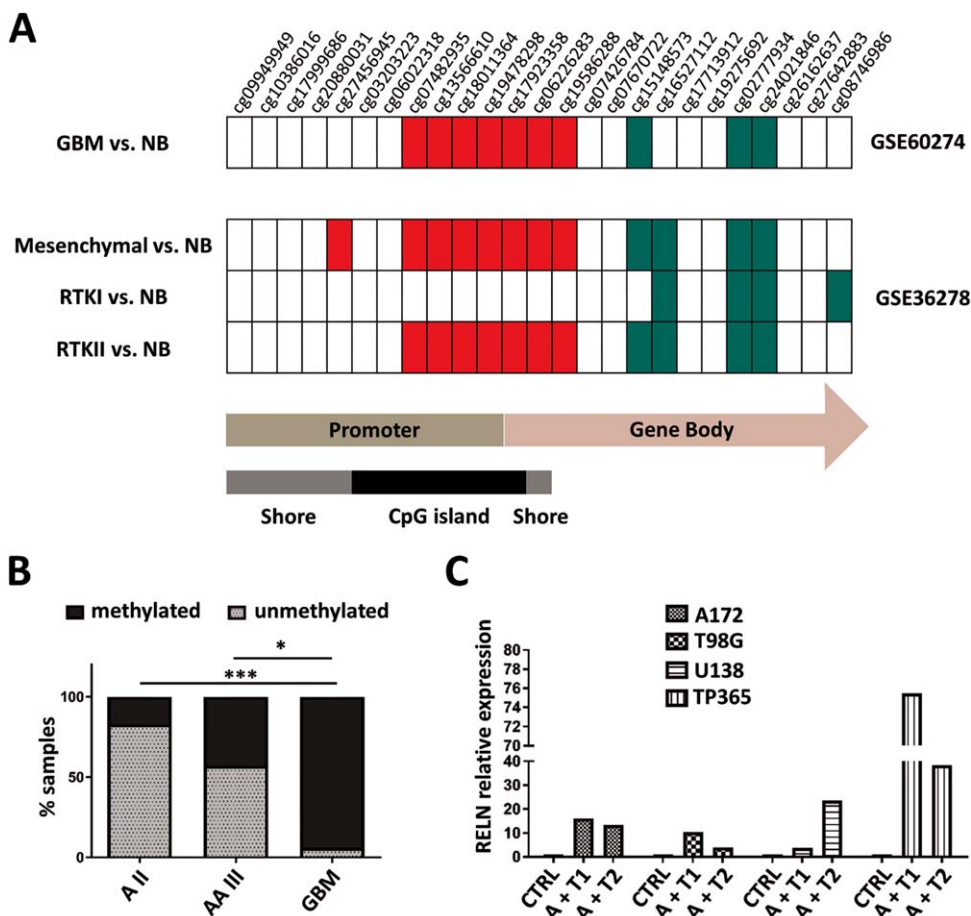
Figure 2. *RELN is silenced by promoter hypermethylation in glioblastoma tissues and cell lines.* **A.** Both the array-based dataset from GSE36278 (46) and GSE60274 (22) show significant hypermethylation in the CpG island spanning the transcription start site (TSS). Significantly hypermethylated CpGs in glioblastoma (GBM) in comparison to non-neoplastic brain tissue (NB) (adj. $P < 0.05$) are indicated in red, significantly hypomethylated CpGs in green (adj. $P < 0.05$) and CpGs with no change in white. Hypermethylation is more pronounced in the receptor tyrosine kinase (RTK) II (corresponding to the classical subtype from the TCGA) and mesenchymal subtype that also show reduced RELN mRNA levels. **B.** Bisulfite sequencing of the RELN promoter reveals frequent hypermethylation in glioblastoma (also compare Supporting Information Table 2). Hypermethylation is positively correlated with malignancy grade. Significant changes between WHO grades (A II = diffuse astrocytoma, AA III = anaplastic astrocytoma, GBM = glioblastoma) are indicated (* = $P < 0.05$, ** = $P < 0.01$, *** = $P < 0.001$, **** = $P < 0.0001$; Fisher's exact test). **C.** Treatment with 5′-Azacytidine and trichostatin A leads to reexpression of RELN as measured by real-time PCR. The RELN mRNA level is increased in the glioblastoma cell lines A172, T98G, U138 and TP365 up to 75-fold. Cells were treated with DMSO as control (CTRL), 500 nM 5-Aza-2′-deoxycytidine for 48 h + trichostatin A for 24 h (A + T1) or 1 µM 5-Aza-2′-deoxycytidine for 72 h + 1 µM trichostatin A for 24 h (A + T2).

the different cell lines had integrated full length DAB1-WT and DAB1-5F at equal levels by semi-quantitative PCR as integration artifacts could have potentially caused the length differences. For this assay, we designed the primers in a way that one pair covers the five-prime and one pair covers the three-prime border of the insert. We quantified if the five-prime to three-prime ratio is altered in one of the cell lines what was not the case. The integration of both full-length constructs was equally efficient in U251 and U87. In addition, we amplified the full-length DAB1-WT and DAB1-5F inserts from genomic DNA and verified that they did not contain any mutations (Supporting Information Fig. 4). Thus, it appears most likely that phosphorylation-dependent processing of DAB1—as already described in neuronal cells (6)—might account for the observed differences in western blotting.

Proteomics identifies E2F targets as well as ERK1/2 and STAT3 phosphorylation as downstream mediators of RELN signaling

To identify possible effects of RELN and DAB1 deregulation, we subjected U87 cells expressing DAB1-WT or DAB1-5F to RELN stimulation for 1 h and quantified both protein abundance and phosphorylation status of proteins. The abundance of few individual proteins changed significantly (P-adj.<0.1) comparing DAB1-WT expressing with non-WT (empty vector and 5F) expressing cells (Supporting Information Table 4). No additional changes were observed on RELN stimulation. Interestingly, on a pathway level, E2F target gene sets were significantly downregulated in the U87-DAB1-WT group as compared to empty vector or 5F cells (GSEA; Figure 4A,B).
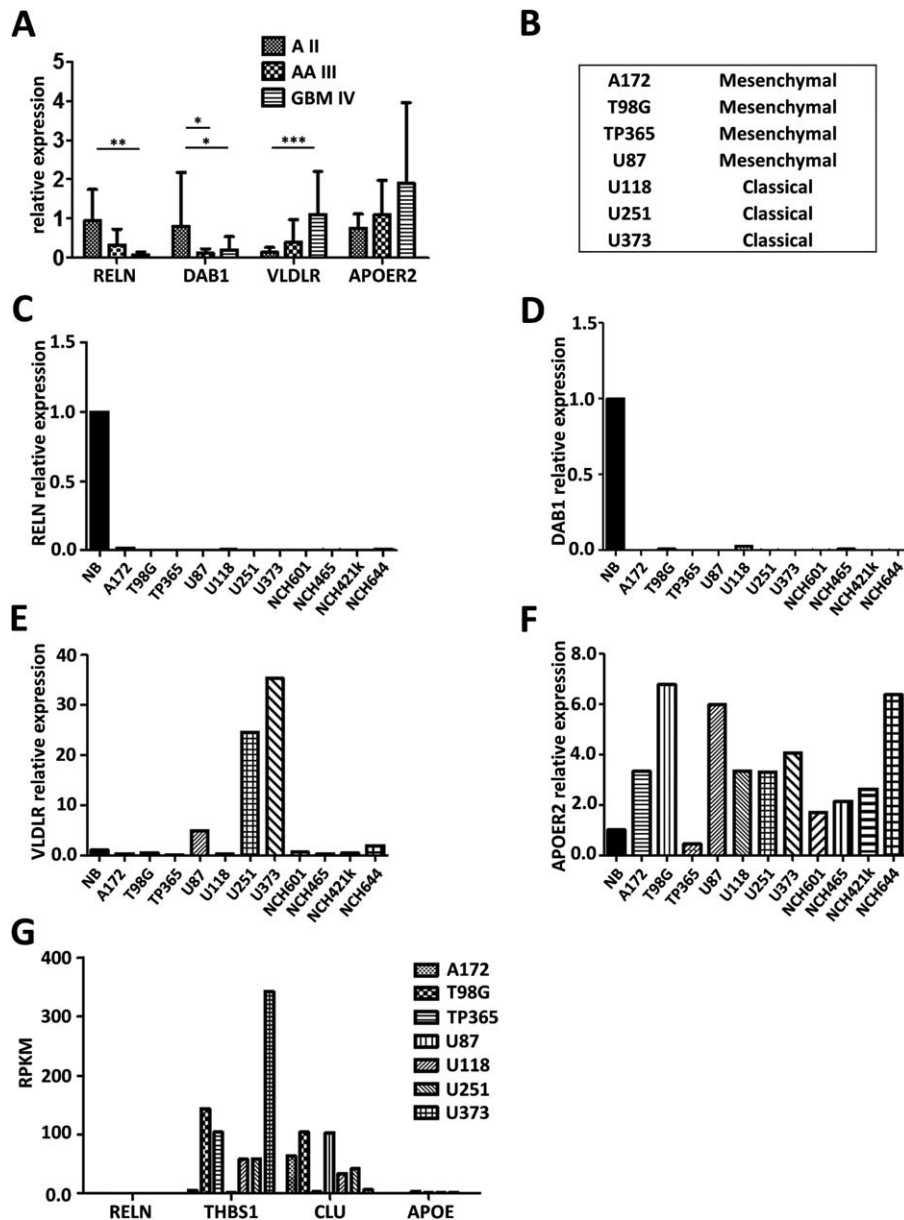
Figure 3. *Classical glioblastoma cell lines recapitulate the changes found in glioblastoma tumor tissue.* **A.** Real-time PCR of RELN, DAB1, VLDLR and APOER2 in astrocytic tumors of different grades (A II: n = 11; AA III: n = 6; GBM IV: n = 9) relative to four non-neoplastic brain samples (set to 1). Shown are means + SD. RELN expression is inversely correlated with tumor grade and significantly higher in WHO grade II astrocytomas than in glioblastomas. All significant changes between WHO grades are indicated (* = $P < 0.05$, ** = $P < 0.01$, *** = $P < 0.001$, **** = $P < 0.0001$; Kruskal-Wallis test followed by Dunn's multiple comparison test). **B.** GSEA prediction of the glioblastoma subtype of the cell lines based on next generation sequencing data. All cell lines tested belong to the mesenchymal or classical subtype. **C–F.** Real-time PCR of RELN (C), DAB1 (D), VLDLR (E) and APOER2 (F) expression in different glioblastoma cell lines as compared to non-neoplastic brain tissue (*NB*). ARF1 was used as an internal control. **G.** Expression of different APOER2 and VLDLR ligands based on next generation sequencing data. While clusterin (*CLU*) and Thrombospondin1 (*THBS1*) are expressed in different glioblastoma cell lines, RELN and APOE are not expressed *in vitro*.

In addition, the proteome profiler array that measures the phosphorylation level of a number of kinases, indicated that phosphorylation of STAT3, MAPK and p27 in U87 cells were all lower in DAB1 expressing cells and that this effect was potentiated by RELN stimulation and statistical analysis indicated significant differences between groups for all four phosphoproteins (one-way ANOVA, Figure 4C-F). The expression of DAB1-WT and -5F protein and the effectiveness of RELN stimulation was controlled by western blotting (Figure 4G). Results of the proteome profiler were then confirmed by ELISA in all
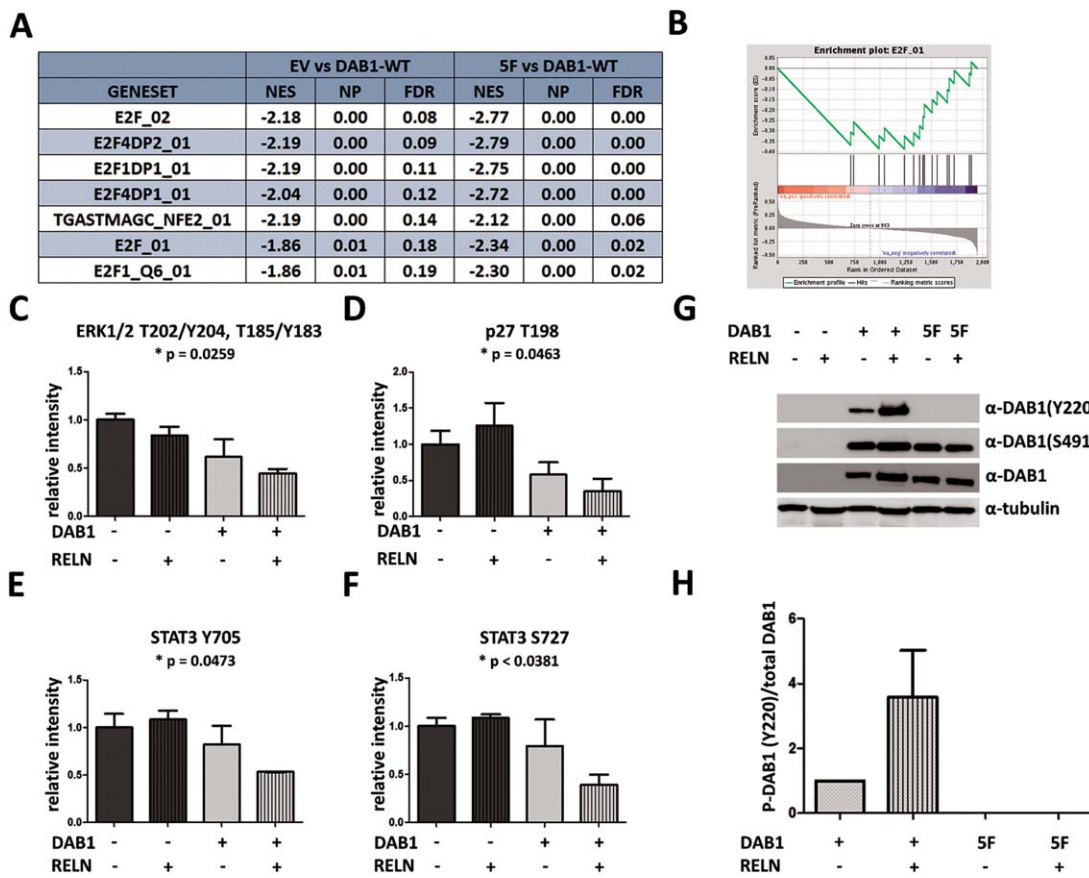
Figure 4. *Proteomic analysis reveals enrichment for E2F pathway components in control cells compared to DAB overexpressing cells.* **A.** GSEA of proteomic data based on fold changes as calculated by DESeq2. N = 5 in each group. E2F signaling is the main deregulated pathway after DAB1-WT expression, represented by several significant gene sets at $P < 0.05$ and FDR < 0.2. **B.** Enrichment plot for the E2F gene set for DAB1-WT vs. empty vector cells. **C–F.** Quantification of the proteome profiler analysis. Phosphorylation of ERK1/2 on T202/Y204 and T185/Y183 (C), of STAT3 on Y705 (D) and S727 (F) as well as phosphorylation of p27 on T198 are markedly decreased after DAB1 expression and RELN stimulation. One-way ANOVA indicates significant differences between groups for all four phosphorylation sites. Shown are means + SD, n = 2. **G, H.** Representative western blot and quantification of n = 3 western blots probed with P-DAB1 Y220, P-DAB1 S491 and total DAB1 antibody, shown are means + SEM.

stable cell lines (Figure 5). In U87, there was a highly significant reduction of both ERK1(T202/Y204)/ERK2(T185/Y187) and STAT3(Y705) phosphorylation in DAB1-WT cells (both RELN and GFP-stimulated) as compared to empty vector cells treated with GFP ($P < 0.001$ or <0.01, one-way ANOVA followed by Dunnett's post hoc test of all conditions vs. empty vector + GFP). Also, in U87 and U251 cells, ERK1/2 activity was significantly reduced in empty vector and DAB1-5F transfected cells stimulated with RELN as compared to empty vector cells treated with GFP ($P < 0.01$ and $P < 0.001$, one-way ANOVA followed by Dunnett's post hoc test of all conditions vs. empty vector + GFP). For STAT3 in U251, there was no difference in protein phosphorylation after RELN stimulation, but even a slight increase in WT-GFP cells as compared to EV-GFP cells. Thus, overlappingly between both cell lines we found a reduction in ERK1/2 phosphorylation following RELN stimulation. Importantly, this effect could be rescued by the function blocking CR-50 antibody, indicating its RELN-specificity (Supporting Information Fig. 5).

Activation of RELN signaling leads to a reduction in proliferation but does not affect chemosensitivity

Activation of the DAB1/RELN signaling axis led to significantly decreased cell numbers on day four and five in both U251 and U87 cells expressing DAB1-WT with or without RELN stimulation (repeated measures, two-way ANOVA with Bonferroni corrected post-test, $P < 0.001$, Figure 6A,B). The DAB1-5F mutant did not achieve comparable effects to DAB1-WT overexpression, strongly arguing for the fact that RELN stimulated tyrosine phosphorylation is important to convey DAB1 inhibitory effects on proliferation. Only in U87 cells, there was a significant decrease in cell numbers on day five when EV + GFP cells were compared to 5F + RELN cells (repeated measures, two-way ANOVA with Bonferroni corrected post-test, $P < 0.05$). Together with the observation that RELN stimulation itself in DAB1-WT cells was not able to reduce the proliferation further, it thus may not be excluded that other ligands contribute to influence this pathway *in vitro*, too. We analyzed if this change in proliferation is because of senescence,
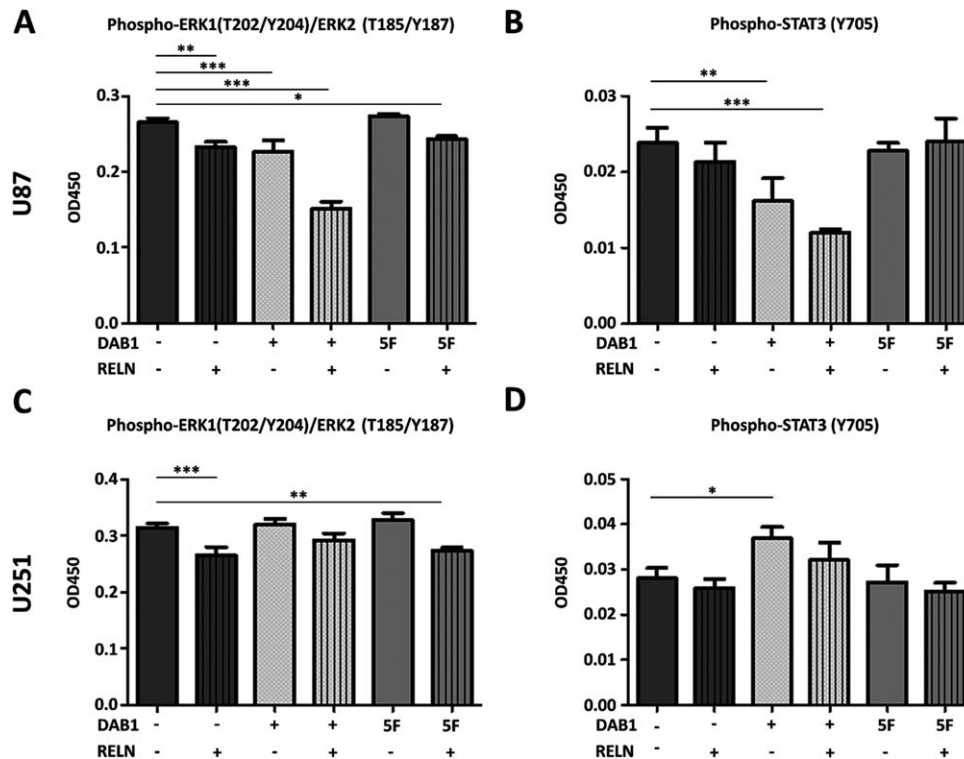
Figure 5. *ELISA assays corroborate influences of RELN signaling on ERK1/2 and STAT3 phosphorylation.* Phospho-STAT3(Y705) and Phospho-ERK1(T202/Y204)/ERK2 (T185/Y187) DuoSet IC ELISAs in U87–**A**, **B** and U251–**C**, **D**. Groups were compared with one-way ANOVA followed by Dunnett's post hoc test. Significant changes are indicated (* = $P < 0.05$, ** = $P < 0.01$, *** = $P < 0.001$, **** = $P < 0.0001$). Shown are means + SD, n = 3. DAB1-WT expressing U87 cells show reduced

Phospho-STAT3 and Phospho-ERK1/2 levels under control (GFP stimulation) conditions. In DAB1-WT cells, RELN treatment reduces the phoshorylation further. In U251 cells, there is a RELN-induced reduction of ERK1/2 phosphorylation that is DAB1 (tyrosine phosphorylation)-independent. In contrast to U87 cells, in U251 RELN does not alter the phosphorylation levels of STAT3(Y705), suggesting cell line-specific effects of RELN on STAT3 activity.

apoptosis or alterations in the cell cycle in U251 cells. There was no sign of senescence in our stable cell cultures as analyzed by ß-galactosidase staining (data not shown). In addition, the cleaved form of caspase-3 was undetectable. In contrast, the amount of cells in G2/M was increased significantly in DAB1-WT as compared to empty vector transfected cells (two-way ANOVA followed by Bonferroni corrected posttests, $P < 0.001$, Supporting Information Fig. 6). There was no significant difference between DAB1-5F and empty vector transfected cells.

The antiproliferative effects of RELN could also be stated in a different fashion. We speculated that adding recombinant RELN to the supernatant of a cell line that expresses at least some DAB1 should select for cells with lower DAB1 expression. We used the U118 cell line for this experiment as it showed the highest endogenous DAB1 expression (Figure 3D). Indeed, after long-term stimulation with RELN-conditioned medium for three weeks, U118 cells showed a significantly lower DAB1 expression as compared to U118 cells cultured in control (GFP-) conditioned medium (Figure 6D).

As DNA damage signaling is known to be influenced by E2F targets (12) and others have reported an influence of RELN on chemoresistance (28), we also assessed chemoresistance following RELN/DAB1 manipulation. However, we could not observe any

change in chemoresistance of U87 cells to lomustine (Figure 6C). DAB1 expression and effectiveness of RELN stimulation were controlled by routine western blotting.

RELN has both DAB1-dependent and DAB1 tyrosine phosphorylation independent effects on cell migration

We studied tumor cell migration following DAB1-WT and -5F overexpression in our two cell lines (U251 and U87) under two different matrix conditions (fibronection and laminin) (Figure 7A–D). Across both cell lines and matrix conditions RELN-stimulated DAB1-WT cells had markedly reduced migration in comparison to empty vector (GFP) and 5F (GFP) cells. These comparisons were concordantly significant in U251 cells on fibronectin and laminin and on U87 cells on laminin. U87 RELN-stimulated DAB1-WT cells on fibronectin showed significantly lower migration in comparison to 5F (GFP) cells and still a trend toward reduced migration in comparison to empty vector (GFP) cells (one-way ANOVA, followed by Tukey's multiple comparison test, $P < 0.05$ for all significant comparisons). Thus, these findings argue for strong DAB1 tyrosine phosphorylation dependent suppressive RELN effects on glioma cell migration.
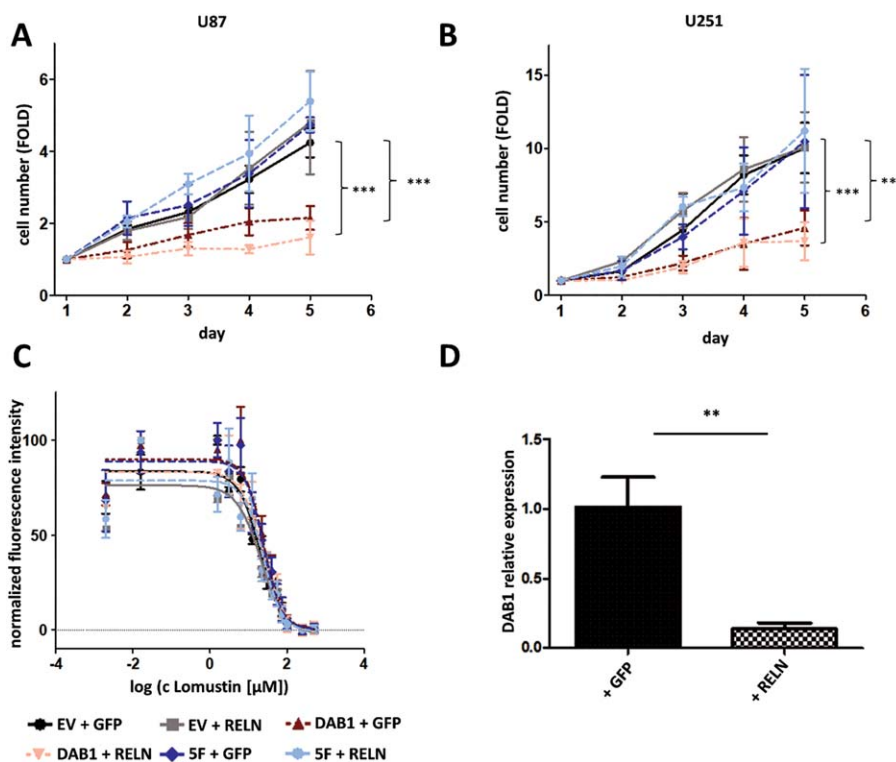
Figure 6. *Activation of RELN signaling inhibits cellular proliferation.* **A, B.** Proliferation assay in U87 (A) and U251 (B) cells stably expressing DAB1-WT or DAB1-5F stimulated with supernatants from HEK293T cells expressing mRELN or GFP as a control. The influence of DAB1-WT expression on the cell number with or without RELN stimulation was highly significant (repeated measures, two-way ANOVA followed by Bonferroni corrected post-tests, $P < 0.001$ on day 4 and 5). Shown are means $\pm$ SD, n = 3. **C.** DAB1 expression and RELN treatment do not alter resistance toward the chemotherapeutic agent lomustine. Neither RELN treatment nor DAB1 expression did influence the IC50 of U87 cells toward lomustine, n = 2. **D.** DAB1 expression is strongly decreased in U118 cells after long-term treatment with mRELN. The expression was measured via real-time PCR. Shown are means + SD, n = 3.

Interestingly, we also observed DAB1 (tyrosine phosphorylation)-independent RELN effects: There was a significant decrease in migration comparing U87 5F (RELN) to U87 5F (GFP) cells on fibronection (one-way ANOVA, followed by Tukey's multiple comparison test, $P < 0.05$). A similar (although non-significant) trend was observed- independently of the matrix condition used- in both cell lines not only for the comparison 5F (RELN vs. GFP-stimulated) but also for the comparison empty vector (RELN vs. GFP-stimulated). Overall, particularly when considering the U251 experiments on fibronection, it appeared that the DAB1 (tyrosine phosphorylation)-independent RELN effects were lower in U251 than in U87. Importantly, the reduction of velocity could be rescued by addition of CR-50, again indicating that the observed effect is RELN-specific. DAB1 expression and effectiveness of RELN stimulation were controlled by routine western blotting (Figure 7E,F; representative example).

In addition, we checked if DAB1 or RELN regulate the expression of the adhesion molecules ITGA3, ITGA5, ITGB1, FAK or PXN (paxillin). However, there was no consistent significant difference between the empty vector cells and (RELN-treated) DAB1-transfected cell lines (one-way ANOVA followed by Dunnett's post hoc test, Supporting Information Fig. 7).

DISCUSSION

The reelin signaling pathway plays a pivotal role in brain development by regulating neuronal migration and cortical layering (19). In contrast to these physiological functions, the role of reelin signaling in glioblastoma had not yet been investigated. We here can show that the *RELN* gene is silenced via promoter hypermethylation in glioblastoma tumors and cell lines, a mechanism that had also been observed in breast, pancreatic and gastric cancers (13, 44). Importantly, we found that DAB1 expression was also strongly reduced in high-grade brain tumors. This suggests that downregulation of RELN in brain tumor cells alone is not sufficient to inactivate the pathway. It is well possible that either RELN from the surrounding healthy brain parenchyma and/or other ligands can bind to the RELN receptors APOER2 and VLDLR, activate DAB1 and thereby exert effects on the tumor cells. Indeed, it had been shown that thrombospondin 1, clusterin or ApoE can all bind to APOER2 and VLDLR and interfere with RELN *in vitro* and *in vivo* (5, 27). Our *in vitro* findings suggest that particularly thrombospondin 1 is expressed by glioma cells.

We next assessed the correlation of RELN and DAB1 expression with WHO grade, glioblastoma expression subtype and overall survival. RELN and DAB1 expression were significantly inversely associated with WHO malignancy grade. Moreover,
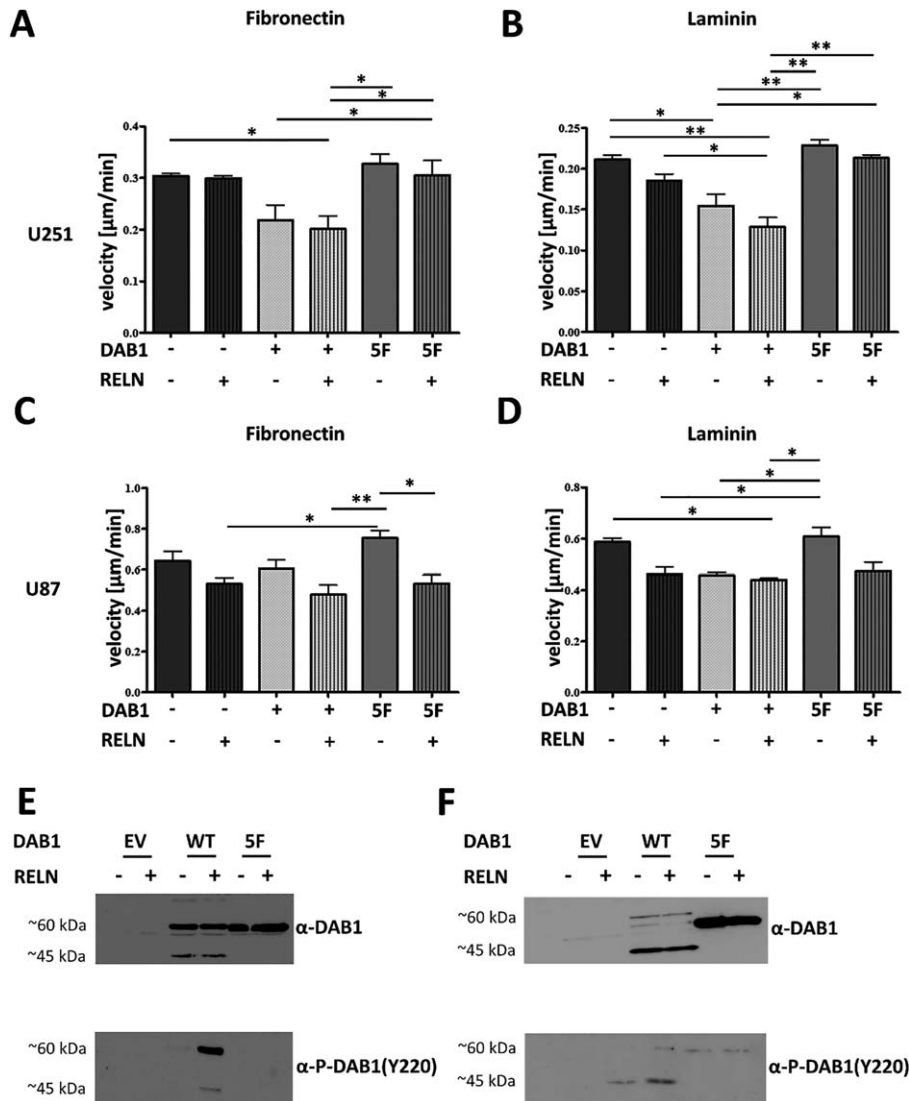
Figure 7. *Activation of RELN signaling alters migration in a DAB1 (tyrosine phosphorylation)-dependent and -independent fashion.* Groups were compared with one-way ANOVA followed by Tukey's multiple comparison test. Significant changes are indicated ($* = P < 0.05$, $** = P < 0.01$, $*** = P < 0.001$, $**** = P < 0.0001$). Shown are means + SEM, n = 2–3. **A, B.** Velocity of U251 cells on fibronectin (A) and laminin (B). DAB1-WT expressing cells that are stimulated with RELN migrate markedly slower than cells expressing the inactive 5F mutant or EV transfected cells. There is a trend toward slower overall migration after RELN stimulation on laminin also in EV and 5F cells, indicative of DAB1 (tyrosine phosphorylation)-independent effects on cell migration. **C, D.** Velocity of U87 cells on fibronectin (C) and laminin (D). On fibronectin, DAB1-WT expressing cells that are stimulated with RELN migrate markedly slower than GFP-stimulated cells expressing the inactive 5F mutant or EV-transfected cells. On laminin, RELN stimulated DAB1-WT cells show a significantly slower migration in comparison to 5F (GFP) cells and still a trend toward reduced migration in comparison to empty vector (GFP) cells. In addition, RELN stimulated 5F cells migrate significantly slower on fibronectin than GFP-stimulated cells and there is a trend toward slower overall migration after RELN stimulation on laminin and fibronectin for 5F and EV cells, indicative of DAB1 (tyrosine phosphorylation)-independent effects on cell migration. **E, F.** Western blot of DAB1 protein and P-DAB1 Y220 in U87 (E) and U251. (F). While in U87 the predominant band is visible at 60 kDa for both DAB1-WT and 5F, in U251 the predominant band of the DAB1-WT protein is visible at 45 kDa, indicating higher basal activity of RELN signaling in U251 cells.

high RELN transcriptional levels were associated with significantly longer overall survival in large glioblastoma patient cohorts. This suggests the RELN/DAB1 signaling axis as a novel candidate diagnostic and prognostic marker and potential therapeutic target. Interestingly, when comparing the expression of RELN and DAB1 between the different transcriptional glioblastoma subtypes (49) highest expression levels were observed in the neural subtype. This is in accord with the physiological function of RELN signaling as the neural expression subtype is suggestive of cells with a differentiated phenotype and typified by the expression of neuron markers, such as NEFL, GABRA1, SYT1 and SLC12A5 (49).

In light of Reelin's physiological function, it is somewhat astonishing that the potential association between RELN signaling and brain cancer pathology had not yet been systematically assessed. This might be caused by hindrances in modelling this pathway, that is, the cumbersome size of the RELN protein, the low expression of RELN (and DAB1) in most glioma cell lines and the lack of vector constructs to overexpress human reelin in glioma cells. On account of these limitations and the simultaneous downregulation of DAB1 in glioblastomas described above, for our functional analyzes we decided to take an approach in which DAB1 was stably overexpressed in two different qualities: (i) as DAB1-WT with the full functionality of the DAB1 protein and (ii) DAB1-5F mutant with point mutations at all five Dab1 tyrosine phosphorylation sites (Tyr185, tyr198, Tyr200, Tyr220 and Tyr232). This DAB1-5F mutant has been previously well characterized and is devoid of all RELN-mediated tyrosine phosphorylation-dependent downstream signaling effects (20). Empty vector cells served as an additional control. As such, we were able to assess the common final signaling pathway with and without reelin stimulation but also completely free of endogenous RELN effects (5F-mutant and CR-50 blocking antibody experiments).

In this experimental setting, we observed major effects on RELN/DAB1 signaling on glioma cell proliferation and migration. DAB1-WT overexpression led to a significant decrease in proliferation and this effect was RELN-dependent as it could not be observed in cells expressing the DAB1-5F mutant. Consistently with this finding, E2F signaling was the major pathway altered in our proteomic screen comparing DAB1-WT and DAB1-5F expressing U87 cell lines. E2F transcription factors are important regulators of cell cycle progression (15). They are also known to be frequently altered in glioblastoma, as for example mediated by other well-known molecular alterations like *RB1* mutations, *CDK4* amplification or *CDKN2A* deletion (7, 49). Our findings therefore describe a new mechanism of E2F control, previously probably not observed because of the fact that RELN signaling via DAB1 was examined mostly in post-mitotic neurons.

In addition, we described cell line-specific effects of RELN signaling on ERK1/2 as well as on STAT3 activity. In U87, DAB1 expression and RELN stimulation were able to reduce ERK1/2 and STAT3 activity. Moreover, short term RELN stimulation after medium exchange was able to reduce ERK1/2 activity in both U251 and U87 cells. As U251 DAB1-WT cells in the proliferation assays grew nonetheless much slower after longer (3–5 days) growth factor removal and ERK and STAT3 phosphorylation were not reduced in these cells, we speculate that alternative ligands, secreted factors or adaptive responses to growth factor removal may trigger this behavior. In contrast to neuronal migration, where alterations in p-cofilin levels after RELN stimulation have been reported (10, 11), we could not find any change in p-cofilin to the total cofilin ratio or a qualitative change in the actin cytoskeleton (data not shown).

Nevertheless, functionally we observed a relevant impact of RELN/DAB1 signaling on glioma cell migration. This suggests that RELN acts only in small areas of the cell (precluding the analysis of a quantitative phenotype) or by a cofilin-independent mechanism, for example by regulation of N-WASP (48). In our rather elaborated setting of migration assays involving different DAB1-overexpressing clones under different matrix conditions with and without RELN stimulation, the most consistent finding was a

significant negative impact of RELN-dependent DAB1 activation on tumor cell migration. However, as outlined above, we also observed DAB1 (tyrosine phosphorylation)-independent RELN effects and these appeared to be gradually different between the cell lines (less pronounced in U251 on fibronectin than in U87). Although both lines are PTEN-deficient (26), they differ in their expression subtype and p53 status what might account for the cell-line specific differences. More importantly, U251 (in comparison to U87) also contains a much higher content of thrombospondin (Figure 3G). Thus, alternative ligand binding might mitigate the DAB1 (tyrosine phosphorylation)-independent RELN effects in U251 cells. As thrombospondin has also been described to specifically bind to fibronectin, this interaction might additionally account for the slightly different migrational behavior of U251 cells on this specific matrix (24). We highlight this example here to underline the advantage of our approach studying RELN signaling by mainly comparing DAB1-WT and DAB1-5F cells over an approach solely relying on stimulation with recombinant RELN. The latter approach may be more prone to uncontrolled interference with endogenous alternative ligand binding and might thereby obscure distinct results.

In summary, we show that the canonical RELN signaling cascade via DAB1 exerts tumor suppressive functions and is a yet unknown barrier to cellular transformation in gliomagenesis. These effects are mediated via suppression of E2F activity by the DAB1-WT protein and harbor strong prognostic implications. Our findings might thereby unearth novel, yet unrecognized treatment options in glioblastomas.

ACKNOWLEDGMENTS

AUTHOR CONTRIBUTIONS

Conception and design: MJ Riemenschneider, M Schulze
Development of methodology: MJ Riemenschneider, C Violonchi, M Schulze, S Swoboda

Acquisition of data: M Schulze, C Violonchi, S Swoboda, J Simbürger, T Welz, S Hoja

Analysis and interpretation of data: M Schulze, MJ Riemenschneider, J Reinders, E Kerkhoff

Writing, review and/or revision of the manuscript: M Schulze, MJ Riemenschneider

Administrative, technical or material support: MJ Riemenschneider, J Reinders, E Kerkhoff

Study supervision: MJ Riemenschneider

CONFLICT OF INTEREST

The authors declare no potential conflicts of interest.

REFERENCES

1. Ahluwalia MS, de Groot J, Liu WM, Gladson CL (2010) Targeting SRC in glioblastoma tumors and brain metastases: rationale and preclinical studies. *Cancer Lett* **298**:139–149.

2. Alcantara Llaguno S, Chen J, Kwon CH, Jackson EL, Li Y, Burns DK *et al* (2009) Malignant astrocytomas originate from neural stem/progenitor cells in a somatic tumor suppressor mouse model. *Cancer Cell* **15**:45–56.

3. Barski D, Wolter M, Reifenberger G, Riemenschneider MJ (2010) Hypermethylation and transcriptional downregulation of the TIMP3 gene is associated with allelic loss on 22q12.3 and malignancy in meningiomas. *Brain Pathol* **20**:623–631.

4. Becker J, Frohlich J, Perske C, Pavlakovic H, Wilting J (2012) Reelin signalling in neuroblastoma: migratory switch in metastatic stages. *Int J Oncol* **41**:681–689.

5. Blake SM, Strasser V, Andrade N, Duit S, Hofbauer R, Schneider WJ, Nimpf J (2008) Thrombospondin-1 binds to ApoER2 and VLDL receptor and functions in postnatal neuronal migration. *EMBO J* **27**:3069–3080.

6. Bock HH, Jossin Y, May P, Bergner O, Herz J (2004) Apolipoprotein E receptors are required for reelin-induced proteasomal degradation of the neuronal adaptor protein Disabled-1. *J Biol Chem* **279**:33471–33479.

7. Brennan CW, Verhaak RG, McKenna A, Campos B, Noushmehr H, Salama SR *et al* (2013) The somatic genomic landscape of glioblastoma. *Cell* **155**:462–477.

8. Carpenter AE, Jones TR, Lamprecht MR, Clarke C, Kang IH, Friman O *et al* (2006) CellProfiler: image analysis software for identifying and quantifying cell phenotypes. *Genome Biol* **7**:R100.

9. Castellano E, Molina-Arcas M, Krygowska AA, East P, Warne P, Nicol A, Downward J (2016) RAS signalling through PI3-Kinase controls cell migration via modulation of Reelin expression. *Nat Commun* **7**:11245.

10. Chai X, Forster E, Zhao S, Bock HH, Frotscher M (2009) Reelin acts as a stop signal for radially migrating neurons by inducing phosphorylation of n-cofilin at the leading edge. *Commun Integr Biol* **2**:375–377.

11. Chai X, Forster E, Zhao S, Bock HH, Frotscher M (2009) Reelin stabilizes the actin cytoskeleton of neuronal processes by inducing n-cofilin phosphorylation at serine3. *J Neurosci* **29**:288–299.

12. Dimova DK, Dyson NJ (2005) The E2F transcriptional network: old acquaintances with new faces. *Oncogene* **24**:2810–2826.

13. Dohi O, Takada H, Wakabayashi N, Yasui K, Sakakura C, Mitsufuji S *et al* (2010) Epigenetic silencing of RELN in gastric cancer. *Int J Oncol* **36**:85–92.

14. Dulabon L, Olson EC, Taglienti MG, Eisenhuth S, McGrath B, Walsh CA *et al* (2000) Reelin binds alpha3beta1 integrin and inhibits neuronal migration. *Neuron* **27**:33–44.

15. Dyson NJ (2016) RB1: a prototype tumor suppressor and an enigma. *Genes Dev* **30**:1492–1502.

16. Evangelisti C, Florian MC, Massimi I, Dominici C, Giannini G, Galardi S *et al* (2009) MiR-128 up-regulation inhibits Reelin and DCX expression and reduces neuroblastoma cell motility and invasiveness. *FASEB J* **23**:4276–4287.

17. Friedmann-Morvinski D, Bushong EA, Ke E, Soda Y, Marumoto T, Singer O *et al* (2012) Dedifferentiation of neurons and astrocytes by oncogenes can induce gliomas in mice. *Science* **338**:1080–1084.

18. Hoja S, Schulze M, Rehli M, Proescholdt M, Herold-Mende C, Hau P, Riemenschneider MJ (2016) Molecular dissection of the valproic acid effects on glioma cells. *Oncotarget* **7**:62989–63002.

19. Honda T, Kobayashi K, Mikoshiba K, Nakajima K (2011) Regulation of cortical neuron migration by the Reelin signaling pathway. *Neurochem Res* **36**:1270–1279.

20. Howell BW, Herrick TM, Hildebrand JD, Zhang Y, Cooper JA (2000) Dab1 tyrosine phosphorylation sites relay positional signals during mouse brain development. *Curr Biol* **10**:877–885.

21. Kam R, Chen J, Blumcke I, Normann S, Fassunke J, Elger CE *et al* (2004) The reelin pathway components disabled-1 and p35 in gangliogliomas–a mutation and expression analysis. *Neuropathol Appl Neurobiol* **30**:225–232.

22. Kurscheid S, Bady P, Sciuscio D, Samarzija I, Shay T, Vassallo I *et al* (2015) Chromosome 7 gain and DNA hypermethylation at the HOXA10 locus are associated with expression of a stem cell related HOX-signature in glioblastoma. *Genome Biol* **16**:16.

23. Kwon IS, Cho SK, Kim MJ, Tsai MJ, Mitsuda N, Suh-Kim H, Lee YD (2009) Expression of Disabled 1 suppresses astroglial differentiation in neural stem cells. *Mol Cell Neurosci* **40**:50–61.

24. Lahav J, Lawler J, Gimbrone MA (1984) Thrombospondin interactions with fibronectin and fibrinogen. Mutual inhibition in binding. *Eur J Biochem* **145**:151–156.

25. Lakoma J, Garcia-Alonso L, Luque JM (2011) Reelin sets the pace of neocortical neurogenesis. *Development* **138**:5223–5234.

26. Lee JJ, Kim BC, Park MJ, Lee YS, Kim YN, Lee BL, Lee JS (2011) PTEN status switches cell fate between premature senescence and apoptosis in glioma exposed to ionizing radiation. *Cell Death Differ* **18**:666–677.

27. Leeb C, Eresheim C, Nimpf J (2014) Clusterin is a ligand for apolipoprotein E receptor 2 (ApoER2) and very low density lipoprotein receptor (VLDLR) and signals via the Reelin-signaling pathway. *J Biol Chem* **289**:4161–4172.

28. Lin L, Yan F, Zhao D, Lv M, Liang X, Dai H *et al* (2016) Reelin promotes the adhesion and drug resistance of multiple myeloma cells via integrin beta1 signaling and STAT3. *Oncotarget* **7**:9844–9858.

29. Livak KJ, Schmittgen TD (2001) Analysis of relative gene expression data using real-time quantitative PCR and the 2(-Delta Delta C(T)) Method. *Methods* **25**:402–408.

30. Love MI, Huber W, Anders S (2014) Moderated estimation of fold change and dispersion for RNA-seq data with DESeq2. *Genome Biol* **15**:550.

31. Madhavan S, Zenklusen JC, Kotliarov Y, Sahni H, Fine HA, Buetow K (2009) Rembrandt: helping personalized medicine become a reality through integrative translational research. *Mol Cancer Res* **7**:157–167.

32. McAvoy S, Zhu Y, Perez DS, James CD, Smith DI (2008) Disabled-1 is a large common fragile site gene, inactivated in multiple cancers. *Genes Chromosomes Cancer* **47**:165–174.

33. Molla Kazemiha V, Shokrgozar MA, Arabestani MR, Shojaei Moghadam M, Azari S, Maleki S *et al* (2009) PCR-based detection and eradication of mycoplasmal infections from various mammalian cell lines: a local experience. *Cytotechnology* **61**:117–124.

34. Nagai S, Moreno O, Smith CA, Ivanchuk S, Romagnuolo R, Golbourn B *et al* (2011) Role of the cofilin activity cycle in astrocytoma migration and invasion. *Genes Cancer* **2**:859–869.

35. Perez-Martinez FJ, Luque-Rio A, Sakakibara A, Hattori M, Miyata T, Luque JM (2012) Reelin-dependent ApoER2 downregulation uncouples newborn neurons from progenitor cells. *Biol Open* **1**:1258–1263.

36. Ramaker RC, Lasseigne BN, Hardigan AA, Palacio L, Gunther DS, Myers RM, Cooper SJ (2017) RNA sequencing-based cell proliferation analysis across 19 cancers identifies a subset of proliferation-informative cancers with a common survival signature. *Oncotarget* **8**: 38668–38681.

37. Riemenschneider MJ, Mueller W, Betensky RA, Mohapatra G, Louis DN (2005) In situ analysis of integrin and growth factor receptor signaling pathways in human glioblastomas suggests overlapping relationships with focal adhesion kinase activation. *Am J Pathol* **167**: 1379–1387.

38. Riemenschneider MJ, Reifenberger J, Reifenberger G (2008) Frequent biallelic inactivation and transcriptional silencing of the DIRAS3 gene at 1p31 in oligodendroglial tumors with 1p loss. *Int J Cancer* **122**: 2503–2510.

39. Sato N, Fukushima N, Chang R, Matsubayashi H, Goggins M (2006) Differential and epigenetic gene expression profiling identifies frequent disruption of the RELN pathway in pancreatic cancers. *Gastroenterology* **130**:548–565.

40. Schneider CA, Rasband WS, Eliceiri KW (2012) NIH Image to ImageJ: 25 years of image analysis. *Nat Methods* **9**:671–675.

41. Sekine K, Kawauchi T, Kubo K, Honda T, Herz J, Hattori M *et al* (2012) Reelin controls neuronal positioning by promoting cell-matrix adhesion via inside-out activation of integrin alpha5beta1. *Neuron* **76**: 353–369.

42. Simburger JM, Dettmer K, Oefner PJ, Reinders J (2016) Optimizing the SWATH-MS-workflow for label-free proteomics. *J Proteomics* **145**:137–140.

43. Smalheiser NR, Costa E, Guidotti A, Impagnatiello F, Auta J, Lacor P *et al* (2000) Expression of reelin in adult mammalian blood, liver, pituitary pars intermedia, and adrenal chromaffin cells. *Proc Natl Acad Sci USA* **97**:1281–1286.

44. Stein T, Cosimo E, Yu X, Smith PR, Simon R, Cottrell L *et al* (2010) Loss of reelin expression in breast cancer is epigenetically controlled and associated with poor prognosis. *Am J Pathol* **177**:2323–2333.

45. Stupp R, Hegi ME, Mason WP, van den Bent MJ, Taphoorn MJ, Janzer RC *et al* (2009) Effects of radiotherapy with concomitant and adjuvant temozolomide versus radiotherapy alone on survival in glioblastoma in a randomised phase III study: 5-year analysis of the EORTC-NCIC trial. *Lancet Oncol* **10**:459–466.

46. Sturm D, Witt H, Hovestadt V, Khuong-Quang DA, Jones DT, Konermann C *et al* (2012) Hotspot mutations in H3F3A and IDH1 define distinct epigenetic and biological subgroups of glioblastoma. *Cancer Cell* **22**:425–437.

47. Subramanian A, Tamayo P, Mootha VK, Mukherjee S, Ebert BL, Gillette MA *et al* (2005) Gene set enrichment analysis: a knowledge-based approach for interpreting genome-wide expression profiles. *Proc Natl Acad Sci USA* **102**:15545–15550.

48. Suetsugu S, Tezuka T, Morimura T, Hattori M, Mikoshiba K, Yamamoto T, Takenawa T (2004) Regulation of actin cytoskeleton by mDab1 through N-WASP and ubiquitination of mDab1. *Biochem J* **384**:1–8.

49. Verhaak RG, Hoadley KA, Purdom E, Wang V, Qi Y, Wilkerson MD *et al* (2010) Integrated genomic analysis identifies clinically relevant subtypes of glioblastoma characterized by abnormalities in PDGFRA, IDH1, EGFR, and NF1. *Cancer Cell* **17**:98–110.

50. Wiśniewski JR, Zougman A, Nagaraj N, Mann M (2009) Universal sample preparation method for proteome analysis. *Nat Methods* **6**: 359–362.

SUPPORTING INFORMATION

Additional Supporting Information may be found in the online version of this article at the publisher's web-site:

Figure 1. Analysis of RELN expression and recurrent mutations in GBM. While there is no significant difference between EGFR-, NF1-, TP53-, PIK3CA-, PIK3R1-, PTEN- and RB1-mutant vs. wildtype (WT) tumors, there is a small but significant difference between IDH1-mutant and WT-tumors (Bonferroni corrected two-sided Mann-Whitney test, $P < 0.05$).

Figure 2. Depiction of the region of the RELN promoter analyzed by bisulfite sequencing. CpG dinucleotides (red) are numbered according to their position relative to the transcription start site (TSS). Primers are marked with grey arrows.

Figure 3. Reln protein expression as assessed by immunohistochemistry. Reln is expressed in non-neoplastic brain tissue with strongest staining in neurons of the grey matter (A, x400) but positivity also in the white matter (B, x200, showing the transition zone between grey and white matter). Reln is also expressed in tumor cells but in a very heterogeneous fashion C (×400) and D (×200) show regions of differential Reln expression within a single case of IDH-wildtype glioblastoma. (E, x200 and F, x200) Two further cases of glioblastoma with one (E) completely devoid of Reln protein expression and the other (F) exhibiting only interspersed Reln positive cells with some of the cells most likely corresponding to intermixed reactive astrocytes. (G, x200) A case of IDH-mutant anaplastic astrocytic with very low to absent Reln protein expression. (H, x400) A case of IDH-mutant WHO grade II diffuse astrocytoma with uniform Reln expression close to the levels observed in non-neoplastic brain tissue.

Figure 4. A) Outline of the strategy for semiquantitative PCR. The five-prime PCR product is located in the CMV promoter, followed by the DAB1 full length ORF. The three-prime product is amplified from a site between the ORF and the IRES site. B) Semiquantitative PCR of the regions flanking the DAB1-WT and DAB1-5F expression construct on the three-prime and five-prime end. All cell lines tested show integration of the full-length construct at an equal level. M, Marker (100 bp DNA ladder plus); +, positive control (20 ng DAB1-WT DNA construct); −, negative control (ultrapure water). A-F, Five-prime region PCR of stably transfected U87MG and U251 cell lines: A, U87-MG + EV; B, U87-MG + DAB1-WT; C, U87-MG + DAB1-5F; D, U251 + EV; E, U251 + DAB1-WT; F, U251 + DAB1-5F. G-L, PCR of the three-prime region from stably transfected U87-MG and U251 cell lines: G, U87-MG + EV; H, U87-MG + DAB1-WT; I, U87-MG + DAB1-5F; J, U251+ EV; K, U251 + DAB1-WT; L, U251 + DAB1-5F. C) Quantification of the PCR as shown in -B). The fluorescence intensities were calculated as ratio of the five-prime PCR intensity divided by the three-prime PCR intensity. +, positive control A, U87-MG + EV; B, U87-MG + DAB1-WT; C, U87-MG + DAB1-5F; D, U251 + EV; E, U251 + DAB1-WT; F, U251 + DAB1-5F. D) PCR of full length DAB1 inserts. M, Marker (100 bp DNA ladder plus); A, U87-MG + DAB1-WT; C, U87-MG + DAB1-5F; D, U251 + DAB1-WT; E, U251 + DAB1-5F.

Figure 5. Both reduction of ERK1/2 phosphorylation (A and B) and migration (C and D) can be rescued by addition of the CR-50 antibody that blocks the function of mRELN. Shown are means + SD. Groups were compared by one-way ANOVA followed by Tukey's post hoc test.

Figure 6. A) Cell cycle distribution of stably transfected U251 cells. While the fraction of cells in G1 is significantly reduced, the fraction of cells in G2/M is significantly increased in DAB1-WT expressing cells as compared to empty vector cells (two-way ANOVA followed by Bonferroni corrected posttests, $P < 0.001$). In contrast, there are no significant differences between empty vector and DAB1-5F expressing cells. B) Caspase 3 western blot analysis in U251 cells. Only full-length caspase 3 can be detected in all stable cell lines, while cleaved caspase 3 is absent.

Figure 7. Real-time PCR analysis of the adhesion molecules PXN, FAK, ITGA3, ITGA5 and ITGB1. Shown are means + SD, n=2. There was no consistent significant difference between the empty vector cells and (RELN-treated) DAB1-transfected cell lines (one-way ANOVA followed by Dunnett's post hoc test, all conditions vs. empty vector + GFP).

Table 1. Primers used for bisulfite sequencing and real-time PCR analyses.

Table 2. Overview of the methylation status (+/-), the methylation score and the methylation pattern of RELN as detected by direct sodium bisulfite sequencing of the RELN promoter region (CpGs sites in Supporting Information Fig. 1). mRNA expression levels are also provided. Allmost all glioblastomas show hypermethylation of the RELN promoter (for % samples hypermethylated in the different WHO grades compare Fig. 2B). For promoter methylation scoring, the CG sites were first semiquantitatively assigned to the categories unmethylated (no cytosine detectable, =0), weakly methylated (peak for cytosine detectable, but smaller that thymine, =1), moderately methylated (C and T at equal amounts detectable, =2) and strongly methylated (thymine peak smaller than cytosine, =3). Then, the scores for each individual sample were summed across the whole investigated CpG site to determine the overall methylation score. Tumors with a score ≥ 22 were considered as hypermethylated (+), tumors with a score < 22 as not hypermethylated (-) compared to the non-neoplastic controls.

Table 3. Methylation analysis of the RELN promoter after 5-Aza-2′deoxycytidine treatment in different cell lines. Treatment with 5-Aza-2′deoxycytidine in combination with trichostatin A reduces the methylation in all cell lines, although significant methylation still remains.

Table 4. Differentially abundant proteins as identified by DESeq2 at P-adjusted < 0.1. Proteins that are less abundant in DAB1-WT cells are labeled in green, whereas proteins that are more abundant in DAB1-WT cells are shown in red.